Petrography, mineralogy and geochemistry of the rock formations of the Zululand Basin based on borehole NZA

Brandon Evan Landman

10116509

Submitted in fulfilment of the requirements for the MSc degree in Geology at the Faculty of Natural and Agricultural Sciences, University of Pretoria

9 June, 2017

The financial assistance of the South African Centre for Carbon Capture and Storage towards this research is hereby acknowledged. Opinions expressed and conclusions arrived at, are those of the author and not necessarily to be attributed to SACCCS.

DECLARATION OF ORIGINALITY / DECLARATION ON PLAGIARISM

The ***Department of Geology (University of Pretoria)*** places great emphasis upon integrity and ethical conduct in the preparation of all written work submitted for academic evaluation. While academic staff teaches you about referencing techniques and how to avoid plagiarism, you too have a responsibility in this regard. If you are at any stage uncertain as to what is required, you should speak to your lecturer before any written work is submitted.

You are guilty of plagiarism if you copy something from another author's work (e.g. a book, an article or a website) without acknowledging the source and pass it off as your own. In effect you are stealing something that belongs to someone else. This is not only the case when you copy work word-for-word (verbatim), but also when you submit someone else's work in a slightly altered form (paraphrase) or use a line of argument without acknowledging it. You are not allowed to use work previously produced by another student. You are also not allowed to let anybody copy your work with the intention of passing if off as his/her work.

Students who commit plagiarism will not be given any credit for plagiarised work. The matter may also be referred to the Disciplinary Committee (Students) for a ruling. Plagiarism is regarded as a serious contravention of the University's rules and can lead to expulsion from the University.

The declaration which follows must accompany all written work submitted while you are a student of the ***Department of Geology (University of Pretoria)***. No written work will be accepted unless the declaration has been completed and attached.

I, the undersigned, declare that:
1. I understand what plagiarism is and am aware of the University's policy in this regard.
2. I declare that this assignment (e.g. essay, report, project, assignment, dissertation, thesis, etc) is my own original work. Where other people's work has been used (either from a printed source, Internet or any other source), this has been properly acknowledged and referenced in accordance with Departmental requirements.
3. I have not used work previously produced by another student or any other person to hand in as my own.
4. I have not allowed, and will not allow, anyone to copy my work with the intention of passing it off as his or her own work.

Full names of student: Brandon Evan Landman

Student number: 10116509

Date submitted: 9 June 2017

Topic of work: MSc dissertation

Signature: _____

Supervisor: _____

ABSTRACT

The drill core of borehole NZA, drilled in the southwest margin of the onshore Zululand Basin to a depth of ca. 571 m was investigated in this study. In this thesis descriptions of the geochemistry, mineralogy and physical properties of major lithofacies of the NZA drill core are followed by an interpretation of the suitability of NZA rock units for injection of carbon dioxide (CO_2). A representative NZA sandstone was subjected to reaction with super critical (sc)CO_2 and water under reservoir conditions for two weeks to gain insight into the effects of rock-CO_2 interactions on rock porosity. Rock porosity was estimated by petrographic study for clastic sedimentary rocks of NZA.

Petrographic study served to identify major lithofacies associations of the NZA drill core, as well as the depositional environments; interpreted after studying primary sedimentary structures, chemistry and biogenic features. Trends within the lithofacies were used to discriminate various formations of the Zululand Group observed in the NZA drill core. The Zululand Group rocks of the NZA drill core were generally deposited in a shallow shelf environment, while the pyroclastic rocks of the Fenda Formation identified in the drill core were deposited in a subaerial volcanic environment. Calcareous sandstones, greywackes, coquina limestone, beachrock, lapilli-stone, lapilli-tuff, tuff-breccia and tuff were identified as the major lithofacies of the NZA drill core and are consistent with literature data.

Major element XRF results and mineralogical results formed an integral role in investigating the chemistry and its effects on the mineralogy of the NZA drill core's rocks. Major element analysis was further utilised for discriminating tectonic setting and provenance of siliciclastic rocks. From geochemical data the source area of the Zululand Group sedimentary rocks of the NZA core is consistent with the inferred continental rift setting for the Zululand Basin. The provenance of the NZA drill core's siliciclastic rocks is consistent with chemically immature terrigenous detritus, sourced from the proximal Lebombo Group volcanic rocks.

Borehole NZA was drilled to a relatively shallow depth which is insufficient, when considering its use for geological storage of CO_2. Furthermore, the low porosity of ca. 1-2 %, identified in the rock samples suggests low storage potential. Dissolution after CO_2 injection may significantly increase porosity after reaction with scCO_2 while rock stability could be severely compromised due to dissolution of carbonates. Lastly, lithologies of the NZA drill core do not correlate well with the adjacent ZA, ZB and ZC drill core lithologies; thus the NZA borehole is a seemingly unsuitable site for geological storage of CO_2 as CCS technology requires lateral continuity of suitable rock packages. Further study of the chemistry and physical properties of the ZA, ZB and ZC drill core could reveal a suitable site for injection of CO_2 in the onshore Zululand Basin.

TABLE OF CONTENTS

LIST OF FIGURES

LIST OF TABLES

APPENDICES

1. Introduction

The mean atmospheric CO_2 concentration has varied between 180-280 ppm during the absence of human influence (Bala, 2013). Recently, global mean atmospheric concentration of CO_2 increased to 400 ppm (Monastersky, 2013). Increasing atmospheric CO_2 concentration is directly related to exploitation of fossil fuels to sustain mankind's enormous energy needs; contributing two-thirds of total global emissions (Barr *et al.,* 2011, Monastersky, 2013; IEA, 2015). Rising CO_2 levels lead to climate change and is also linked to ocean acidification causing extinction of species (Barr *et al.,* 2011, Bala, 2013). Furthermore, elevated atmospheric CO_2 concentration causes increased cases of diseases such as skin cancer and disruption of marine life due to increased sea levels from melting of polar ice caps (Barr *et al.,* 2011, Bala, 2013).

Fossil fuels are used extensively because current technology is functional and more importantly affordable compared with untested, expensive, environmentally-friendly, alternative energy sources (Mwakasonda and Winkler, 2005). Several countries have pledged to reduce their CO_2 emissions through the Kyoto Protocol as well as Intended Nationally Determined Contributions (INDC's) (IEA, 2015). Countries that have submitted pledges contribute ca. 90 % of world-wide CO_2 emissions and will work toward reducing CO_2 emissions per capita, setting absolute GHG emission targets and implementing various climate change policies (IEA, 2015). Presently countries such as Germany, the United States of America and Japan reduced CO_2 emissions by utilising renewable energy in nearly half their new power generation capacity (IEA, 2015).

Greenhouse gas (GHG) emissions contributing to climate change include CO_2, N_2O, CH_4, O_3 and water vapour (DEA, 2014). CO_2 has been identified as the most prolific GHG after CH_4 and N_2O (DEA, 2014) because it is the most abundant and stable GHG produced (Bachu, 2000). It has a long residence time in the atmosphere of ca. 100-3000 yr (Bala, 2013). Thus, CO_2 is able to contribute to climate change many years after it is emitted. For this reason climate change mitigation efforts concentrate on reducing CO_2 emissions. Under the United Nations Framework Convention for Climate Change (UNFCCC) South Africa, which produces up to ca. 440 Mt of CO_2 annually, is obligated to mitigate climate change and compile strict inventories concerning GHG emissions (DEA, 2014).

Between the years 2000 and 2010 coal combustion contributed ca. 66 % of South Africa's energy supply (DEA, 2014). The much cleaner burning oil and gas, contribute significantly less to the country's energy budget, ca. 21.5 % and 2.8 % respectively (DEA, 2014). From these statistics CO_2 emissions are expected to increase each year as a result of burning of more coal for increasing energy needs. For this reason an effective strategy for reducing South Africa's CO_2 emissions is required. In the paragraphs that follow a brief description of carbon capture and storage (CCS) is given as well as reasons for South Africa undertaking this climate change mitigation technology.

1.1 What is carbon capture and storage?

There are several methods of storing CO_2 including biological, deep ocean disposal and injection into geological formations (IPCC, 2005). Through preliminary studies conducted by the Council for Geoscience (CGS) the South African CO_2 Technical Report was published (Viljoen *et al.,* 2010). After careful consideration the most cost effective, environmentally sound and globally established method for mitigating CO_2 in South Africa is geological storage of CO_2 (Viljoen *et al.*, 2010).

CCS is a broad, intricately linked chain of capturing CO_2 produced at point sources and transporting it to geologically suitable sites for injection into stable rock formations (Lotz and Brent, 2008). CCS stems from a similar technology used in the oil and gas industry, specifically in enhanced oil recovery (EOR) (Bachu, 2000; IPCC, 2005). It involves the injection of CO_2 into the Earth's crust at relatively shallow levels, at ca. 800-2500 m into suitable geological formations (Cloete, 2010). Injected CO_2 can be kept in the earth's crust by closed traps in highly porous reservoir rocks such as sandstones, at depths of ca. 800 m or more over geological time frames. Trapping injected CO_2 in sandstone is made possible by an overlying impermeable caprock such as shale. Another means of storing CO_2 is hydrodynamic trapping or mineral immobilisation whereby CO_2 reacts with rock and pore water forming stable mineral phases permanently trapping the CO_2 in mineral phases (Cloete, 2010). Both techniques are intended for permanent, safe storage of CO_2 without degrading the environment, both now and in the future (IPCC, 2005). Presently, CCS technology has been safely implemented at relatively large scales in test sites such as In Salah, Algeria storing 3.8 Mt of CO_2 until 2011; Sleipner, Norway storing 1 Mt of CO_2 per annum since 1996 and Weyburn, Canada storing 1,8 Mt of CO_2 per annum since 2000 (Viljoen *et al.,* 2010).

The roadmap outlined for South Africa's CCS goals includes up-scaling endeavours once the geology of potential storage reservoirs has been considered (Cloete, 2010). Firstly, the strategy aims to have a test injection site by 2017, in which tens of thousands of tonnes of CO_2 can be injected and monitored. Secondly, this project will upscale before 2020 to safely store hundreds of thousands of tonnes of CO_2 (Cloete, 2010). The final goal of the CO_2 roadmap is a fully operational, commercial plant storing millions of tonnes of CO_2 by 2025 (Cloete, 2010).

1.2 Why use carbon capture and storage?

South Africa, like other developing countries faces the challenge of mitigating climate change while simultaneously reducing CO_2 emissions and supplying energy necessary to sustain economic growth (Mwakasonda and Winkler, 2005). Thus, a multi-disciplinary integrated portfolio of energy technologies is required for mitigation of GHG emissions (Viljoen *et al.,* 2010). According to Viljoen *et al.* (2010), CCS technology will form an integral part of the country's multi-platform CO_2 emission mitigation strategy. CCS is an attractive option whereby South Africa can meet its energy demands while simultaneously cutting CO_2 emissions (Mwakasonda and Winkler, 2005). South Africa's CCS objective is a 5 % reduction

of annual CO_2 emissions (Cloete, 2010); however this value could vary as the certainty of CCS capacity in South Africa changes.

CCS can be a cost saving climate change mitigation technology if sources of CO_2 are proximal to geological units to be used for storage. For this reason, limited transport costs and infrastructure upgrades are required. In other cases the transportation costs are cut by building pipelines to distal areas (Cloete, 2010). According to the South African CO_2 Atlas (Cloete, 2010), the entire country's current storage potential is calculated to accommodate 150 Gt of CO_2. Approximately 98 % of this storage potential is available in offshore Mesozoic sedimentary rocks, while the remaining 2 % storage potential is available in onshore basins (Viljoen *et al.,* 2010).

Pertinent to this project is the onshore Zululand Basin, with an estimated storage capacity of approximately 460 Mt of CO_2, as well as being located within 400 km of major CO_2 sources (Viljoen *et al*., 2010). According to IPCC (2005), important factors to consider for CCS include short distances between CO_2 point sources and storage areas. This is especially apparent in South Africa's interest in increasing research and technological capacity for the onshore Zululand Basin as compared to actively studying the larger, more expensive, offshore basins.

1.3 Objectives of the study

Assembling reliable geological data and using purposeful techniques to precisely characterise the physical, geochemical and mineralogical features of potential reservoir rocks as well as caprocks are the primary aims of this study. The porosity variation of host rock was investigated in this study, before and after autoclave experiments in which rocks reacted with $scCO_2$ under reservoir conditions. These experiments provide an overview of potential outcomes of the rocks suitability for injecting CO_2. Understanding the geochemistry and mineralogy of rock units of the NZA drill core is important for predicting potential reactions of CO_2 reacting with rock units. While deciphering the depositional environment of the NZA lithofacies provides insight into correlating rock units of adjacent Zululand Basin boreholes. Thus, the suitability of laterally continuous host rocks can be determined across the Zululand Basin. These objectives are consistent with refining preliminary insights to provide geological information necessary to show that, as far as can be discerned prior to injection, the site will perform effectively and safely for geological storage of CO_2 (Groenenberg *et al.,* 2008).

2. Regional geology of the onshore Zululand Basin

The onshore Zululand Basin is located in KwaZulu-Natal Province, along the north-eastern coast of South Africa, indicated by the circled area in Figure 1. Along its western margin the basin extends 250 km from the town of St Lucia into the southernmost portion of Mozambique where it becomes the Mozambique Basin (Kennedy and Klinger, 1972; Chabangu *et al.,* 2014). The basin is bounded to the west by the 180-140 Ma Lebombo Group volcanics (Watkeys, 2002), interpreted as a rifted volcanic margin contributing continental clastic sediment to the Zululand Basin. East of the limited Zululand Group outcrops are the Cenozoic deposits of the Maputaland Group (Roberts *et al.,* 2006).

The sedimentary rocks of the onshore Zululand Basin cover a narrow, north-south trending area of ca. 7500 km^2 extending into southern Mozambique (Broad *et al.,* 2006; Shone, 2006). The basin is divided into two distinct areas by the north-east trending Bumbeni Ridge in Figure 2 extending through the basin from the Lebombo Mountains to the Indian Ocean (Broad *et al.,* 2006; Chabangu *et al.,* 2014). North of the Bumbeni Ridge lies the deeper Kosi Trough comprised of rock units ca. 2000 m thick, while to the south, the St Lucia Trough is comprised of a ca. 1000 m thick package of rocks (SACS, 1980).

Sedimentary units of the Zululand Group of ca. 130-60 Ma as well as ca. 135 Ma, post Karoo volcanic rocks of the Bumbeni Complex are encountered in NZA drill core. The basal pyroclastic rocks of the NZA drill core are part of the Fenda Formation belonging to the Bumbeni Complex. The volcano-sedimentary sequence of the NZA drill core thus encompasses rocks deposited between the Hauterivian and Maastrichtian ages. For the purposes of this study the siliciclastic sedimentary rocks of borehole NZA are classified according to the Zululand Group formations devised by Kennedy and Klinger (1975), because their study makes use of the most recent data from various studies of the area and provide less complicated subdivisions for the rock formations.

According to Watkeys (2002), the formation of the Zululand Basin is related to early disassembly of Gondwana at ca. 175-155 Ma, creating trans-tensional stresses of the continental crust and initiating rift basins along South Africa's east coast. Renewed dextral strike-slip movement along the Davie Fracture Zone resulted in separation of East Gondwana (Antarctica, Australia, Madagascar and India) from West Gondwana (Africa and South America) at ca. 160 Ma (Watkeys, 2002). Volcanism associated with the opening of the South Atlantic and separation of the Falkland Plateau subsequently formed, at ca. 133.5 Ma, a northeast-southwest trending continental rift with the Bumbeni Ridge being a volcanic centre on the northern side of the rift (Watkeys, 2002).

2.1 Pyroclastic rocks

The Bumbeni Ridge is a basement ridge ca. 14 km long by 5 km wide forming a palaeotopographic high with the upper portion consisting of 360 m thick pyroclastic rocks intruded by several sub-volcanic bodies. The Bumbeni Complex is comprised of the lower, ca. 150 m thick conglomeratic Msunduze Formation (Viljoen *at al.*, 2011) followed by the ca. 65 m thick amygdaloidal alkali basalts and trachyandesites of the Mpilo Formation (Viljoen *et*

al., 2011). The upper, terminating Fenda Formation is ca. 135 m thick and comprised of pyroclastic rocks (Viljoen *et al.*, 2011). The uppermost pyroclastic rocks, ca. 133 Ma (Allsopp *et al.,* 1984; Bristow, 1984) intersected in NZA drill core, belong to the Nxwala Member of the Fenda Formation and predate the Zululand Group sedimentary rocks in Table 1.

Table 1. Formations of the Zululand Group and Fenda Formation present in the NZA drill core highlighted in red (SACS, 1980 and written communication with Botha, 1992 after Watkeys *et al.,* 1993).

Era	Sub-Era	Period	Epoch	Group	Formation
Cenozoic	Quaternary	Pleistogene	Holocene	Maputaland	redistributed sand
					high dune sand
			Pleistocene		unconsolidated dune sand
					Port Durnford Formation
	Tertiary	Pliocene to Miocene	Early		calcarenite
			Late		*Pecten* Beds and Uloa Formation
Mesozoic		Cretaceous	Late	Zululand	St. Lucia Formation
			Early		Mzinene Formation
					Makatini Formation
					Bumbeni Complex
					Mpilo and Movene Formations
					Msunduze Formation
		Jurassic	Middle	Lebombo	Jozini Formation

2.2 Siliciclastic rocks

The proto-Indian Ocean opened from the north at ca. 190-160 Ma along a rift on the eastern edge of the Mozambique Basin (Tankard *et al.,* 1982) forming a shallow, pericontinental sea on the continental margin of southeast Africa and only fully developed by 130 Ma when transgression reached the Zululand Basin commencing sedimentation in the Barremian (Kennedy and Klinger, 1972). Rifting, uplift and concomitant north-south tensional faulting tilted topographically high fault blocks eastwards, causing eroded sediment to accumulate in the low lying Zululand Basin (Dingle and Scrutton, 1974; Tankard *et al.,* 1982). The origin of the sediments and volcanics comprising the Zululand Group is important because chemistry and mineralogy of detritus influence the porosity, chemistry and mineralogy of the rocks. The Zululand Group formations are typically thin onshore, but thicken out in their offshore component of the Zululand Basin in Figure 1. Typical of passive margins described by Johnson and Baldwin (1996), the Zululand Basin is hinged on the landward side and thus developed seaward thickening deposits fed by major continental drainage systems.

The lithofacies of the sedimentary rocks in the NZA drill core investigated in this thesis are similar to the units described in the literature, except rock units of each formation are thinner due to sedimentation upon the Bumbeni Complex palaeohigh. In general the Zululand Group formations in Table 1 are described as follows:

The oldest, Makatini Formation, Barremian to Aptian, ca. 125-115 Ma, rests above the Bumbeni Complex and attains a maximum thickness of ca. 80 m. Its deposition occurred during the Barremian transgression linked to drifting of East Gondwana from West Gondwana (Dingle and Scrutton, 1974). According to Tankard *et al.* (1982), the Makatini Formation lithofacies include conglomerates, sandstones and siltstones formed by progradation of braided fluvial deposits into a shallow sea. The uppermost termination of the Makatini Formation is described by McMillian (2003) as a pinkish terrestrial limestone.

The Mzinene Formation, ca. 120-95 Ma, was deposited during the following transgression, unconformably on the Makatini Formation as well as directly overlying the Lebombo Group in some areas (Kennedy and Klinger, 1975; Shone, 2006). The Mzinene Formation is made up of glauconitic siltstones and fossil rich sandstone units attaining a maximum thickness of ca. 642 m (Shone, 2006), terminating due to a repeated regional regression (Kennedy and Klinger, 1975).

The St Lucia Formation was deposited during renewed transgression spanning the Coniacian to Maastrichtian, ca. 90-65 Ma, attaining a maximum thickness of ca. 876 m. It is strikingly similar to the Mzinene Formation (Kennedy and Klinger, 1975; Shone, 2006), and was deposited under similar, transgressive conditions as the Mzinene Formation. A disconformity extending shorewards to an unconformity separates both formations and is difficult to recognise in distal, basinwards facies.

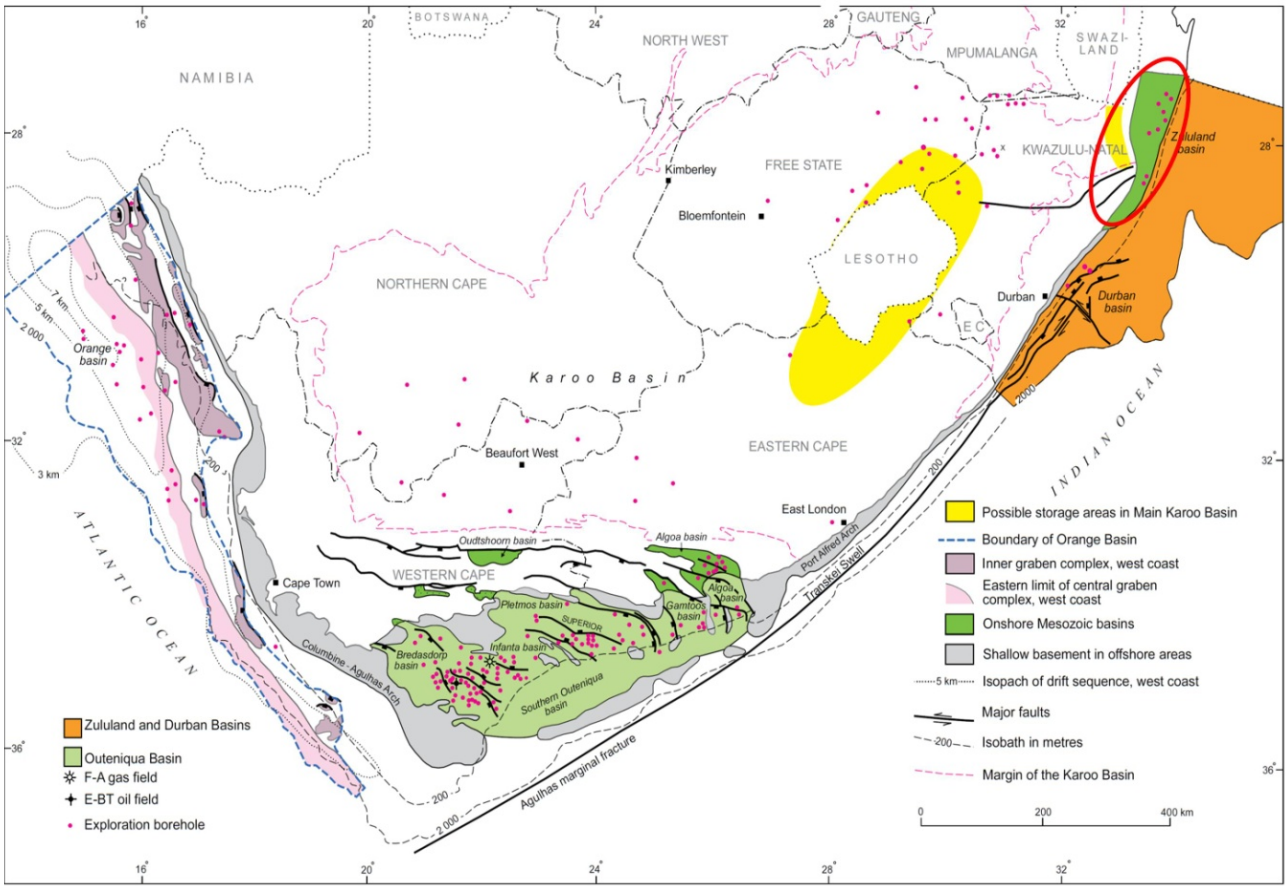

Figure 1. **Map of Mesozoic basins along South Africa's coast with the onshore Zululand Basin circled in red after Van Vuuren *et al.* (1998) in Viljoen *et al.* (2010).**

3. Materials and methods

Ten boreholes were drilled between 1967 and 1968 by the South African Exploration Corporation (SOEKOR) in the Zululand Basin (McLachlan and McMillan, 1979). Thereafter, exploration by SOEKOR was abandoned because the boreholes yielded insignificant quantities of oil and natural gas. The drill cores NZA, ZA, ZB and ZC in Figure 2 were donated to the CGS and stored in the National Core Library, in Donkerhoek, Pretoria, for almost five decades. After the Zululand Basin was chosen in 2010 as one of the possible sites for experimental CO_2 storage new interest arose in the old cores. The core trays for borehole NZA were laid out and logged in detail for the purpose of the project in Figure 3. The following paragraphs describe the procedures carried out at the National Core Library as well as at the University of Pretoria as part of the investigations that led to the herein presented thesis.

3.1 Geological core logging

Due to storage conditions the drill core was weathered and extremely dusty. Meticulous, repeated washing of the drill core with water removed detectable surface debris and dirt obscuring visual study. Changes in lithology were documented at a centimetre and decimetre scale, starting from the base of the drill core and logging to shallower depths. Rocks of interest for the purpose of CO_2 storage are porous sandstones that can serve as potential reservoir rocks and impermeable shales that can act as a potential caprock. Such rocks were given special attention during the core logging procedure.

The thickness's of different lithologies with sedimentary structures were noted to construct the detailed borehole log in Figure 5. The NZA borehole log was designed plotting the data into a *Strater* software package with the intent of providing a straightforward representation of NZA rock units. Using this borehole log, correlation between other onshore Zululand Basin drill cores can provide information on lateral extent and thickness of suitable rock units with adjacent boreholes, which were investigated by my fellow students in different MSc and BSc Honours projects. The compiled borehole log was also used for deciding where samples should be taken for the study.

The NZA drill core was logged from base depth ca. 571 m to the surface with forty samples taken at changes in lithology to gain a representative sample population of the rock units present in the core. Sampling as many lithologies as possible is important to account for the effects of grain size, petrologic evolution and sediment maturation (Roser and Korsch, 1986). During core logging the primary sedimentary structures, grain sizes, fossil content and textures present in the NZA drill core were described from hand specimens in Table 2.

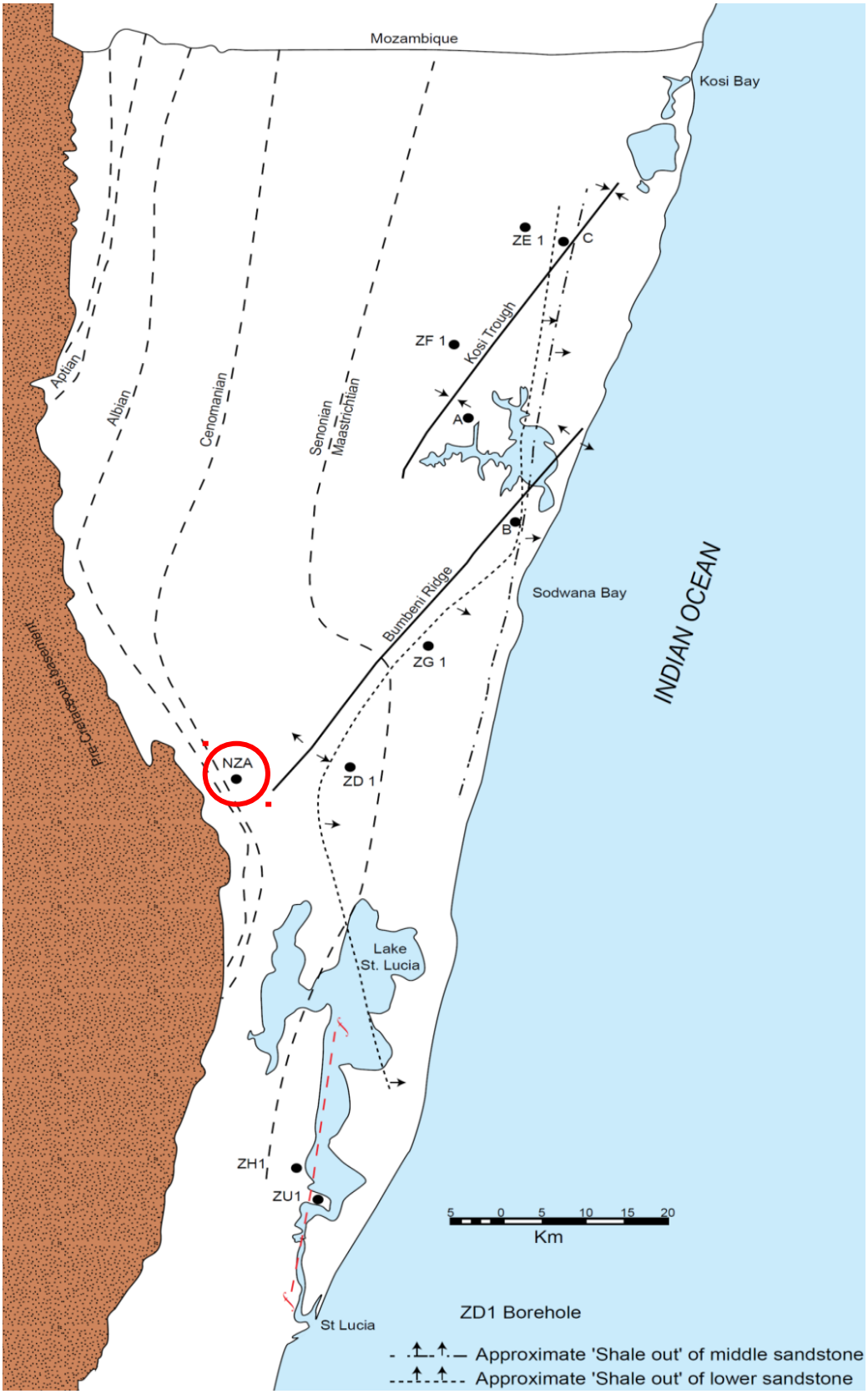

Figure 2. **Map of the onshore Zululand Basin indicating positions of the ten exploration boreholes drilled by SOEKOR with borehole NZA circled in red (Viljoen *et al.*, 2010).**

Figure 3. The National Core Library seen with core trays of various Zululand Basin boreholes investigated by my fellow students in different MSc and BSc Honours projects.

3.2 Lithofacies analysis

Forty samples taken from the NZA drill core were studied in thin section using a Leica polarising light microscope to identify changes in lithofacies of the NZA drill core. Petrographic study aided in accurately compiling NZA's borehole log, and gaining insights into mineral components. Petrographic observations were the main source of reliable information as initial hand specimen descriptions, are confined to broad, general classification of grain sizes and features such as colour or friability of the rocks (Pettijohn *et al.,* 1972).

Descriptions of the sedimentary structures, grain size, mineralogy and fossil content during petrographic study were used to designate the lithofacies of the NZA drill core. Similarities in the identified features contributed to assigning lithofacies associations that were overlooked in hand specimens during core logging. In this way fine-grained sandstones and medium-grained sandstones comprising predominant calcite cement were grouped as calcareous sandstone lithofacies. The sandstone packages were of interest during this study, and assessed for their suitability as a reservoir rock for injected CO_2. Fine-grained sandstones comprising predominantly clay matrix hosting immature, poorly sorted lithoclasts were grouped as greywacke lithofacies. Due to their high clay content, and impermeable nature, the greywackes are assessed for their suitability as a caprock. The carbonate-rich rocks include coquina limestone and beachrock lithofacies. Pyroclastic lithofacies were identified according to size and proportion of volcanic components and include lapilli-stone, lapilli-tuff, tuff-breccia and tuff consistent with classification by Bristow (1984).

3.3 Chemical bulk rock analysis

XRD analysis identified mineralogical composition of usually unidentifiable minerals during petrographic studies, and thus aided in consolidating the understanding of mineralogical variation among the rocks samples taken from the NZA drill core. Ensuring accurate and reliable analyses required milling of samples to a ca. 75 µm powder. A customised single unit swing mill and tungsten carbide milling pot were used to mill samples at the University of Pretoria. Samples were then analysed at the Stoneman X-Ray facility, Department of Geology, University of Pretoria.

The analytical techniques used to provide bulk rock composition include major element analysis by XRD analysis in Table 7 and XRF analysis in Table 8. Major element results are not only used to interpret the chemistry of the rock samples but were also utilised in discrimination plots to geochemically classify sandstones in Figure 21 and Figure 22 and geochemically elucidate their tectonic setting in Figure 23 and Figure 24. Furthermore, major element results were used to ascertain the degree of chemical alteration of the NZA sandstone lithofacies in Figure 25 and Figure 26 and determine the chemistry of the pyroclastic rocks in Figure 27.

3.3.1 XRD analysis preparation

XRD analysis performed at the University of Pretoria's Stoneman X-Ray facility provided mineralogical composition results for each sample, proving invaluable in distinguishing and identifying mineralogical composition in Table 7. After representative sampling, crushing each sample and using a riffle splitter, each sample was ground to ca. <75 µm powder in a tungsten carbide vessel and prepared according to the standardized PANalytical back loading system, which provides nearly random distribution of the milled powder. Samples were analyzed using a PANalytical X'Pert Pro powder diffractometer in θ–θ configuration with an X'Celerator detector and variable divergence and fixed receiving slits with Fe-filtered Co-Kα radiation (λ=1.789Å). The mineral phases were identified using X'Pert Highscore plus software. The relative phase amounts in wt-% were estimated using the Rietveld method (Autoquan Program).

Limitations of XRD analysis include poor reproducibility when compared to XRF and microscopy of the sample because the exact part analysed by each method differs from the aliquot used for the thin section. For this reason, minerals seen in the thin section might not feature in the XRD results. This problem can be overcome by using a more homogenous sample. Furthermore, amorphous and very fine-grained clays constituting matrix of the NZA calcareous sandstones are not easily detected by XRD because the detection limit for XRD is relatively low. Thus, microscopy and spectral imaging provided the main source of reliable mineralogical information; especially very fine-grained clay minerals which cannot be differentiated by microscopy.

3.3.2 XRF analysis preparation

Glass disks were prepared by fusing 1 g roasted sample and 10 g flux consisting of 49.5% $Li_2B_4O_7$, 49.5 % $LiBO_2$ and 0.50 % LiI at 1150 °C. Quality assurance was done by

using an in-house amphibolite reference material (sample 12/76). Samples were mixed with PVA binder and pressed in an Al cup at 10 t. The Thermo Fisher ARL Perform'X Sequential XRF with OXSAS software was used for analyses after Loubser and Verryn (2008).

3.4 Spectral imaging

The *GeoSpectral Imaging* technique provides a wealth of continuous spectral information across the NZA drill core. The sisuMobi mobile spectrometer unit in Figure 4 captured images of individual NZA core trays providing spectral, mineralogical and chemical characteristics of the drill core (Harris, 2012). The system uses a RGB camera and two spectrometers covering the visible and near-infrared (VNIR) and short-wave infrared (SWIR) wavelength region from 400-2500 nm. The RGB camera is a three channel system capturing images of the drill core in the red (620-750 nm), green (495-570 nm) and blue (450-495 nm) wavelength (Harris, 2012). These RGB images provide a base image for control and geometric adjustment of the spectrometer information with a direct link to the spectral data of the drill core (Harris, 2012).

The SWIR (1.0-2.5 µm) cameras capture the spectral characteristics from the core's surface by reflectance spectroscopy. These spectral characteristics result from the chemical and mineralogical composition of the rocks. Rocks and minerals show unique spectral information due to the fingerprint interaction of the incoming light (electromagnetic energy) with the minerals under investigation. These interactions depend on the individual behaviour of bonding of electrons and molecules in the materials. Spectral imaging technology in the wavelength field from 0.4-2.5 µm can detect iron minerals, hydroxyl and carbonate groups thus identifying goethite versus haematite, carbonates and clay minerals (Harris, 2012). Clay mineral identification in this project is especially important for ascertaining chemistry and the mineralogy of potential caprock lithology.

Data sheets of the imaged core include geological coordinates, depth information and spectral information in digital format (Harris, 2012). These data allow further analysis via specific spectral processing software, *IntelliCore*, to locate and identify specific mineral associations in Figure 16. Spectral imaging is a powerful tool because of its passive and non-destructive nature while providing continuous *in situ* chemical and mineralogical characterisation at high spatial and spectral resolution. Data extracted from the spectral image data include element abundance results, similar to XRF as well as mineralogical composition results, similar to XRD. Chemical and mineralogical data are presented as depth interval data providing count values throughout the core. The chemical and mineralogical information extracted from the spectral database can be superimposed on the RGB images of each core tray in Figure 17 to gain a visualisation of the distribution of detected mineralogical compositions across the length of the core.

Distinct disadvantages of the spectral imaging include the lack of 3D analysis, because this method only measures the reflectance from the drill core surface. In addition, dust residue as well as any moisture present on the surface of the core even after cleaning and washing can potentially contribute to misleading results. Furthermore, the intensity of the signal detected by the scanner is not uniform across the cylindrical drill core and needs to be corrected. As the field of reflectance spectrometry develops, the use of long-wave infrared (LWIR) (7-13 µm) will account for detection of pyroxenes, feldspars, silica and sulphates which are currently not directly detectable using only the SWIR spectrum.

Figure 4. **The sisuMobi device scanning and imaging a core tray in the National Core Library in Donkerhoek, Pretoria.**

4. Results

This chapter presents the results acquired from geological core logging, lithofacies analysis from petrographic study, spectral imaging and chemical bulk rock analysis. The similarities and differences of the techniques are detailed towards the end of this chapter in section 4.5.

4.1 Geological core logging results

The basal pyroclastic rocks of the NZA drill core at ca. 571-521 m depth grade upward from well sorted, upward fining tuff lithofacies to poorly sorted structureless lapilli-stone, tuff-breccia and lapilli-tuff. A single cream coloured tuff bed, ca. 30 cm thick forms a sharp contact with several ash flow deposits of ca. 12 m thickness each. The thicker, poorly sorted ash flow deposits comprise lapilli-sized pumice, accidental rock fragments as well as larger blocks of pumice hosted in a fine-grained volcanic ash matrix. Several consecutive ash flow deposits were observed in the NZA drill core. Each unit varies in colour, ranging from cream coloured, greyish-black to pinkish coloured units. The total thickness of the pyroclastic rocks is ca. 50 m for the NZA drill core.

Overlying the pyroclastic rocks are siliciclastic and carbonate lithofacies exhibiting an upward fining character. Two thin, ca. 2 m thick, cream coloured medium-grained sandstones display indistinct cross-laminae at ca. 514 m depth and grade into overlying, ca. 30 m thick brown, poorly bedded and massive fine-grained sandstones. Breaks in the monotonous brown, fine-grained sandstone lithofacies of the NZA drill core include thin ca. 1 m thick beachrock at depths of ca. 486m and 341 m. A coquina limestone, ca. 4 m thick, at ca. 340 m depth directly overlies a beachrock. The recrystallised beachrocks are massive, indurated horizons in the drill core exhibiting a brownish appearance. The coquina limestone has a reddish colour and comprises well sorted bivalve fossils and lesser gastropod fossils ca. 30 mm in diameter coated in reddish clay and cemented in calcite. Furthermore, thin, ca. 30 cm dark brown greywacke horizons occur intercalated with fine-grained calcareous sandstone and are entirely devoid of fossil fragments. The NZA drill core thus comprises predominantly fine-grained calcareous sandstone lithofacies with interbedded carbonate lithofacies underlain by pyroclastic rocks.

Table 2. Core logging sheet including sample depths and depth interval descriptions.

Sample ID	Depth		Sample length (m)	Description
	From (m)	To (m)		
	0.00	22.86		Missing
	22.86	31.39		Disaggregated, dark brown, fossiliferous, massive fine-grained calcareous sandstone.
N1	31.39	31.55	0.15	Brownish-grey, bioturbated, massive fine-grained calcareous sandstone unit, with black organic matter, large thin shelled bivalve fossils and small chips of plant fossils.
	31.55	35.33		Brownish, massive, fine-grained calcareous sandstone with clusters of invertebrate fossils intercalated with indurated horizons of calcareous sandstone.
N2	35.33	35.48	0.15	Brownish-grey, bioturbated, massive, fine-grained calcareous sandstone with clusters of thin and thick shelled bivalve fossils, black organic matter and large plant fossils and indistinct bedding
	35.48	38.71		Brownish, massive, fine-grained calcareous sandstone with clusters of invertebrate fossils intercalated with indurated horizons of calcareous sandstone.
N3	38.71	38.86	0.15	Light grey, indistinctly cross-bedded, bioturbated fine-grained calcareous sandstone unit with small intact gastropod and thin shelled bivalve fossils and black organic matter.
	38.86	56.31		Brownish, massive, fine-grained calcareous sandstone with clusters of invertebrate fossils and black organic matter.
N4	56.31	56.44	0.13	Greyish-brown poorly bedded, fine-grained calcareous sandstone with clusters of thin and thick shelled bivalves and gastropod fossils and traces of black organic matter.
	56.44	106.38		Brownish, massive, fine-grained calcareous sandstone with clusters of bivalve and gastropod fossils and thin indurated horizons devoid of plant, gastropod and bivalve fossils fragments.
	106.38	110.95		Highly weathered and disaggregated brownish fine-grained calcareous sandstone with small bivalve and gastropod fossils.
	110.95	116.69		Light brown, massive fine-grained calcareous sandstone with sparse invertebrate fossils and fossiliferous indurated horizons of calcareous sandstone.
N5	116.69	116.97	0.28	Brownish massive, fine-grained calcareous sandstone grading into light brown-grey, bioturbated, poorly bedded, fine-grained calcareous sandstone with heavily recrystallised bivalve fossils.
	116.97	118.11		Light brown-grey, massive fine-grained calcareous sandstone with sparse invertebrate fossils and indurated horizons of fossiliferous, calcareous sandstone.
N6	118.11	118.31	0.20	Light brown, fine-grained greywacke unit of porous and friable appearance, rare bivalve fossils with black organic matter.
	118.31	154.23		Light brown, massive fine-grained calcareous sandstone with sparse invertebrate fossils and indurated fossil rich horizon of calcareous sandstone.
	154.23	154.84		Thin, brownish, muddy fine-grained calcareous sandstone with no visible fossils.
	154.84	156.39		Light brown, massive, fine-grained calcareous sandstone with sparse invertebrate fossils and indurated fossiliferous, calcareous sandstone horizons.
N7	156.39	156.56	0.18	Brownish-grey, bioturbated, fine-grained calcareous sandstone with thin and thick shelled bivalve fossils, black organic matter and geopetal gastropod fossils.
	156.56	169.09		Brownish-grey, massive, fine-grained calcareous sandstone with sparse bivalve fossils and black organic matter.
N8	169.09	169.32	0.23	Brownish-grey, bioturbated poorly bedded fine-grained calcareous sandstone with sparse bivalve, gastropod and broken oyster shell fossils, grading into a dark brown muddy fossiliferous horizon.
	169.32	184.40		Brownish-grey, massive, fine-grained calcareous sandstone with sparse invertebrate fossils and indurated horizons.
N9	184.40	184.63	0.23	Brownish-grey, massive, fine-grained greywacke unit has a muddy appearance, few gastropod fossils and rich in black organic matter.
	184.63	184.86		Brownish-grey, massive, fine-grained calcareous sandstone with sparse invertebrate fossils, black organic matter and indurated horizons.
	184.86	185.93		Light brown, massive, bioturbated, fine-grained calcareous sandstone with sparse invertebrate fossils and traces of organic matter.
N10	185.93	186.08	0.15	Light brown, massive, bioturbated, fine-grained calcareous sandstone with black organic matter and limited thin shelled bivalve fossils.
	186.08	209.40		Light brown, massive, bioturbated fine-grained calcareous sandstone with sparse invertebrate fossils and black organic matter.
N11	209.40	209.55	0.15	Brownish-grey, massive, fine-grained calcareous sandstone with rare, thin shelled bivalve fossils, black laminae of organic matter and grading into dark brown muddy horizon with coarse sand grade quartz grains.
	209.55	210.01		Brown, thin, massive, fine-grained calcareous sandstone layer, no visible fossils.
	210.01	212.29		Brownish-grey, massive, fine-grained calcareous sandstone units intercalated with greyish calcareous sandstones and sparse invertebrate fossils.
	212.29	229.38		Dark brown to grey, massive, bioturbated fine-grained calcareous sandstone with isolated invertebrate fossil clusters and thin indurated calcareous sandstone horizons.
N12	229.38	229.53	0.15	Greyish-brown, massive, bioturbated fine-grained calcareous sandstone with isolated invertebrate fossil clusters grading into darker, organic-rich horizon with muddy appearance and coarse sand grade grains of quartz.
	229.53	230.12		Greyish-brown massive, fine-grained calcareous sandstone with isolated invertebrate fossil clusters and thin calcareous sandstone horizons.
N13	230.12	230.30	0.18	Dark brown-grey, thin, fine-grained greywacke, no visible fossils, traces of black organic matter and small plant fossils, the core has a porous and friable surface appearance with indistinct bedding.
	230.30	231.04		Dark brown-grey, massive fine-grained calcareous sandstone with isolated invertebrate fossil clusters and isolated calcareous sandstone horizons.
	231.04	237.31		Dark brown-grey, massive fine-grained calcareous sandstone with isolated invertebrate fossil clusters and isolated calcareous sandstone horizons.
N14	237.31	237.46	0.15	Greyish-brown massive fine-grained calcareous sandstone with black organic matter, scattered coarse sand sized quartz, no fossil fragments except an upper recrystallised fossil layer.
	237.46	243.71		Greyish-brown massive fine-grained calcareous sandstone with isolated invertebrate fossil clusters and isolated calcareous sandstone horizons.
N15	243.71	244.09	0.38	Greyish-brown massive fine-grained calcareous sandstone rich in black organic matter, containing few thick shelled and thin shelled bivalve and oyster fragments and geopetal gastropods, rock is porous and friable.
	244.09	244.60		Dark brown-grey, muddy intercalation in massive fine-grained calcareous sandstone.
N16	244.60	244.88	0.28	Brownish-grey, porous, fine-grained calcareous sandstone with black organic matter and rare fossil fragments and coarse sand grade quartz.
	244.88	257.25		Brownish-grey, porous, fine-grained calcareous sandstone with black organic matter, coated in reddish mineral and rare fossil fragments and coarse sand grade quartz.
	257.25	267.87		Brownish-grey, porous, fine-grained calcareous sandstone with black organic matter, coated in reddish mineral and rare fossil fragments and coarse sand grade quartz.
N17	267.87	268.15	0.28	Brownish-grey, porous, fine-grained calcareous sandstone with black organic matter and rare fossil fragments.
	268.15	278.64		Brownish-grey, porous, fine-grained calcareous sandstone with black organic matter and rare fossil fragments.

Sample ID	From (m)	To (m)	Sample length (m)	Description
N18	278.64	278.84	0.20	Light brown-grey, indurated, organic rich fine-grained sandstone comprised of thin shelled bivalves with sparse plant fossil fragments. Muddy intercalations occur between indurated calcareous sandstone horizons.
	278.84	296.93		Greyish-brown, indurated, organic rich fine-grained calcareous sandstone with sparse plant fossil fragments.
N19	296.93	297.13	0.20	Brownish-grey, massive fine-grained calcareous sandstone, no visible calcareous fossils but abundant black organic matter.
	297.13	298.37		Brownish-grey, massive fine-grained calcareous sandstone, no visible calcareous fossils but abundant black organic matter.
N20	298.37	298.60	0.23	Brownish-grey, poorly bedded fine-grained calcareous sandstone, no visible calcareous fossils but abundant black organic matter.
	298.60	299.41		Brownish-grey, poorly bedded fine-grained calcareous sandstone, no visible calcareous fossils but abundant black organic matter and small plant fossils coated in red mineral.
N21	299.41	299.64	0.23	Greyish-brown, poorly bedded fine-grained calcareous sandstone, rare fragments of thin shelled bivalves, abundant organic matter and small plant fossils coated in red mineral.
	299.64	324.48		Greyish-brown, massive fine-grained calcareous sandstone with muddy intercalations.
N22	324.48	324.74	0.25	Brownish-grey, massive, bioturbated, fine-grained calcareous sandstone with large, visible oyster fossils and large fragments of thick shelled bivalves, large chips of plant fossils and scattered black organic matter is coated in red mineral. The calcareous sandstone grades into a fine-grained muddy horizon devoid of fossils.
	324.74	325.22		Brownish-grey, massive fine-grained calcareous sandstone with large, visible oyster fossils.
	325.22	340.46		White and reddish, weathered coquina comprised of thin and thick shelled fragments of bivalves, gastropods, echinoderm spines and coarse sand clasts of quartz with visible glauconite.
N23	340.46	340.61	0.13	White and reddish, weathered coquina limestone comprised of thin shelled bivalves, gastropods and visible glauconite grains.
	340.61	341.07		Brownish, beachrock comprised of quartz grains and thin shelled bivalves.
N24	341.07	341.22	0.15	Greyish brown porous beachrock with scattered medium sand sized quartz grains, rare thin shelled bivalve fragments and glauconite. Rock grades into dark brown layer rich in quartz clasts and small fossils.
	341.68	367.89		Cream coloured, massive fine-grained calcareous sandstone interlayered with highly weathered calcareous sandstone.
	367.89	408.05		Highly weathered and disaggregated fine-grained calcareous sandstone with intact portions of calcareous sandstone.
N25	408.05	408.36	0.30	Brownish-grey, weathered, poorly bedded fine-grained calcareous sandstone with patches of organic matter and rare bivalve fossils.
	408.36	437.08		Brownish, indurated, massive fine-grained calcareous sandstone with rare bivalves and gastropod fossils.
	437.08	451.26		Brownish, weathered fine-grained calcareous sandstone with friable and porous intercalations.
N26	451.26	451.41	0.15	Greyish-brown, bioturbated, fine-grained calcareous sandstone, no visible fossils but abundant organic matter.
	451.41	455.12		Greyish-brown, bioturbated fine-grained calcareous sandstone, no visible fossils but abundant organic matter.
N27	455.12	455.27	0.15	Brown, massive, porous extremely weathered fine-grained calcareous sandstone with plant fossils and organic matter coated in reddish mineral.
	455.27	486.16		Brown, massive, porous extremely weathered fine-grained calcareous sandstone, rare shelly fossils but abundant organic matter and plant fossils coated in reddish mineral.
N28	486.16	486.41	0.25	Pinkish-reddish, beachrock with plant fossils, rare thin shelled bivalve fossils and indistinctly laminated organic material coated in reddish minerals.
	486.41	499.01		Light brown to grey, bioturbated, massive fine-grained calcareous sandstone comprised of poorly laminated organic matter coated in a reddish mineral with rare thin shelled bivalve fragments.
N29	499.01	499.44	0.43	Light brown to grey, bioturbated, massive fine-grained calcareous sandstone comprised of poorly laminated plant fossils coated in a reddish mineral with rare thin shelled bivalve fragments.
	499.44	500.18		Light brown to grey, fossiliferous, massive fine-grained calcareous sandstone.
N30	500.18	500.66	0.48	Light brown to grey, massive fine-grained calcareous sandstone with rare subrounded to rounded coarse-grained volcanic clasts, rare fragments of large thick shelled bivalves and poorly laminated plant fossils.
	500.66	513.23		Reddish, massive fine-grained calcareous sandstone with rare bivalve and gastropod fossils, and black organic matter.
N31	513.23	513.41	0.18	Greyish-brown, well sorted, medium-grained, indistinctly cross-laminated calcareous sandstone with traces of black organic matter.
	513.41	514.71		Greyish-brown, well sorted, medium-grained calcareous sandstone exhibiting indistinct cross-laminae and traces of black organic matter.
N32	514.71	514.96	0.25	Greyish-brown, well sorted, medium-grained calcareous sandstone exhibiting indistinct cross-laminae and traces of black organic matter.
	514.96	521.06		Grey-black volcanic rock displaying upward coarsening sequence of whitish medium-grained angular pumice.
N33	521.06	521.31	0.25	Grey-black volcanic rock displaying upward fining sequence of whitish medium-grained angular pumice.
	521.31	532.05		Poorly sorted, creamish-pink lapilli-tuff composed of lapilli-sized pumice and lithic fragments in weathered ash matrix of creamy colour.
N34	532.05	532.18	0.13	Poorly sorted, creamish-pink lapilli-tuff composed of lapilli-sized angular pumice and lithic fragments in weathered powdery ash matrix, creamy in colour.
	532.18	549.15		Poorly sorted, cream-pink lapilli-stone composed of lapilli-sized angular pumice and lithic fragments in weathered powdery ash matrix, creamy in colour.
N35	549.15	549.27	0.12	Poorly sorted, creamish-brown lapilli-stone composed of lapilli-sized angular pumice and lithic fragments in weathered powdery ash matrix, creamy and green in colour.
	549.27	553.06		Poorly sorted, creamish-brown lapilli-stone composed of lapilli-sized angular pumice and lithic fragments in weathered powdery ash matrix.
N36	553.06	553.29	0.23	Poorly sorted grey-black tuff-breccia comprised of angular blocks of pumice and accidental fragments hosted in fine-grained dark green-grey ash matrix.
	553.29	557.12		Poorly sorted, grey lapilli-stone composed of lapilli-sized angular pumice and lithic fragments in weathered matrix.
N37	557.12	557.35	0.23	Highly porous, poorly sorted, cream lapilli-stone composed of subrounded lapilli-sized pumice and lithic fragments in whitish ash matrix.
	557.35	562.89		Poorly sorted, cream lapilli-stone composed of subrounded lapilli-sized pumice and lithic fragments in a weathered ash matrix.
N38	562.89	563.07	0.18	Poorly sorted, cream-grey lapilli-stone composed of lapilli-sized pumice and lithic fragments in weathered whitish-greenish ash matrix.
	563.07	564.62		Poorly sorted, cream- grey lapilli-stone composed of lapilli-sized pumice and lithic fragments in weathered whitish-greenish ash matrix.
N39	564.62	564.79	0.18	Poorly sorted, cream lapilli-stone composed of lapilli-sized pumice and lithic fragments in weathered whitish-greenish ash matrix.
	564.79	571.09		Poorly sorted, cream lapilli-stone composed of lapilli-sized pumice and lithic fragments in weathered whitish-greenish ash matrix.
N40	571.09	571.20	0.10	Upward fining, cream coloured tuff displaying sharp contact between very fine and fine-grained ash.

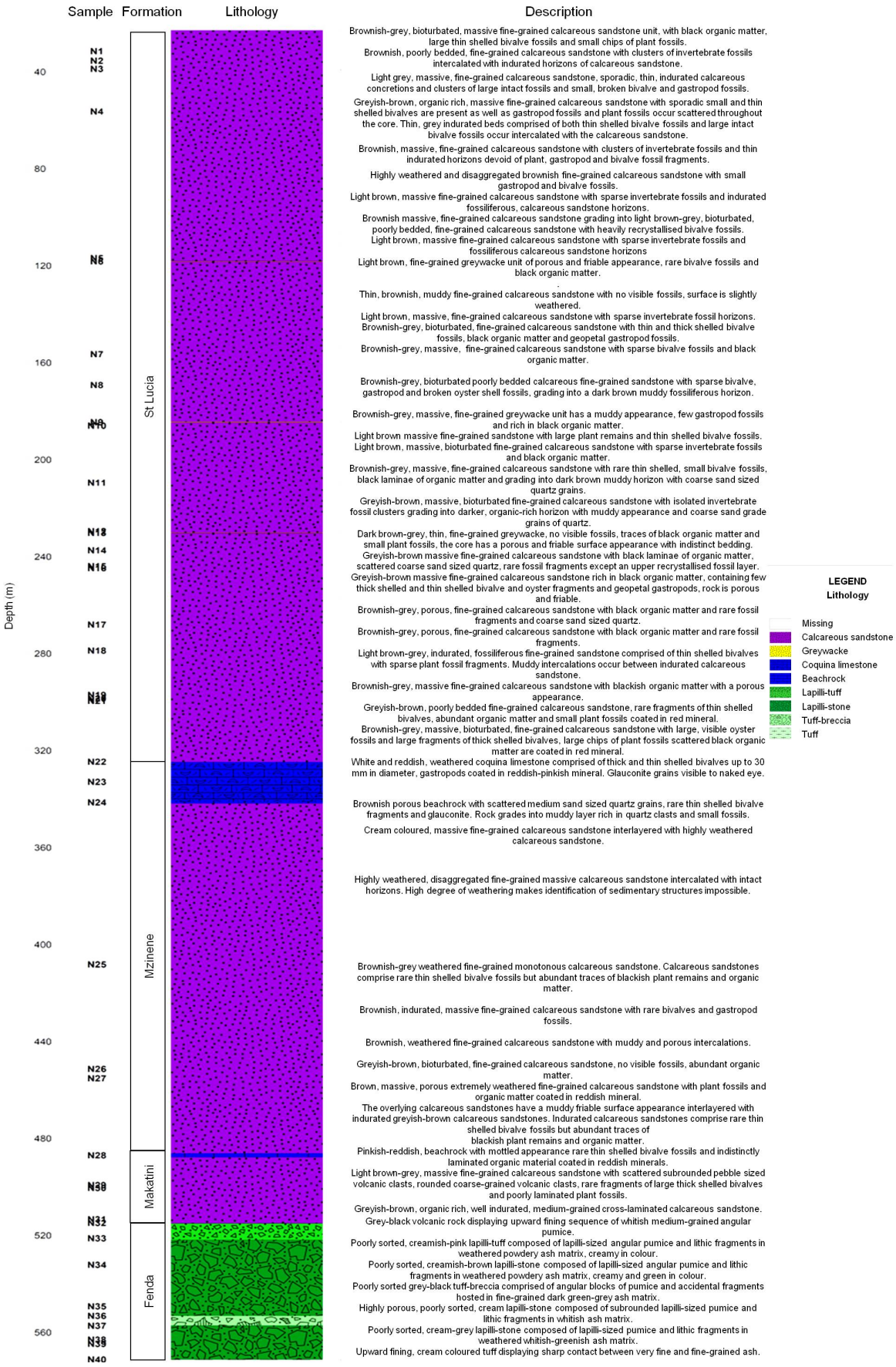

Figure 5. **Borehole log of the NZA drill core including sample depths, various rock formations and hand specimen descriptions.**

4.2 Lithofacies analysis results

Lithofacies of the NZA drill core were categorised based on observed sedimentary structures, grain size, mineralogy and biological features of the NZA drill core. The NZA drill core was divided into the following lithofacies: medium-grained calcareous sandstone, fine-grained calcareous sandstone, fine-grained greywacke, coquina limestone, beachrock, lapilli-stone, lapilli-tuff, tuff-breccia and tuff.

Among the lithofacies a series of upward fining trends, and breaks in the siliciclastic succession were identified in the NZA drill core. Medium-grained sandstones were overlain by fine-grained sandstones as well as coquina limestones and beachrock overlain by fine-grained sandstones. This upward fining trend is consistent with ongoing basin subsidence described by McMillian (2003) as well as ongoing increased sea-level due to basin subsidence later illustrated in Figure 35. Changes in depositional environments, observed in the NZA rocks, due to rising and falling sea-levels resulted in regressive and transgressive cycles consistent with those described by Kennedy and Klinger (1972) and McMillian (2003).

The medium-grained cross-laminated calcareous sandstones of the NZA drill core are well sorted and comprise rounded detritus, and indistinct cross-laminae consistent with reworking of shoreface facies. The fine-grained calcareous sandstones and fine-grained greywackes of the NZA drill core comprise poorly sorted compositionally immature detritus consistent with proximal sedimentation in offshore-transition zone facies and offshore zone facies. These lower energy facies are consistent with the inferred continental shelf environment for the deposition of sediments in the Zululand Basin. Coquina limestone lithofacies and beachrock lithofacies are indicative of foreshore facies, while pyroclastic lithofacies are consistent with ignimbrite facies composed predominantly of poorly sorted pumice and volcanic ash.

4.2.1 Calcareous sandstone lithofacies results

Calcareous sandstones are the dominant lithofacies of NZA drill core and were identified throughout all three formations of the Zululand Group. The samples include N1, N2, N3, N4, N5, N7, N8, N10, N11, N12, N14, N15, N16, N17, N18, N19, N20, N21, N22, N25, N26, N27, N29, N30, N31 and N32 in Table 3. The NZA calcareous sandstones comprise monocrystalline quartz grains, plagioclase grains, orthoclase grains, rare microcline grains, muscovite grains, invertebrate fossils, plant fossils, fine-grained siderite, traces of organic matter, glauconite grains as well as volcanic fragments cemented in prominent, sometimes poikilotopic fabric of carbonate cement. The sandstones are predominantly poorly to moderately sorted due to rapid erosion and sedimentation of detritus derived from the proximal Lebombo Mountain source. Furthermore, bioturbation and sporadic storm events contribute to the poorly sorted nature of the NZA calcareous sandstones. However, the medium-grained calcareous sandstones are well sorted, reflecting higher energy facies.

Table 3. Description of components and observations of calcareous sandstone lithofacies identified in the NZA drill core.

Sample ID	Depth		Lithofacies	Components	Observations
	From (m)	To (m)			
N1	31.39	31.55	Fine-grained calcareous sandstone	Subangular monocrystalline quartz (30%), angular plagioclase (10%), volcaniclastics (5%), plant fossils (10%), organic matter (10%), invertebrate fossils (5%), subrounded to rounded glauconite (<1%) and calcite cement (30%).	Poorly to moderately sorted, massive, fine-grained sandstone dominated by angular to subangular quartz and plagioclase grains ca. 0.1mm cemented in sparry calcite.
N2	35.33	35.48	Fine-grained calcareous sandstone	Subangular monocrystalline quartz (20%), angular plagioclase (5%), invertebrate fossils (15%), plant fossils (5%), organic matter (10%), siderite (5%), subrounded glauconite (10%) and calcite cement (30%).	Poorly to moderately sorted, massive, fine-grained sandstone comprised of angular to subangular quartz and feldspar grains ca. 0.1 mm and ca. 0.3mm invertebrate fossil cemented in sparry calcite. Authigenic glauconite indicates marine water typically shallower than 200 m.
N3	38.71	38.86	Fine-grained calcareous sandstone	Subangular monocrystalline quartz (30%), angular to subrounded plagioclase (10%), subrounded orthoclase (5%), invertebrate fossils (20%), volcaniclastics (5%), subrounded glauconite (5%) and calcite cement (25%).	Poorly to moderately sorted, massive, fine-grained sandstone comprised of angular to subangular quartz and feldspar grains as well as ca. 0.1 mm and ca. 0.3mm invertebrate fossils cemented in sparry calcite. Authigenic glauconite indicates marine water typically shallower than 200 m.
N4	56.31	56.44	Fine-grained calcareous sandstone	Subangular monocrystalline quartz (25%), angular plagioclase (10%), invertebrate fossils (25%), plant fossils (5%), organic matter (10%), subrounded glauconite (5%) and calcite cement (20%),	Poorly to moderately sorted massive, fine-grained sandstone comprised of angular to subangular quartz and feldspar grains as well as ca. 0.1 mm and ca. 0.3mm invertebrate fossils cemented in sparry calcite.
N5	116.69	116.97	Fine-grained calcareous sandstone	Subangular monocrystalline quartz (25%), angular plagioclase (10%), invertebrate fossils (10%), organic matter (10%), smectite (7%), volcanic fragments (5%), rounded glauconite (2%) and calcite cement (30%).	Poorly to moderately sorted, massive, fine-grained sandstone dominated by angular to subangular grains of quartz and feldspar cemented in sparry calcite. Authigenic glauconite indicates marine water typically shallower than 200 m.
N7	156.39	156.56	Fine-grained glauconitic calcareous sandstone	Angular monocrystalline quartz (25%), subangular plagioclase (10%), invertebrate fossils (10%), plant fossils (5%), organic matter (5%), orthoclase (5%), subrounded glauconite (10%) clay matrix (10%) and calcite cement (20%).	Moderately sorted massive fine-grained glauconitic sandstone comprised of subangular to angular detritus cemented in sparry calcite. Authigenic glauconite indicates marine water typically shallower than 200 m.
N8	169.09	169.32	Fine-grained glauconitic calcareous sandstone	Angular monocrystalline quartz (20%), subangular plagioclase (10%), invertebrate fossils (15%), organic matter (5%), angular orthoclase (5%), subrounded glauconite (10%), smectite matrix (10%) and calcite cement (25%).	Moderately sorted massive, fine-grained sandstone comprised of subangular to angular ca. 0.1 mm detritus cemented in sparry calcite. Authigenic glauconite indicates marine water typically shallower than 200 m.
N10	203.40	203.63	Fine-grained glauconitic calcareous sandstone	Angular monocrystalline quartz (15%), angular plagioclase (10%), volcanic fragments (5%), invertebrate fossils (10%), plant fossils (5%), organic matter (5%), subrounded glauconite (10%), siderite infilling fossils (10%) and calcite cement (30%).	Moderately sorted fine-grained sandstone comprised of subangular to angular, ca. 0.1 mm detritus cemented in sparry calcite. Authigenic glauconite indicates marine water typically shallower than 200 m.

Table 3 cont.

Sample ID	Depth		Lithofacies	Components	Observations
	From (m)	To (m)			
N11	209.40	209.55	Fine-grained glauconitic calcareous sandstone	Angular monocrystalline quartz (15%), angular plagioclase (15%), invertebrate fossils (5%), plant fossils (5%), organic matter (10%), subrounded glauconite (10%), siderite infilling fossils and matrix (10%) and calcite cement (30%).	Poorly sorted fine-grained glauconitic sandstone comprised of subangular to angular, ca. 0.1 mm detritus cemented in sparry calcite. Authigenic glauconite indicates marine water typically shallower than 200 m.
N12	229.38	229.53	Fine-grained glauconitic calcareous sandstone	Subrounded monocrystalline quartz (20%), tabular plagioclase (10%), invertebrate fossils (5%), organic matter (5%), plant fossils (5%), subrounded glauconite (20%), siderite (5%) and calcite cement (30%).	Moderately sorted fine-grained glauconitic sandstone comprised of subangular to angular, ca. 0.1 mm detritus cemented in sparry calcite. Authigenic glauconite indicates marine water typically shallower than 200 m.
N14	237.31	237.46	Fine-grained glauconitic calcareous sandstone	Subangular monocrystalline quartz (15%), angular and euhedral plagioclase (10%), subangular orthoclase (5%), muscovite (2%), invertebrate fossils (10%), plant fossils (3%), weathered angular volcaniclastics (5%), subrounded glauconite (20%) and calcite cement (30%).	Moderately sorted fine-grained glauconitic sandstone comprised of subangular to angular, ca. 0.1 mm detritus cemented in sparry calcite. Authigenic glauconite indicates marine water typically shallower than 200 m.
N15	243.71	244.09	Fine-grained glauconitic calcareous sandstone	Subrounded monocrystalline quartz (20%), angular plagioclase (7%), plant fossils (3%), organic matter (20%), invertebrate fossils (10%), subrounded glauconite (15%), siderite (5%) and calcite cement (20%),	Moderately sorted fine-grained glauconitic sandstone comprised of subangular to angular ca. 0.1 mm grains cemented in sparry calcite. Authigenic glauconite indicates marine water typically shallower than 200 m.
N16	244.60	244.88	Fine-grained glauconitic calcareous sandstone	Subangular quartz (20%), angular plagioclase (10%), plant fossils (5%), invertebrate fossils (10%), organic matter (15%), subrounded glauconite (10%), fine-grained siderite (10%) and calcite cement (20%).	Moderately sorted fine-grained glauconitic sandstone comprised of subangular to angular ca. 0.1 mm grains cemented in sparry calcite. Authigenic glauconite indicates marine water typically shallower than 200 m.
N17	267.87	268.15	Fine-grained calcareous sandstone	Subangular monocrystalline quartz (20%), angular plagioclase (10%), orthoclase (5%), plant fossils (10%), organic matter (10%) invertebrate fossils (10%), siderite (10%), rounded glauconite (5%) and calcite cement (20%).	Moderately sorted fine-grained sandstone comprised of subangular to angular ca. 0.1 mm grains cemented in sparry calcite. Authigenic glauconite indicates marine water typically shallower than 200 m.
N18	278.64	278.84	Fine-grained calcareous sandstone	Angular monocrystalline quartz (15%), subangular plagioclase (10%), invertebrate fossils (10%), organic matter (25%), fine-grained siderite (10%) and subrounded glauconite (5%) and calcite cement (25%).	Moderately sorted fine-grained sandstone comprised of subangular to angular ca. 0.1 mm grains cemented in sparry calcite. Authigenic glauconite indicates marine water typically shallower than 200 m.
N19	296.93	297.13	Fine-grained glauconitic calcareous sandstone	Subangular monocrystalline quartz (20%), rounded and tabular plagioclase (15%), invertebrate fossils (10%), plant fossils (5%), organic matter (10%), siderite (10%), subrounded glauconite (15%) and calcite cement (15%).	Moderately sorted fine-grained, massive, glauconitic sandstone comprised of subangular to angular ca. 0.1 mm grains cemented in sparry calcite. Authigenic glauconite indicates marine water typically shallower than 200 m.
N20	298.37	298.60	Fine-grained glauconitic calcareous sandstone	Subrounded monocrystalline quartz (15%), rounded and tabular plagioclase (15%), plant fossils (10%), organic matter (15%), volcanic clasts (5%), siderite (10%), subrounded glauconite (10%) and calcite cement (20%).	Moderately sorted fine-grained, massive, glauconitic sandstone comprised of subangular to angular ca. 0.1 mm grains cemented in sparry calcite. Authigenic glauconite indicates marine water typically shallower than 200 m.

Table 3 cont.

Sample ID	Depth		Lithofacies	Components	Observations
	From (m)	To (m)			
N21	299.41	299.64	Fine-grained calcareous sandstone	Angular to subrounded monocrystalline quartz (20%), angular plagioclase (20%), rounded orthoclase (5%), plant fossils (10%), organic matter (15 %), rounded glauconite (5%) and siderite (10%) and calcite cement (15%).	Moderately sorted fine-grained massive sandstone comprised of subangular to angular ca. 0.1 mm grains cemented in sparry calcite. Authigenic glauconite indicates marine water typically shallower than 200 m.
N22	324.48	324.74	Fine-grained glauconitic calcareous sandstone	Subangular monocrystalline quartz (20%), angular plagioclase (10%), subrounded orthoclase (5%), invertebrate fossils (5%), organic matter (20%), subrounded glauconite (10%) and siderite coating organic matter (10%) and calcite cement (20%).	Moderately sorted sandstone comprised of subangular to angular ca. 0.1 mm grains cemented in sparry calcite. Authigenic glauconite indicates marine water typically shallower than 200 m.
N25	408.05	408.36	Fine-grained calcareous sandstone	Subrounded monocrystalline quartz (30%), subrounded plagioclase (10%), subrounded orthoclase (5%), volcanic clasts (10%), invertebrate fossils (5%), organic matter (10%), subrounded glauconite (5%) and calcite cement (25%).	Moderately sorted fine-grained, massive sandstone comprised of subangular to angular ca. 0.1 mm grains cemented in sparry calcite. Authigenic glauconite indicates marine water typically shallower than 200 m.
N26	451.26	451.41	Fine-grained glauconitic calcareous sandstone	Subrounded monocrystalline quartz (20%), subangular plagioclase (10%), subrounded orthoclase (5%), volcanic clasts (5%), organic matter (10%), smectite matrix (5%), subrounded glauconite (10%) and calcite cement (35%).	Poorly to moderately sorted, massive, fine-grained glauconitic sandstone comprised of subangular to angular plagioclase and monocrystalline quartz of ca. 0.1 mm cemented in sparry calcite. Glauconite grains and volcanic clasts are highly weathered.
N27	455.12	455.27	Fine-grained calcareous sandstone	Subangular monocrystalline quartz (25%), angular plagioclase (20%), tabular muscovite (5%), plant fossils (5%), invertebrate fossils (5%), organic matter (20%), subrounded glauconite (5%) and calcite cement (15%).	Moderately sorted fine-grained, massive sandstone comprised of subangular to angular ca. 0.1 mm grains cemented in sparry calcite. Authigenic glauconite indicates marine water typically shallower than 200 m.
N29	499.01	499.44	Fine-grained calcareous sandstone	Subangular monocrystalline quartz (30%), angular and tabular plagioclase (10%), plant fossils (5%), organic matter (5%), invertebrate fossils (10%), subrounded glauconite (5%), siderite coating (5%) and calcite cement (30%).	Poorly sorted, massive fine-grained sandstone comprised of subangular to angular ca. 0.1 mm grains cemented in sparry calcite. Authigenic glauconite indicates marine water typically shallower than 200 m.
N30	500.18	500.66	Fine-grained calcareous sandstone	Subangular to subrounded monocrystalline quartz (20%), subangular plagioclase (10%), volcanic fragments (15%), plant fossils (5%), organic matter (10%), invertebrate fossils (5%), subrounded glauconite (1%), siderite coating (4%) and calcite cement (30%).	Poorly sorted, massive sandstone comprised of subangular to angular grains ca. 0.1 mm cemented in sparry calcite.
N31	513.23	513.41	Medium-grained calcareous sandstone	Subrounded monocrystalline quartz (30%), subrounded plagioclase (25%), volcanic fragments (15%), plant fossils (4%), subrounded orthoclase (5%), subrounded glauconite (1%), and calcite cement (20%).	Well sorted medium-grained sandstone faintly exhibiting low angle cross-laminae dominated by subrounded to rounded quartz and plagioclase hosted in calcite cement.
N32	514.71	514.96	Medium-grained calcareous sandstone	Subrounded monocrystalline quartz (30%), subrounded plagioclase (25%), plant fossils (4%), volcanic fragments (15%), subrounded orthoclase (5%), subrounded glauconite (1%), and calcite cement (20%).	Well sorted medium-grained sandstone exhibiting indistinct low angle cross-laminae dominated by subrounded to rounded monocrystalline quartz and plagioclase hosted in calcite cement.

Detritus of the calcareous sandstones are predominantly, massive to indistinctly bedded, fine-grained in Figure 7 to rarely medium-grained and indistinctly cross-laminated in Figure 6. Detritus is commonly subrounded to subangular implying varied bedload transport or short transport distance. Generally, the sandstones are structurally immature with input of proximal volcanic sources contributing volcanic clasts larger than fine-grained siliciclastic detritus. Medium grade sand detritus and less resistant detritus are commonly rounded.

Sedimentary structures are not clearly discernible in the NZA sandstones because of the poor preservation state of the core. The fine-grained sandstones appear typically massive due to pervasive bioturbation, caused by activity of several invertebrates preserved in the drill core, as well as rare, indistinct bedding. The medium-grained sandstones at ca. 521 m depth possess indistinct cross-laminae in Figure 6c identified by orientation of siliciclastic components. Medium-grained, cross-laminated sandstones are consistent with shoreface facies typically developed in shallow water ca. 50-100 m depth (Blatt, 1980) below the fair weather wave base (Nichols, 2009). Indistinct cross-laminations in the sandstones indicate directional flow of sediment prior to sedimentation consistent with the subtidal zone during which ocean currents distributed sediment. Increased water depth during Barremian transgression of the Indian Ocean is consistent with later deposited fine-grained sandstones forming in water deeper than 200 m (Blatt, 1980; Nichols, 2009) consistent with offshore-transition zone and offshore zone facies on the continental shelf (Nichols, 2009). The transition between medium-grained sandstones, shoreface facies, and fine-grained sandstones, offshore transition zone facies, are inferred to indicate increased sea-level consistent with Albian basin subsidence identified by McMillian (2003).

Clastic components identified by petrographic study include subangular, ca. 0.1-0.2 mm monocrystalline quartz grains consistent with suspension and saltation transport whereas subrounded ca. 0.3-0.5 mm monocrystalline quartz grains are consistent with saltation transport creating more rounded detritus. Subangular to subrounded polycrystalline quartz grains ca. 0.2 mm in diameter occur rarely throughout the calcareous sandstones of NZA, indicating a low metamorphic origin (Basu *et al.,* 1975). Slight undulose extinction observed in monocrystalline quartz grains also indicates a low metamorphic origin, most likely attributed to overburden of thick volcanic deposits of the Lebombo Mountains.

Subangular ca. 0.1 mm plagioclase grains and larger, 0.2-0.4 mm subrounded orthoclase grains and microcline grains were identified whereby the former are prominent in NZA calcareous sandstones. Plagioclase grains are identified by multiple lamellar twinning, whereas microcline grains were identified by unmistakable cross-hatched twinning. The survival of rounded microcline grains, transported by saltation, and lesser suspension implies proximal sedimentation, and derivation from an igneous source rock. The variation of feldspar mineral species, mostly plagioclase and K-feldspar, is consistent with eroded mafic to silicic rocks of the Lebombo Mountains.

Invertebrate fossils include bivalves, gastropods and echinoid spines from 0.3-30 mm size. Bivalves and gastropod shells are well preserved, unless obliterated by diagenesis, indicating limited transport from where they once lived in shallow marine water. Fragments of echinoid spines, oysters and fossil sponges are attributed to sporadic storm events depositing detritus in distal environments (Flügel, 2004), of the onshore Zululand Basin continental shelf.

Detrital micas, such as muscovite, occur rarely in sandstones of NZA. Typically sourced from granites these minerals have lower settling velocity and are typically associated with silt and sand sized plagioclase and quartz detritus (Pettijohn *et al.,* 1972). Clay sized minerals include Al-smectite and Mg-smectite, hosted in glauconite, derived from weathered mica grains and feldspar grains (Hillier, 1995). Less common clay minerals of the NZA calcareous sandstones include fine-grained illite and chlorite, identified by XRD analysis, derived from unstable volcanic minerals comprising varying abundances of matrix in NZA calcareous sandstones. Most weathered clay minerals however form part of the glauconite grains observed throughout siliciclastic rocks of the NZA drill core.

Plant fossils occur throughout the NZA drill core sandstones. The plant fossils often contain infilling of diagenetic chalcedony and calcite preserving their internal structure. Kennedy and Klinger (1972) and Tankard *et al.* (1982), observed logs of ca. 6 m occurring in rock units of the Zululand Group. However, for NZA drill core, only small ca. 0.2-20 mm plant remains were observed. Preservation of plant fossils is strongly linked to pervasive reducing conditions (Reineck and Singh, 1980) which inhibit decomposition of organic material, also consistent with the presence of glauconite in the NZA calcareous sandstones. Plant chips are tabular in form and deposited in lowest energy state indicating horizontal plane of deposition. Randomly oriented, poorly preserved organic material is also observed throughout the thin sections.

The common occurrence of authigenic glauconite observed in the NZA rock packages confirms slow, steady sedimentation rates in a developing shelf environment with oceanic current upwelling as well as prevailing reducing conditions in the onshore Zululand Basin. Sandstones of the NZA drill core are characterised by massive bedding, probably due to bioturbation of newly deposited sediments resulting in sediment mixing as well as destruction of pre-existing depositional structures by sporadic storm events (Reineck and Singh, 1980). Intraskeletal geopetal fillings of material similar to the surrounding sediment indicate slow sedimentation rates (Flügel, 2004) which are observed in a number of gastropod shells throughout NZA calcareous sandstones in Figure 7c. The subrounded to rounded nature of the glauconite grains is consistent with longshore movement along the shelf by waves, tides or storm events.

The majority of sandstones in the NZA drill core contain ca. 30 % of sparry ca. 20-50 µm diameter calcite cement. Calcite cement is prominent; up to two generations are identifiable in some rocks, typically leading to complete destruction of primary porosity. The prominence of sparry pore-filling calcite cement, often displaying a poikilotopic fabric, in NZA sandstones indicates rapid cementation and recrystallisation commonly associated with shallow, near surface burial diagenesis of porous sandstones (Flügel, 2004).

Several mechanisms of calcite cement formation can be offered for NZA calcareous sandstones; each may have occurred independently or together. Precipitation of calcite from $CaCO_3$ saturated marine pore water is favoured by increased pH and reducing conditions (Pettijohn *et al.,* 1972) from escape of CO_2 due to decomposition of organisms. The fossil rich sedimentary rocks encountered in the NZA drill core support such a diagenetic history. The dissolution of shell fragments by expelled pore water reprecipitating higher in the sedimentary sequence also offers another likely explanation for calcite cements and obliteration of some invertebrate fossils (Pettijohn *et al.,* 1972 and Flügel, 2004). According to Flügel (2004), formation of carbonate cement is rapid in the marine phreatic realm. Shallow, near surface burial diagenesis of originally highly porous and permeable sands created a poikilotopic fabric of calcite cement (Flügel, 2004).

Dolomite was detected sporadically, via XRD analysis, in NZA calcareous sandstones and formed by introduction of Mg^{2+} into the $CaCO_3$ crystal lattice during diagenesis. Mg^{2+} ions are likely introduced by surrounding Mg-smectite dissolved in pore waters and releasing Mg^{2+} ions. Small abundant nucleation sites afford an explanation for the lack of large dolomite crystals, but rather formation of pseudomorphic dolomite and sporadic dolomitisation of calcite (Tucker and Wright, 1990). Siderite occurs throughout the calcareous sandstones of the NZA drill core, mixed with clays and organic matter. The occurrence of fine-grained iron and hydrated Al-oxides in the presence of abundant organic matter evidence reducing conditions upon burial (Curtis *et al.,* 1975), invariably leading to formation of interstitial siderite and coatings of siderite on organic matter. Such conditions are also supported by the widespread occurrence of glauconite grains. These conditions are consistent with shallow marine and transitional environments (Curtis *et al.,* 1975), of the onshore Zululand Basin.

Medium-grained calcareous sandstone (N32)
514.71-514.96 m

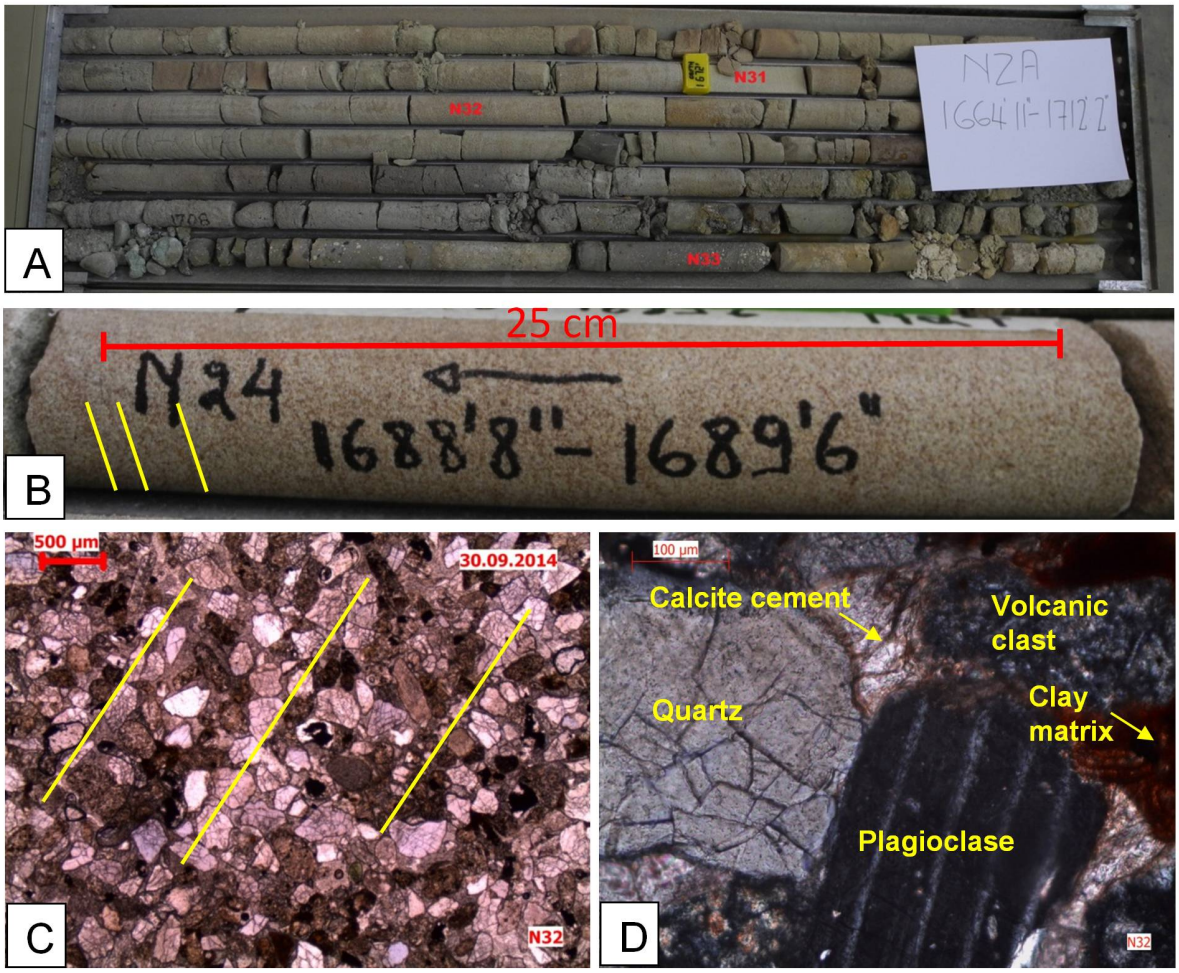

Figure 6. **Photographs, descriptions and observations of a medium-grained calcareous sandstone rock sample from the NZA drill core. (A) Core grades from older pyroclastic material into younger, greyish monotonous medium-grained calcareous sandstone. (B) Cream coloured, well sorted medium-grained sandstone displaying indistinct cross-laminae (yellow lines) comprising quartz grains cemented in calcite. (C) PPL photomicrograph showing cracked subrounded to rounded ca. 0.3 mm quartz grains and subrounded volcanic clasts hosted in calcite cement with poikilotopic fabric. Yellow lines indicate the indistinct cross-laminae. (D) XPL photomicrograph comprising subrounded, cracked monocrystalline quartz grain, weathered volcanic clasts and subangular, twinned plagioclase grains occurring in calcite cement with reddish clay matrix. Pore space is assumed to be greater along cross-laminae; however carbonate cements probably destroyed primary porosity resulting in estimates of low certainty of ca. 1 %.**

Fine-grained calcareous sandstone (N14)
237.31-237.46 m

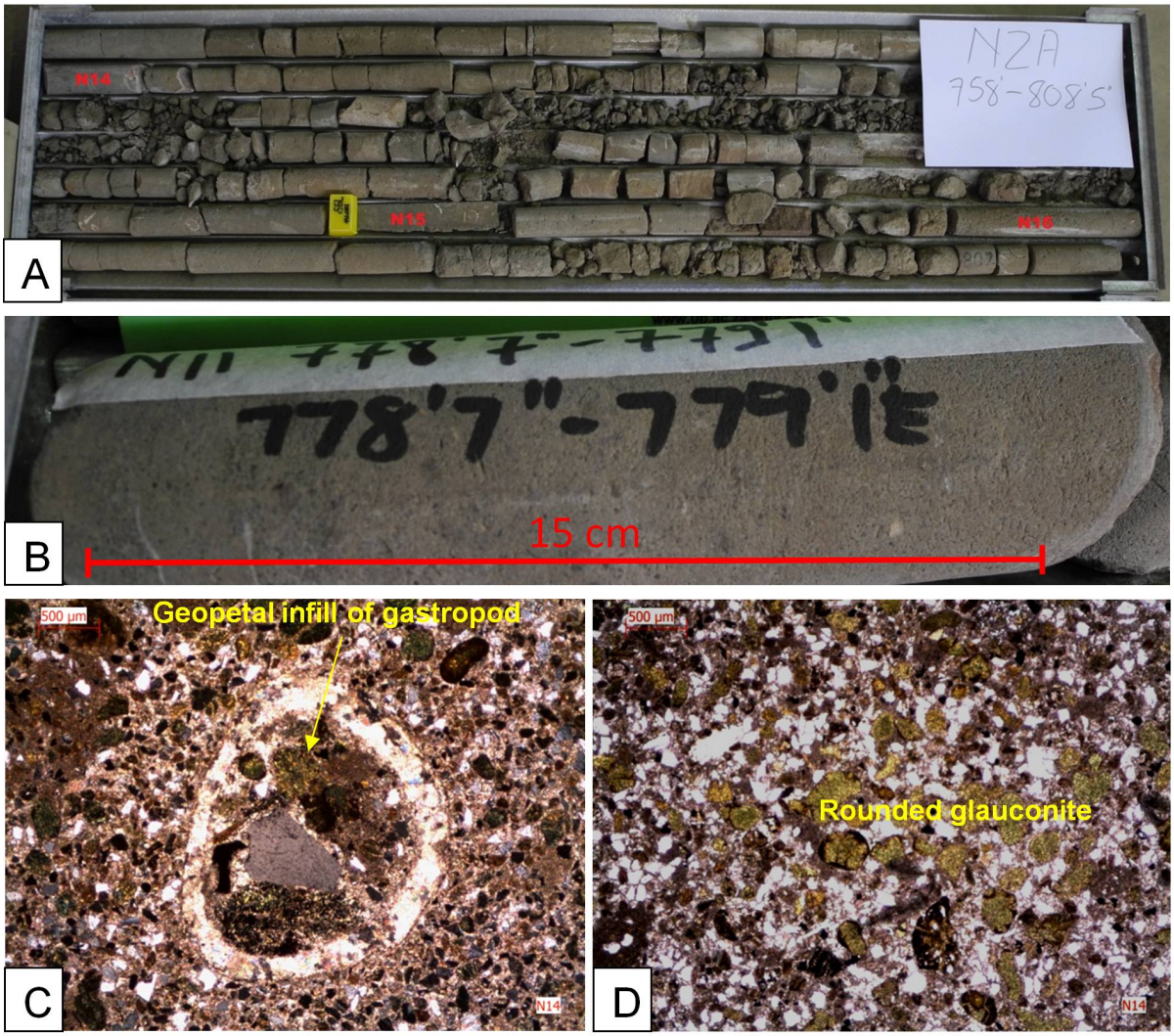

Figure 7. **Photographs, descriptions and observations of a fine-grained calcareous sandstone rock sample from the NZA drill core. (A) Grey, fine-grained calcareous sandstone is darker in colour compared to brown calcareous sandstones. (B) Thin shelled, horizontally deposited fossil fragments are visible in the drill core. (C) XPL photomicrograph of geopetal infill of an invertebrate skeleton, probably a gastropod, comprising distinctive subrounded ca. 0.5 mm monocrystalline quartz grain, smaller subrounded monocrystalline quartz grains, subrounded glauconite and calcite cement. Infill is similar to surrounding material. (D) XPL photomicrograph of subrounded to angular ca. 0.1 mm monocrystalline quartz grains hosted in brownish calcite cement with large subrounded slightly oxidised glauconite and brown organic material. Rock porosity estimates are ca. 2 % but cannot be made with a high degree of certainty because of well distributed calcite cement**

4.2.2 Greywacke lithofacies results

Table 4. Description of components and observations of greywacke lithofacies identified in the NZA drill core.

Sample ID	Depth		Lithofacies	Components	Observations
	From (m)	To (m)			
N6	118.11	118.31	Fine-grained greywacke	Angular monocrystalline quartz (25%), angular plagioclase (20%), plant fossils (5%), invertebrate fossils (5%), organic matter (10%), calcite cement (1%), subrounded glauconite (4%) and smectite matrix (30%)	Poorly sorted greywackes dominated by angular quartz and plagioclase hosted in a matrix of smectite. Authigenic glauconite indicates marine water typically shallower than 200 m.
N9	184.62	184.77	Fine-grained glauconitic greywacke	Angular to subrounded monocrystalline quartz (20 %), angular plagioclase (10%), orthoclase (5%), volcaniclastics (5%), invertebrate fossils (5%), plant fossils (10%), organic matter (10%), clay matrix (25%), rounded glauconite (10%)	Poorly sorted greywackes dominated by angular quartz and plagioclase hosted in a matrix of smectite. Authigenic glauconite indicates marine water typically shallower than 200 m.
N13	230.27	230.44	Fine-grained glauconitic greywacke	Subrounded monocrystalline quartz (25%), angular plagioclase (10%), subrounded orthoclase (5%), plant fossils (10%), organic matter (10%) smectite matrix (30%) and subrounded glauconite (10%).	Poorly sorted greywackes dominated by angular quartz and plagioclase hosted in a matrix of smectite. Authigenic glauconite indicates marine water typically shallower than 200 m.

Sandstones constituting 15-75 % clay minerals as matrix hosting terrigenous material with an insignificant amount of carbonate cement are considered greywackes (Williams *et al.,* 1954; Pettijohn *et al.,* 1972). In the NZA drill core three thin, ca. 50 cm greywacke beds, N6, N9 and N13 were identified, intercalated with fine-grained calcareous sandstones, at ca. 118 m, 184 m and 230 m depths respectively. Other muddy horizons less than ca. 5 cm were observed and are thought to have formed under similar conditions to the above mentioned greywackes. The greywacke beds constitute similar components to calcareous sandstones recognised under the microscope; however calcite cement is poorly developed and clay matrix comprises Mg-smectite and other unidentified clay minerals. The poorly sorted components include subangular to subrounded monocrystalline quartz grains, ca. 0.1-0.2 mm in diameter, angular twinned plagioclase grains, ca. 0.2 mm and lesser subrounded, ca. 0.2 mm orthoclase grains hosted in smectite matrix.

Invertebrate fossil fragments of ca. 0.2 mm occur rarely and calcite cement is poorly developed in the NZA greywackes. Plant fossils occur sporadically and resemble small wood chips of ca. 0.2 mm length. Glauconite grains are present in varying abundances in the studied greywacke beds indicating input of a shallow marine environment. In general, greywackes are typically related to rapid deposition of compositionally immature sediment of mixed provenance, sourced from tectonically active regions and are deposited on shelf and slope areas by currents and turbidity currents (Pettijohn *et al.,* 1972). However, no graded bedding or other markers for turbulent deposition were observed in NZA greywackes.

Fine-grained greywacke (N9)184.62-184.77 m

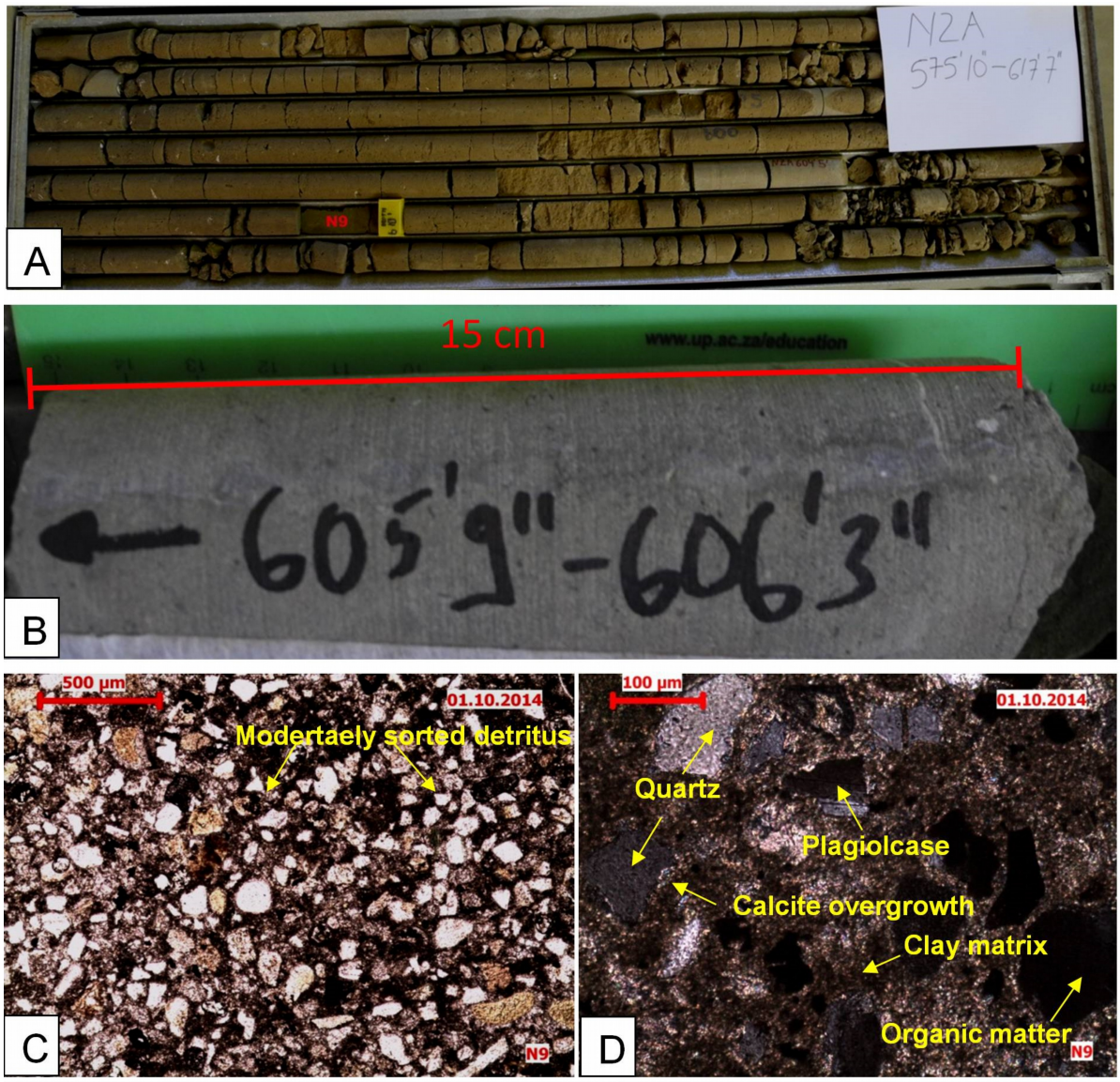

Figure 8. **Photographs, descriptions and observations of a fine-grained greywacke rock sample from the NZA drill core. (A) Light brown to grey coloured drill core identified as greywacke. (B) The rock is well indurated and has a greyish appearance compared to surrounding brown sandstones (C) PPL photomicrograph of poorly sorted, subangular to subrounded 0.2 mm diameter granular quartz grains and similarly sized angular plagioclase grains in a smectite matrix. Weathered limonitic, 0.3 mm fine-grained, yellowish glauconite grains occur sparsely in the matrix. (D) XPL photomicrograph of subangular monocrystalline quartz grains and subangular twinned plagioclase in a predominantly dark brown to black clay matrix with lesser calcite cement seen as faint whitish colour around detritus. Rock porosity could not be confidently estimated but is presumably below ca. 2% and permeability is very low because of well distributed smectite matrix.**

4.2.3 Coquina limestone and beachrock lithofacies results

Table 5. Description of components and observations of coquina limestone and beachrock lithofacies identified in the NZA drill core.

Sample ID	Depth		Lithofacies	Components	Observations
	From (m)	To (m)			
N23	362.46	362.61	Coquina limestone	Large bivalve fragments up to 30 mm (50%), gastropods (10%), echinoid spines (5%), subrounded monocrystalline quartz (5%), calcite cement (20%), smectite matrix (5%) and subrounded glauconite (5%).	Shell lag dominated by 30 mm bivalves and lesser gastropods and echinoid spines cemented in blocky calcite. Sparse glauconite indicates shallow water marine environment.
N24	363.07	363.22	Beachrock	Recrystallised calcite (60%), subrounded monocrystalline quartz (5%), subrounded orthoclase (2%), angular plagioclase (3%), invertebrate fossils (5%), goethite matrix (5%) and subrounded glauconite (20%).	Idiomorphic mosaic of ca. 0.2 mm recrystallised calcite accompanied by minor clay matrix. Glauconite indicates shallow marine environment with early diagenesis.
N28	486.16	487.68	Beachrock	Recrystallised calcite (50%), subrounded monocrystalline quartz (5%), subrounded orthoclase (2%), angular plagioclase (3%), invertebrate fossils (10%), plant fossils (5%), organic matter (5%), siderite coating (10%) and subrounded glauconite (10%).	Idiomorphic mosaic of ca. 0.2 mm recrystallised calcite accompanied by minor clay matrix. Glauconite indicates shallow marine environment with early diagenesis.

Limestone encompasses rocks comprising 50 % and more $CaCO_3$ material (Folk, 1959; Pettijohn *et al.,* 1972). Thus, the carbonate-rich fossiliferous rock, N23, is designated a coquina limestone and the siliciclastic rocks with considerable recrystallised calcite are designated beachrocks. These lithofacies are inferred to indicate changes in the depositional history of the onshore Zululand Basin related to fluctuations in sea level.

The N24 and N28 rocks from NZA drill core comprise an idiotropic fabric of interlocking, equigranular, ca. 0.2 mm calcite crystals in Figure 10d, subrounded volcanic fragments, subangular quartz grains, subrounded feldspar grains, shelly fossil fragments, minor clay matrix, haematite and rounded, 0.3 mm glauconite grains. These rocks are interpreted as beachrock and mark the inferred terminations of both the Makatini Formation at ca. 486 m depth and the Mzinene Formation at ca. 328 m depth. Beachrock comprise beach material bonded by rapidly precipitated carbonate cements, forming seaward dipping rocks along tropical coastlines (Vousdoukas *et al.,* 2007). The original sediment probably resembled a calcarenite prior to rapid crystallisation of calcite crystals. However, the extent of calcite recrystallisation is significant, thus ascertaining the provenance of the sediments is difficult. Although beachrocks rarely provide an accurate indication of sea-level changes these beachrocks are inferred to have formed due to rapid facies changes attributed to strongly decreasing sea-level, as discussed in section 6.2.

Close to 328 m depth of the NZA borehole a ca. 15 m thick coquina limestone, N23, comprised predominantly of moderately sorted ca. 30 mm long bivalve and gastropod shells and echinoid spines, Figure 9d, and directly overlies the N24 beachrock in Figure 10. The haematitic matrix of the coquina limestone indicates subaerial exposure or interaction of Fe-rich hydrothermal fluids with the thick shell lag. After submergence due to increased sea-level, deposition of glauconite occurred and cementation of blocky calcite in pore space

bound invertebrate fragments in Figure 9c. This subaerial exposure is linked to widespread Cenomanian marine regression experienced across the Zululand Basin as described by (McMillian, 2003), and represents the top of the Mzinene Formation in the NZA borehole.

Coquina limestone (N23)
340.46-340.61 m

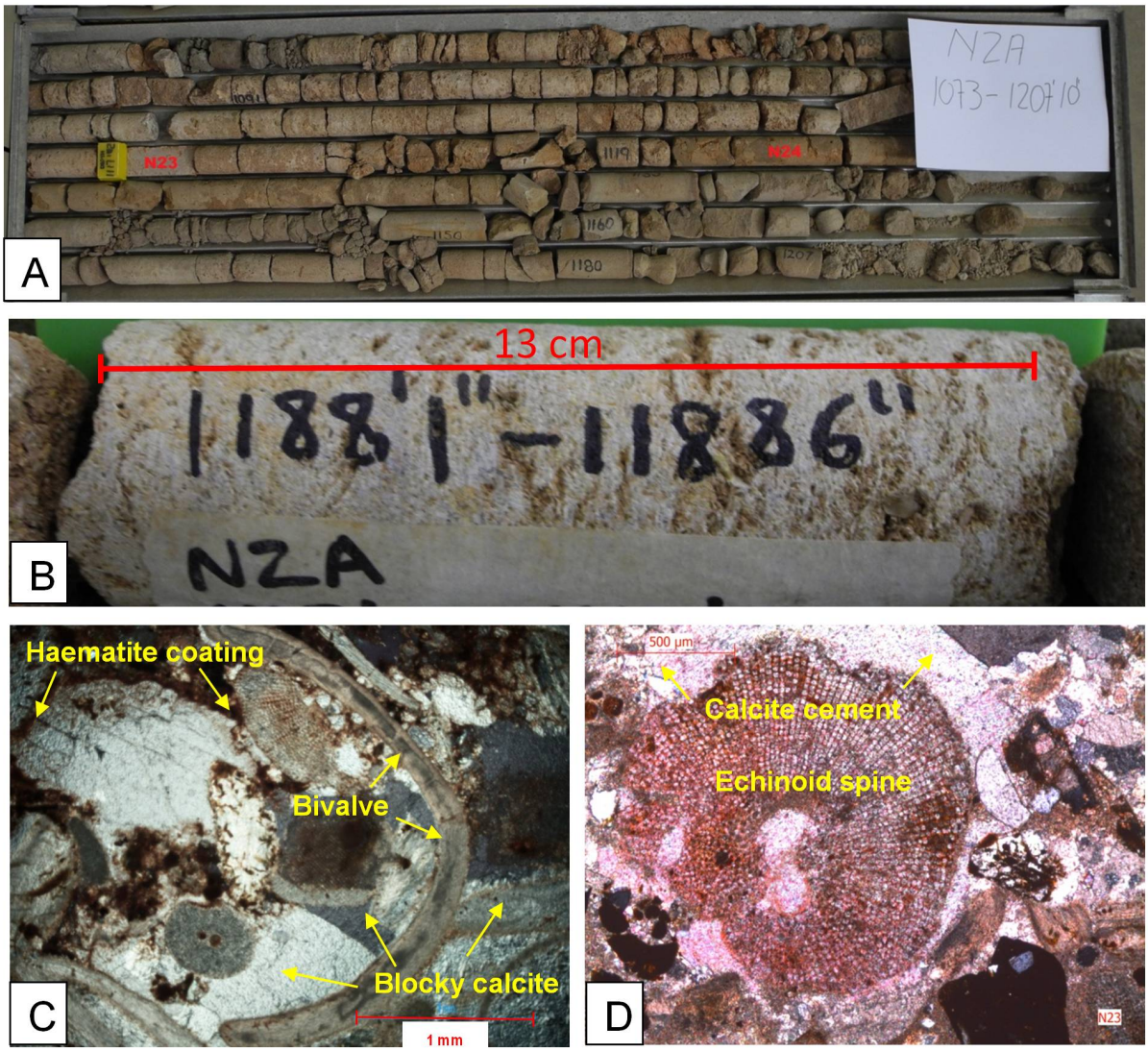

Figure 9. **Photographs, descriptions and observations of a coquina limestone rock sample from the NZA drill core. (A) Weathered, fissile, whitish to reddish coquina limestone ca. 8 m thick, rich in bivalve fossils. (B) Invertebrate fossils are visible and coated in reddish haematite. (C) XPL photomicrograph of a well preserved bivalve fragment and crinoid fragment coated in haematite and cemented in blocky calcite. The matrix comprises smectite, glauconite and very fine-grained quartz. (D) XPL photomicrograph of a recrystallised echinoid spine filled with haematite and bound in calcite cement. Rock porosity of the coquina is estimated to be low, ca. less that 1 % because of pervasive calcite cement.**

Beachrock (N24)
341.07-341.22 m

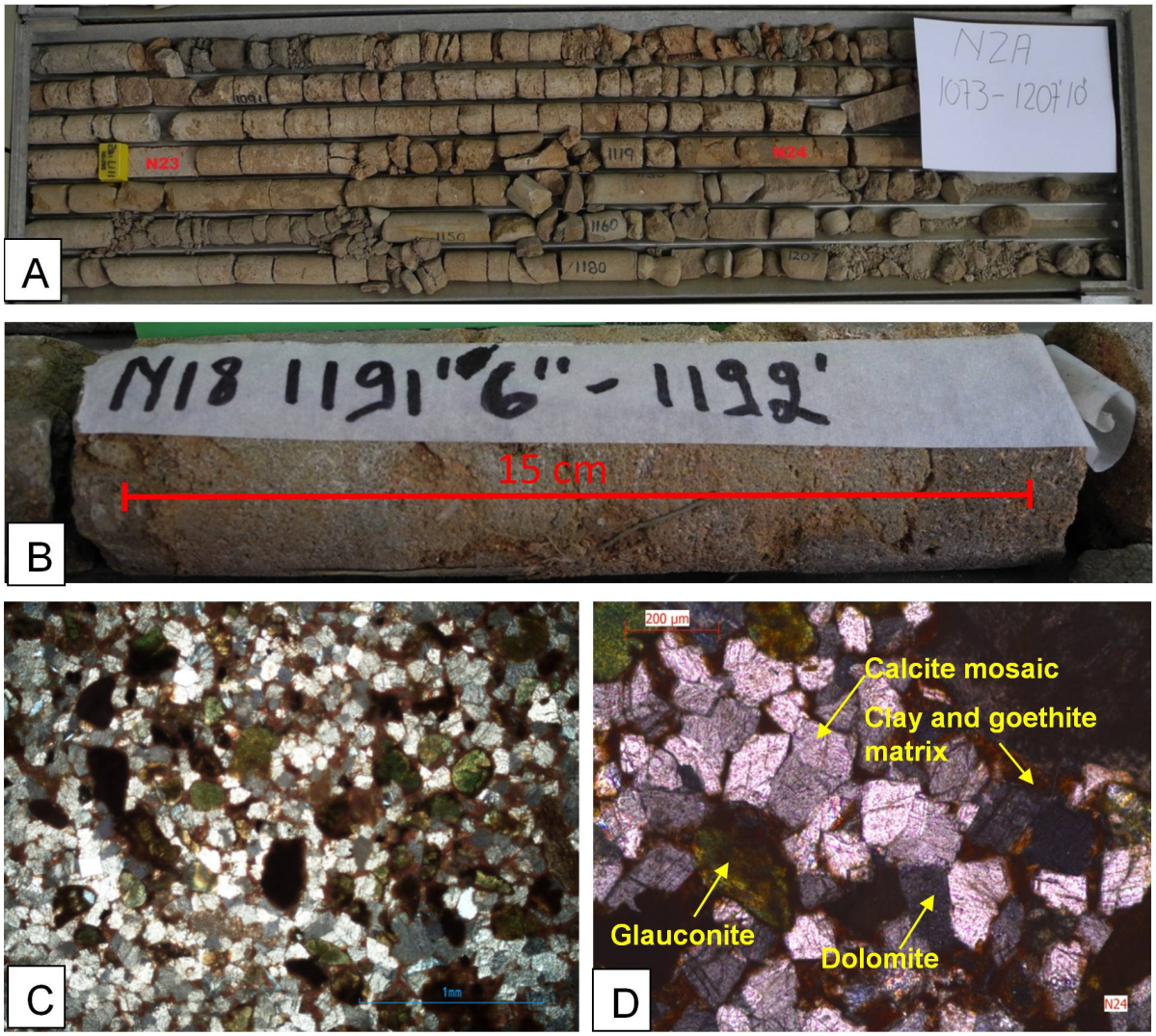

Figure 10. **Photographs, descriptions and observations of a beachrock rock sample from the NZA drill core. (A) The beachrock is ca. 1 m thick and has a brownish-grey weathered appearance. (B) No macroscopic fossils are visible and the rock comprises interlocking carbonate grains surrounded by reddish smectite and presumably goethite. (C) XPL photomicrograph of 0.3 mm, green, rounded glauconite grains present in reddish smectite and goethite matrix supporting an idiomorphic mosaic of calcite and dolomitised calcite grains. (D) XPL photomicrograph of mosaic framework of white and grey, 0.15 mm diameter cracked calcite and dolomite crystallites surrounded by brown matrix and dispersed glauconite grains. Porosity is not visible in this rock and probably below ca. 1 %.**

4.2.4 Pyroclastic lithofacies results

Table 6. Description of components and observations of pyroclastic lithofacies identified in the NZA drill core.

Sample ID	Depth		Lithofacies	Components	Observations
	From (m)	To (m)			
N33	521.06	521.31	Lapilli-tuff	Lapilli size fragments of pumice and accidental fragments (50%), medium sand size quartz (20%) and ash matrix (30%)	Poorly sorted lapilli grade pumice and lithic fragments hosted in extremely fine-grained matrix of zeolitised ash with a welded, darker appearance.
N34	532.05	532.18	Lapilli-tuff	Lapilli size fragments of pumice and accidental fragments (50%), medium sand size quartz (20%) and ash matrix (30%)	Poorly sorted, unwelded lapilli grade pumice and lithic fragments hosted in extremely fine-grained matrix of zeolitised ash.
N35	549.15	549.27	Lapilli-stone	Lapilli size pumice (20%), fine sand grade quartz and plagioclase grains (10%) and ash matrix (70%).	Poorly sorted, unwelded pumice and lithic fragments hosted in extremely fine-grained matrix of zeolitised ash.
N36	553.06	553.29	Tuff-breccia	Lapilli size pumice and block-sized lithic fragments (60%), fine sand size orthoclase and quartz clasts (10%) and ash matrix (30%)	Accidental blocks up to 80mm size as well as lapilli grade pumice are welded in fine-grained matrix of plagioclase needles and clay grade minerals.
N37	557.12	557.35	Lapilli-stone	Lapilli size pumice (30%), medium sand size quartz and orthoclase (<5%) and ash matrix (70%)	The rock constitutes poorly sorted, unwelded comprising lapilli-grade pumice and lithic fragments hosted in fine-grained zeolite ash.
N38	562.89	563.07	Lapilli-stone	Blocks of accessory fragments (20%), lapilli size pumice (30%), medium sand size quartz and orthoclase (10%) and ash matrix (40%)	The rock is dominated by unwelded lapilli sized pumice and few blocks of lithic fragments hosted in a fine-grained matrix of zeolitised ash.
N39	564.62	564.79	Lapilli-stone	Lapilli size pumice (30%), sand size quartz and plagioclase grains (10%) and ash matrix (60%)	The rock constitutes unwelded poorly sorted lapilli pumice and lithic fragments hosted in fine-grained zeolite ash.
N40	571.09	571.20	Tuff	Clay size plagioclase and quartz (20%), fine-grained organic material (5%) and creamish ash matrix (80%)	The rock comprises an upward fining sequence of ash to fine-lapilli sized zeolitised tuff.

The pyroclastic rocks of the NZA drill core can broadly be classified as “tuff” according to contemporary literature by McPhie *et al.* (1993) and Branney and Kokelaar (2002). However, no recent work has been done on these rocks and thus an older classification system is used in this study to remain consistent with Bristow (1984).

Lapilli-stone lithofacies were identified for N35, N37, N38, and N39, in Figure 11, at depths of ca. 549 m, 557 m, 562 m and 564 m respectively. Petrographic study of the lapilli-stones indicate the components are unwelded lapilli-sized fragments of ca. 25 mm angular pumice, ca. 20 mm angular lithic rock fragments and angular sand size grains such as quartz and plagioclase grains scattered in a fine-grained matrix of volcanic ash in Figure 14c and Figure 14d. Furthermore, angular and subrounded pumice fragments comprise inclusions of

plagioclase crystals and quartz crystals indicate overland flow of material produced by volatile rich eruptions as described in Bristow (1984).

Lapilli-tuff lithofacies were identified for samples N33 and N34, in Figure 11, at depths of ca. 521 m and 532 m respectively. Sample N33 however, is darker, presumably altered, and denser compared to sample N34. Petrographically, N33 and N34 are similar to each other, characterised by poorly sorted material. Angular lapilli-sized pumice and sand size quartz grains, orthoclase grains and plagioclase grains are scattered in fine-grained volcanic ash matrix in Figure 12c. Chalcedony and quartz grains typically occur in cavity filling as well as in veins developed in the lapilli-tuffs probably due to hydrothermal alteration.

Tuff-breccia lithofacies is identified for sample N36, in Figure 13 and comprises extremely dense and dark, altered rock compared to surrounding pyroclastic rocks. It is characterised by predominantly block sized lithic fragments ca. 70 mm in diameter and ca. 30 mm lapilli-sized pumice hosted in a matrix of fine-grained volcanic ash. Scattered in the matrix are sand size grains of ca. 0.3 mm subrounded orthoclase, 0.2 mm tabular plagioclase and 0.2 mm angular quartz. Veins developed in the tuff-breccia after deposition are filled with chalcedony, and surrounded by unidentified green minerals in Figure 13c and Figure 13d also formed by hydrothermal alteration.

Tuff lithofacies is identified for sample N40, in Figure 11, at a depth of ca. 570 m, comprising clay sized ash and displaying a contact of coarse and fine-grained ash layers within the sample. The well sorted, graded nature of the tuff is indicative of a distal airfall deposit. Petrographic study indicates that the sharp contact between the volcanic ash layers is disrupted, providing sufficient space for ca. 0.5 mm dolomite rhombs to form in Figure 15c.

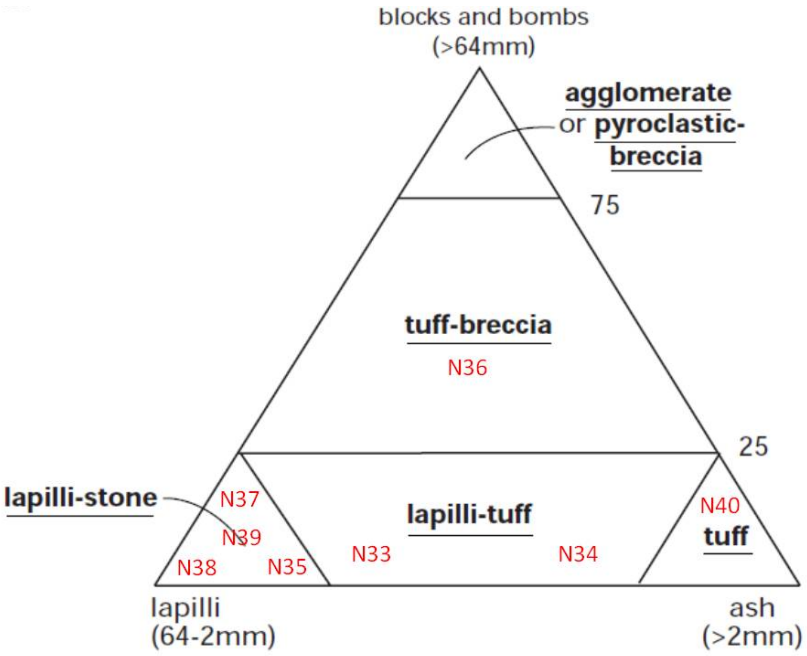

Figure 11. Classification of pyroclastic rocks of borehole NZA after (Fisher and Schminke, 1984) in (Gillespie and Styles, 1999) based on size and proportions of tephra.

Lapilli-tuff (N33)
521.06-521.31 m

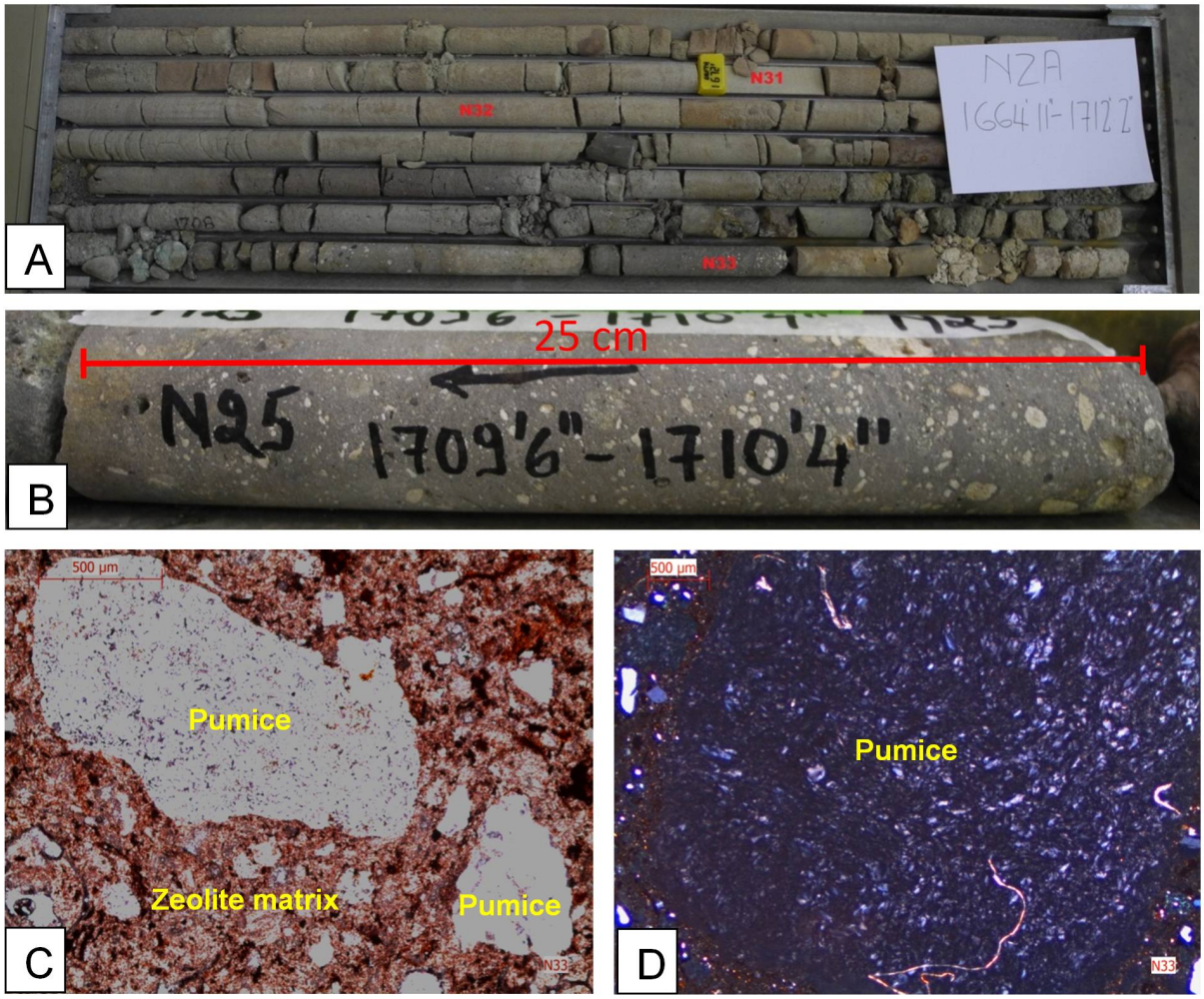

Figure 12. **Photographs, descriptions and observations of a lapilli-tuff rock sample from the NZA drill core. (A) The dark grey lapilli-tuff comprises lithoclasts, pumice and zeolite (B) Angular clasts of upward fining juvenile material and pumice hosted in a dark grey zeolite matrix of ash and clay minerals, presumably chlorite. (C) PPL photomicrograph of large ca. 15 mm in diameter lapilli-sized pumice in a matrix of smaller pumice, angular quartz crystals, orthoclase crystals and plagioclase crystals and volcanic ash. (D) XPL photomicrograph of a ca. 35 mm large pumice fragment with visible infilling of minute vesicles with an unknown white mineral.**

Tuff-breccia (N36)
553.06-553.29 m

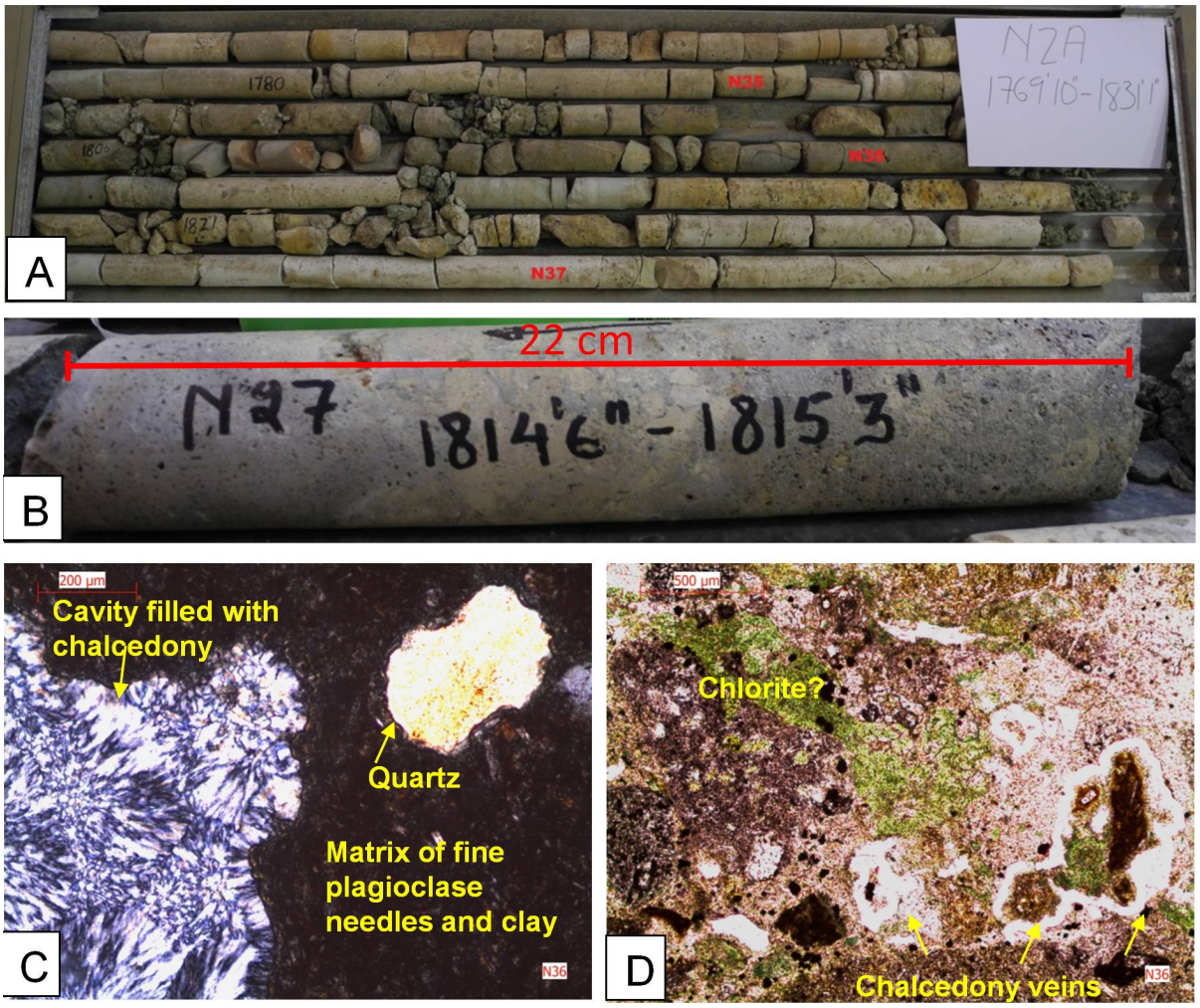

Figure 13. **Photographs, descriptions and observations of a tuff-breccia rock sample from the NZA drill core. (A) Dark grey tuff-breccia comprised of pumice, plagioclase crystals, glass and lithic fragments with weathered, yellowish-green appearance. (B) The tuff-breccia has a pitted appearance where weathering has taken place. Large angular clasts ca. 80 mm in diameter are present among smaller lapilli sized scoria and lithic fragments in a dark glassy matrix of fine zeolite. (C) XPL photomicrograph of a cavity filled with chalcedony alongside a subrounded, indistinctly embayed quartz crystal surrounded by dark brown matrix of plagioclase shards and fine-grained volcanic ash. (D) PPL photomicrograph indicating an unidentified green mineral as well as chalcedony surrounding lithoclasts and pumice within the rock, presumably sourced from silica released by glass transforming to zeolite (Pettijohn *et al.,* 1972).**

Lapilli-stone (N37)
557.12-557.35 m

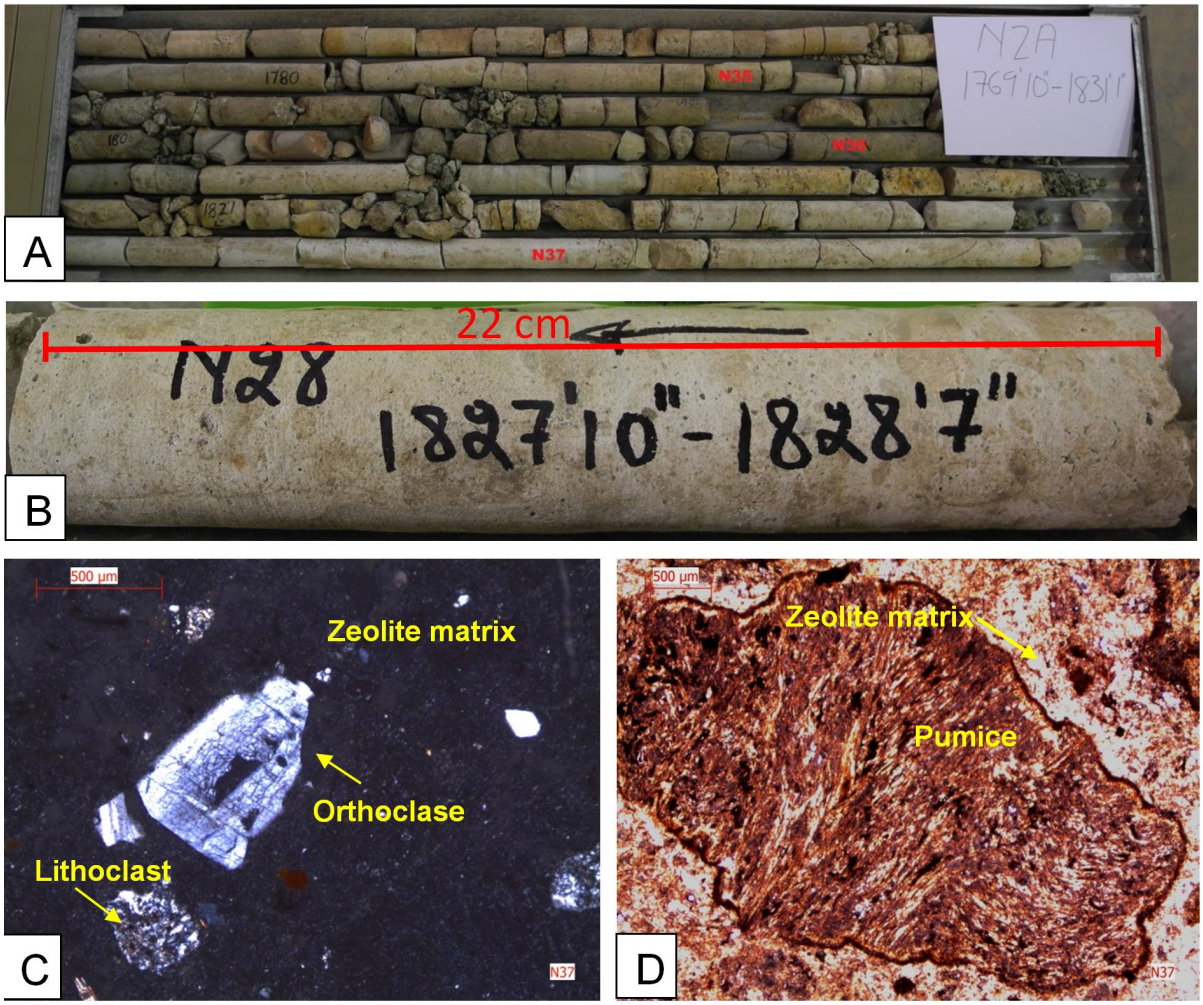

Figure 14. **Photographs, descriptions and observations of a lapilli-stone rock sample from the NZA drill core. (A) Cream coloured lapilli-stone comprising poorly sorted, subangular pumice, angular zeolite crystals and lithic fragments hosted in zeolite matrix. (B) Weathered and altered appearance of the lapilli-stone seen in the NZA drill core. (C) XPL photomicrograph of black fine-grained volcanic ash containing subrounded, ca. 0.4 mm diameter lithoclasts and ca. 0.5 mm diameter orthoclase phenocryst. (D) PPL photomicrograph of a ca. 2.5 mm diameter lapilli-sized pumice fragment covered with a rim of altered glass. The vesicles in the pumice appear flattened and aligned in several directions.**

Tuff (N40)
571.09-571.20 m

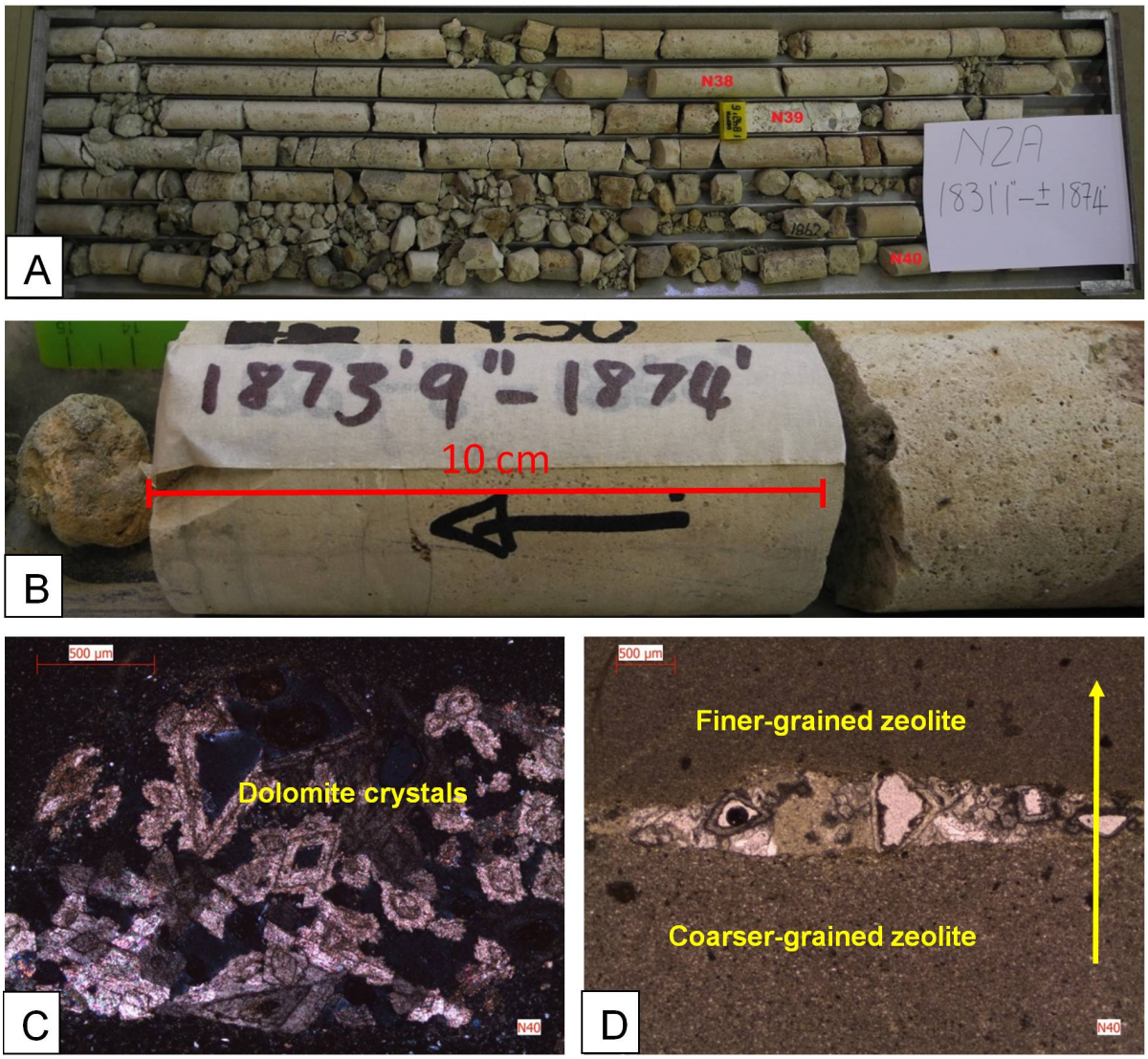

Figure 15. **Photographs, descriptions and observations of a tuff rock sample from the NZA drill core. (A) The tuff is ca. 30 cm in length and comprises fine crystals altered to zeolite and clays with a typical upward fining texture. (B) A sharp contact between the fine-grained tuff layers is visible in the hand specimen. (C) XPL photomicrograph of an opening at a sharp contact in which interlocking, secondary dolomite rhombs formed in several generations between volcanic ash beds. (D) PPL photomicrograph indicating underlying coarser grained grains of volcanic ash compared to overlying finer grains of volcanic ash with the direction of fining indicated by an arrow. The opening is interpreted to have formed due to deformation of sediment prior to lithification.**

4.3 Chemical bulk rock analysis results

4.3.1 Mineralogical composition results of calcareous sandstone lithofacies

Mineralogical composition results are consistent with microscopically observed detrital components in the rocks, namely quartz grains, plagioclase grains, K-feldspar grains, bivalve and gastropod fossils as well as rare volcanic fragments. Quartz detritus abundance varies between 12-50 wt-% in calcareous sandstones of the NZA drill core. Quartz content averages ca. 30 wt-% further indicating the compositional immaturity of the NZA calcareous sandstones. Plagioclase content varies between 6-37 wt-% which is concordant with the compositional immaturity of the NZA sandstones related to proximal source of the detritus (Pettijohn *et al.,* 1972). Samples with plagioclase content over 30 wt-% include N19, N20, N21 and N27 and are consistent with petrographic observations. Orthoclase detritus is rare and occurs in majority of NZA sandstone samples with abundances up to ca. 7 wt-% further implying sedimentation from a felsic source rock (Pettijohn *et al.,* 1972; Nichols, 2009). Volcanic fragments sourced from the Lebombo volcanics are linked to the rare detection of pyroxene and zeolite lithic fragments including heulandite and clinoptillolite in some rock samples.

Calcite content averages ca. 38 wt-% and includes shelly fossils and calcite cement. Low calcite content is linked to sandstones with limited fragments of shelly fossils and poorly developed calcite cement. Organic rich calcareous sandstones of the NZA drill core comprise fine-grained diagenetic siderite between ca. 4-19 wt-% in samples N16, N18, N20, N21, N22 and N27. Siderite is closely associated with organic matter present in the sandstones, often seen coating organic matter and plant fossils similar to observations by Curtis *et al.* (1975), due to reducing conditions created by organic matter. Rhodochrosite content of ca. 9 wt-% was detected in sample N22 and forms under similar reducing conditions to siderite, as described by Curtis *et al.* (1975). Pyrite was not identified during petrographic studies, but was detected by XRD analysis with abundances up to 1-4 wt-% in samples N5, N10, N21 and N22, and is also congruous with the reducing conditions identified within the NZA drill core. Dolomite occurs in samples N17 and N26 and is thought to occur as fine grains or replacing calcite cement. XRD analysis is thus useful in identifying various carbonates which are not easily identified during petrographic study. Apatite content is extremely low, ca. 0.05 wt-%, and is presumably hosted in shelly fossils and minuscule fish bones.

Mica grains such as muscovite are rare in NZA calcareous sandstones. Furthermore, extremely fine-grained clay minerals comprising matrix constituents are largely undetected by XRD because the detection limit is lower than 3 %. However, mica grains were detected in N10, N12, N14, N15, N19 and N31. Lastly, glauconite which is chemically analogous to illite and smectite is not readily detected by XRD analysis. For this reason, spectral imaging was advantageous in detecting and identifying clay minerals in the NZA drill core.

4.3.2 Mineralogical composition results of greywacke lithofacies

The three greywacke samples studied from the NZA drill core have similar appearance and mineralogy. The mineralogical composition analyses indicate quartz content

between ca. 22-50 wt-% agreeing with petrographic descriptions. The low quartz content is also concordant with the chemically immature nature of greywackes. Plagioclase content up to 35 wt-% is congruous with observations made during petrographic study. Microcline occurs only in N6 and comprises 5 wt-%, while orthoclase content of 7 wt-% occurs for both N9 and N13. The variation in feldspar reflects variable source rock composition. Diopside only occurs in N9, ca. 4 wt-% and is attributed to inclusion of volcanic material. Smectite content of ca. 20-56 wt-% is consistent with well distributed clay matrix observed in petrographic studies. The abrasion of volcanic, unstable grains is attributed to smectite present throughout the NZA drill core. No calcite was detected during XRD analysis, as the detection limit is 3 %, however rare, thin shelled bivalve fossils and poorly developed calcite cement are present.

4.3.3 Mineralogical composition results of coquina limestone and beachrock lithofacies

Mineralogical composition results of the coquina limestone indicate a calcite content of 92 wt-% consistent with dominant calcitic fossils as well as calcite cement. Due to winnowing of less dense terrigenous material, quartz and plagioclase do not feature prominently in the coquina limestone. Quartz content is comparatively low, ca. 7 wt-% and plagioclase is less than 1 wt-%, concordant with petrographic observations. Haematite coating invertebrate fossils accounts for ca. 1 wt-% of the coquina limestone, and imparts a pinkish-reddish colour on the rock.

Mineralogical composition results for the beachrocks indicate quartz content of ca. 20 wt-%, attributed to quartz and chalcedony grains observed during petrographic study. Orthoclase content of ca. 5 wt-% and plagioclase content up to 20 wt-% indicate the presence of an eroded volcanic source. Calcite content of ca. 30 wt-% is congruous with shell fragments and recrystallised calcite, however the abundance of calcareous minerals observed during petrographic study is at least 50 %. Dolomitisation of calcites occurs in N24 comprising 32 wt-% of the beachrock. The reddish clay matrix was previously misidentified during petrographic study, as XRD analysis indicates presence of 9 wt-% goethite for sample N24. Goethite presumably formed due to weathering of iron-rich products such as haematite (Pettijohn *et al.,* 1972). Haematite is rare but occurs in abundances up to ca. 5 wt-%, observed as sparse mineral coatings from precipitation of Fe-rich hydrothermal fluids.

4.3.4 Mineralogical composition results of pyroclastic lithofacies

Mineralogical composition of the pyroclastic rocks indicate quartz content averages of ca. 20 wt-% attributed to chalcedony and sparse angular quartz clasts. Albite and K-feldspars are common in NZA pyroclastic rocks averaging ca. 10 wt-%, while plagioclase content averages ca. 11 wt-%. Zeolites formed by alteration of unstable juvenile glassy material comprising 24-84 wt-% of NZA pyroclastic rocks. Enstatite and diopside occur sporadically, up to 13 wt-% for N36, and were most likely included as accessory minerals during volcanic eruptions.

Table 7. Mineralogical results of NZA rock samples after XRD analysis.

Sample ID	Lithofacies	Calcite	Dolomite	Siderite	Rhodochrosite	Haematite	Goethite	Microcline	Orthoclase	Plagioclase	Quartz	Mica	Chlorite	Smectite	Pyrite	Zeolite	Pyroxene	Apatite	Total
N1	Calcareous sandstone	59	0	0	0	0	0	0	4	13	18	0	0	0	0	0	6	0	100
N2	Calcareous sandstone	67	0	0	0	0	0	0	0	8	25	0	0	0	0	0	0	0	100
N3	Calcareous sandstone	55	0	0	0	0	0	0	0	18	26	0	0	0	0	1	0	0	100
N4	Calcareous sandstone	57	0	0	0	2	0	0	0	10	31	0	0	0	0	0	0	0	100
N5	Calcareous sandstone	62	0	0	0	0	0	0	3	15	14	0	0	0	1	0	5	0	100
N6	Greywacke	0	0	0	0	0	0	5	0	22	29	0	7	37	0	0	0	0	100
N7	Calcareous sandstone	39	0	0	0	0	0	0	6	14	18	0	0	23	0	0	0	0	100
N8	Calcareous sandstone	65	0	0	0	0	0	0	5	13	17	0	0	0	0	0	0	0	100
N9	Greywacke	0	0	0	0	4	0	0	7	33	30	0	0	20	2	0	4	0	100
N10	Calcareous sandstone	3	0	0	0	0	0	0	0	22	44	1	0	27	3	0	0	0	100
N11	Calcareous sandstone	53	0	0	0	0	0	0	1	12	14	0	0	20	0	0	0	0	100
N12	Calcareous sandstone	67	0	0	0	1	0	0	0	10	16	6	0	0	0	0	0	0	100
N13	Greywacke	0	0	0	0	0	0	0	7	16	22	0	0	55	0	0	0	0	100
N14	Calcareous sandstone	67	0	0	0	1	0	0	2	10	15	3	0	0	0	2	0	0	100
N15	Calcareous sandstone	31	0	0	0	4	0	0	0	18	44	3	0	0	0	0	0	0	100
N16	Calcareous sandstone	21	0	13	0	0	0	0	0	16	46	0	0	0	0	3	0	1	100
N17	Calcareous sandstone	0	55	0	0	1	0	0	5	15	20	0	0	0	0	0	0	4	100
N18	Calcareous sandstone	68	0	4	0	0	0	0	3	12	12	0	0	0	0	1	0	0	100
N19	Calcareous sandstone	11	0	0	0	5	0	0	0	37	45	2	0	0	0	0	0	0	100
N20	Calcareous sandstone	0	0	19	0	0	0	0	0	35	35	0	0	0	0	5	0	6	100
N21	Calcareous sandstone	0	0	15	0	0	0	0	6	37	32	0	0	0	1	5	0	4	100
N22	Calcareous sandstone	14	0	17	9	0	0	0	7	15	30	0	0	0	3	0	0	5	100
N23	Coquina limestone	92	0	0	0	0.5	0	0	0	0.5	7	0	0	0	0	0	0	0	100
N24	Beachrock	24	32	0	0	0	9	0	6	7	21	0	0	0	0	1	0	0	100
N25	Calcareous sandstone	46	0	0	0	0	0	0	5	16	32	0	0	0	0	1	0	0	100
N26	Calcareous sandstone	48	6	0	0	0	0	0	5	13	25	0	0	0	0	2	1	0	100
N27	Calcareous sandstone	0	0	13	0	0	0	0	0	34	44	0	0	0	0	3	4	2	100
N28	Beachrock	44	0	0	0	0	0	0	5	20	20	0	0	0	4	7	0	0	100
N29	Calcareous sandstone	56	0	0	0	0	0	0	4	17	18	0	0	0	0	5	0	0	100
N30	Calcareous sandstone	59	0	0	0	2	0	0	0	13	26	0	0	0	0	0	0	0	100
N31	Calcareous sandstone	37	0	0	0	0	0	0	0	11	50	2	0	0	0	0	0	0	100
N32	Calcareous sandstone	30	0	0	0	0	0	0	5	25	39	0	0	0	0	0	0	1	100
N33	Lapilli-tuff	0	0	0	0	0	0	0	19	10	47	0	0	0	0	24	0	0	100
N34	Lapilli-tuff	0	0	30	0	0	0	17	0	12	4	0	0	0	0	37	0	0	100
N35	Lapilli-stone	0	0	0	0	0	0	0	7	5	13	0	0	0	0	75	0	0	100
N36	Tuff-breccia	0	0	0	0	0	0	0	29	34	21	3	0	0	0	0	13	0	100
N37	Lapilli-stone	0	0	0	0	0	0	0	5	4	7	0	0	0	0	84	0	0	100
N38	Lapilli-stone	0	0	0	0	0	0	0	7	6	14	4	0	0	0	69	0	0	100
N39	Lapilli-stone	0	0	0	0	0	0	13	0	14	22	0	0	0	0	51	0	0	100
N40	Tuff	0	0	0	0	0	0	0	9	3	32	0	0	0	0	56	0	0	100

4.3.5 Geochemistry results of calcareous sandstone lithofacies

The calcareous sandstones of the NZA drill core comprise allochthonous detritus including quartz grains, orthoclase grains, plagioclase grains, volcanic fragments, shelly fossils, plant fossils, organic matter, glauconite grains, rare micas and smectite matrix hosted in calcite cement. Although bulk rock analysis does not discriminate cements and matrix from detritus, meaningful insights are provided in the following paragraphs and correlated well with findings from spectral imaging and petrography. Cementing the sandstone components is prevalent calcite cement. Major element analyses indicate that the SiO_2 content ranges between ca. 42-75 wt-%. The SiO_2 percentages are attributed to the presence of quartz grains, rare chalcedony grains, feldspar grains and zeolite grains, with SiO_2 content averaging ca. 56 wt-% indicating chemical immaturity of the detritus (Pettijohn *et al.,* 1972).

Al_2O_3 abundance averages ca. 10 wt-% and is attributed to the presence of smectite in glauconite grains and feldspar grains. Al_2O_3 abundance increases with glauconite content in NZA calcareous sandstones, consistent with petrographic observations and spectral imaging results. MgO abundance averages ca. 3.5 wt-% in the NZA calcareous sandstones and is linked to Mg-smectite clays, phyllosilicates and detritus from mafic source rock. Anomalously high levels up to ca. 11 wt-% MgO is attributed to rare dolomite, detected by XRD analysis, as is the case for N17. Dolomite was overlooked during petrographic study, but confirmed by mineralogical results and is presumed to be distributed as fine grains or steadily replacing calcareous fossils and calcite cement.

$Fe_2O_{3(total)}$ content varies between 5-18 wt-% with increased Fe_2O_3 content in NZA sandstones attributed to several mineral phases such as haematite coatings, fine-grained siderite and glauconite grains. Fe_2O_3 content averages ca. 11 wt-%, while samples N19, N20, N21, N22 comprising ca. 15 wt-% Fe_2O_3 are consistent with widespread glauconite and scattered organic matter coated in fine-grained siderite during to reducing conditions. CaO content averages ca. 7 wt-%, with abundant anorthite grains contributing to CaO content. The CaO content from major element analysis was recalculated to exclude calcite cement and invertebrate fossils in order to provide meaningful insight into the chemistry of allochthonous detritus comprising the NZA drill core's siliciclastic rocks. Prior to recalculation of the major element results the CaO content was ca. 35 wt-%, providing misleading results.

Na_2O and K_2O content both average ca. 1.7 wt-% and are attributed to rare orthoclase grains as well as rare mica grains observed in the calcareous sandstones. TiO_2 content averages ca. 1.7 wt-% in calcareous sandstones of the NZA drill core. It is hosted in heavy minerals and fine-grained clays and is found to increase in NZA sandstones comprised of greater clay content. Pettijohn *et al.* (1972), found that TiO_2 is resistant to both mechanical and chemical decomposition and thus persists throughout sedimentary rocks. P_2O_5 content averages ca. 0.15 wt-% and is hosted as a minor component in collophane grains and glauconite grains. Pettijohn *et al.* (1972), also suggest that P_2O_5 is introduced to relatively shallow marine shelves by upwelling of deep nutrient rich water, also supporting the presence of abundant glauconite in the NZA drill. MnO content is low, typically less than ca. 0.6 wt-% and is incorporated in carbonates depending on several controls such as crystallography, mineralogy and concentration of manganese in sea water (Flügel, 2004).

Lastly, loss on ignition (LOI) up to 28 wt-% is consistent with samples comprising scattered plant fossils as well as abundant, small black organic matter distributed throughout the NZA drill core.

4.3.6 Geochemistry results of greywacke lithofacies

Three samples, N6, N9 and N13 represent greywacke lithofacies. In the following paragraphs the results of their major element analyses are briefly discussed. Major element analyses indicate SiO_2 abundance of ca. 60 wt-%, is consistent with the presence of quartz grains, well distributed fine-grained smectite and feldspar detritus observed during petrographic study. The Al_2O_3 abundance between ca. 10-13 wt-% matches the presence of smectite matrix and feldspar grains in the NZA greywackes. Fe_2O_3 content between ca. 9-15 wt-% is attributed to Fe-bearing mineral phases such as fine-grained siderite which are typically intermixed with fine-grained matrix and abundant Fe-bearing glauconite grains. MgO content between 6-8 wt-% is consistent with well distributed Mg-smectite identified by spectral imaging. MgO is typically derived from volcanic glass, phyllosilicates and mafic detritus (Nesbitt and Young, 1984). Due to limited calcite cement and rare fossil fragments CaO abundance is typically low at ca. 2 wt-%, compared to the calcareous sandstones.

Na_2O and K_2O content both average ca. 2 wt-% and are consistent with XRD results indicating the presence of microcline, orthoclase and albite in the NZA greywackes. TiO_2 content between 1.2-2.6 wt-% is comparatively higher than calcareous sandstones of the NZA drill core and is linked to greater abundance of fine-grained smectite, able to host more TiO_2. P_2O_5 content varies insignificantly compared to calcareous sandstones and is also hosted in minuscule phosphate rich fossils and glauconite grains (Pettijohn *et al.,* 1972). Low MnO abundance throughout the greywacke samples averages ca. 0.06 wt-%, consistent with the absence of invertebrate fossils and limited fine-grained siderite which could potentially incorporate MnO into their crystal lattices. LOI is low ca. 0.31 wt-% for the greywackes due to the absence of large plant fossils and rare shelly fossils.

4.3.7 Geochemistry results of coquina limestone and beachrock lithofacies

For the beachrocks, N24 and N28, major element analyses include SiO_2 content of ca. 44 % attributed to monocrystalline quartz grains, plagioclase grains and fine-grained clay minerals observed during petrographic study. MgO content of ca. 2-8 wt-% is related to varying abundance of Mg-smectite and dolomite content, especially for N24, detected by XRD analysis. Al_2O_3 abundance of ca. 7 wt-% is consistent with the presence of smectite among recrystallised calcite grains. Fe_2O_3 content of ca. 10 wt-% is attributed to haematite coatings and siderite matrix constituents as well as Fe-bearing authigenic glauconite grains.

CaO content of ca. 28 wt-% is congruous with the abundant recrystallised calcite mosaic and sparse invertebrate fossils observed in sample N24 and N28. Plagioclase grains and orthoclase grains occur rarely and are linked to low Na_2O and K_2O content of ca. 1 wt-%. The low abundance of immobile elements such TiO_2 ca. 1 wt-% is consistent with the absence of heavy minerals and limited presence of fine-grained clay minerals. P_2O_5 content of ca. 0.15 wt-% is consistent with phosphate-bearing skeletal remains and is also hosted in glauconite grains (Pettijohn *et al.,* 1972).

For the coquina limestone, N23, major element analyses indicate low, ca. 11 wt-%, SiO_2 content due to limited quartz detritus. Al_2O_3 content of ca. 1.5 wt-% is concordant with low smectite abundance. Fe_2O_3 content of ca. 3.5 wt-% is found in secondary iron-rich minerals such as haematite coatings and glauconite grains comprising matrix material. Low MgO content of ca. 1.5 wt-% is consistent with low abundance of fine-grained Mg-smectite, and the absence of dolomite, identified from spectral imaging results.

High CaO content of ca. 80 wt-% is concordant with abundant fossil fragments and blocky calcite cement observed during petrographic study. K_2O and Na_2O content less than 1 wt-% is attributed to low feldspar content. P_2O_5 content is also less than 1 wt-% and attributed to limited presence of glauconite grains and few phosphate-bearing fossils. TiO_2 content of 0.15 wt-% is linked to the absence of Ti-bearing clay minerals which are typically absent in shallow water, high energy environments (Flügel, 2004). MnO content of ca. 0.27 wt-% is hosted in the crystal lattices of calcareous invertebrate remains and is consistent with petrographic observations. LOI up to ca. 27 wt-% is concordant with the abundance of calcareous fossils which liberate CO_2 during heating above 900 °C.

4.3.8 Geochemistry results of pyroclastic lithofacies

The geochemistry of the pyroclastic rocks directly underlying the Zululand Group rocks in the NZA drill core are discussed in the following paragraphs. SiO_2 content averages ca. 75 wt-% related to minerals including quartz grains, fine-grained clinoptillolite crystals, heulandite crystals, plagioclase grains, microcline grains and orthoclase grains. The fine-grained zeolite minerals were identified by XRD analysis. Al_2O_3 content of ca. 12 wt-% indicates high clay content associated with matrix constituents as well as zeolite and volcanic ash. Fe_2O_3 content is low ca. 2 wt-% except for one sample, N34, comprising ca. 8.5 wt-% due to the presence of siderite, presumably introduced by hydrothermal alteration. MgO and CaO are typically hosted in mafic and ultramafic mineralogical compositions. MgO content of ca. 0.5-0.95 wt-% and CaO content of ca. 0.6-1.72 wt-% are low and consistent with typical felsic compositions. Feldspars such as plagioclase, microcline and orthoclase are common in the NZA pyroclastic rocks and are congruous with Na_2O and K_2O content of ca. 3 wt-% respectively.

Table 8. Major element results of NZA rock samples after XRF analysis, recalculated to exclude calcite cement and shelly fossils.

Sample	Lithofacies	SiO_2	TiO_2	Al_2O_3	Fe_2O_3	MnO	MgO	CaO	Na_2O	K_2O	P_2O_5	Cr_2O_3	LOI	Total
N1	Calcareous sandstone	60.83	1.83	11.22	9.83	1.43	3.84	7.00	1.69	1.49	0.29	0.04	0.51	100
N2	Calcareous sandstone	45.00	1.61	8.39	7.70	0.29	1.61	3.44	1.24	1.77	0.10	0.04	28.81	100
N3	Calcareous sandstone	63.87	1.49	11.68	8.51	0.30	3.86	5.79	1.73	2.19	0.12	0.04	0.41	100
N4	Calcareous sandstone	46.67	1.07	8.78	6.11	0.18	2.62	6.90	1.54	1.64	0.09	0.03	24.36	100
N5	Calcareous sandstone	59.07	1.63	12.81	10.28	2.32	4.30	5.99	1.66	0.96	0.44	0.03	0.51	100
N6	Greywacke	62.48	1.22	12.50	9.92	0.07	6.16	2.78	2.38	2.05	0.11	0.03	0.31	100
N7	Calcareous sandstone	57.99	1.55	11.75	9.96	1.67	4.78	7.95	1.86	1.92	0.14	0.04	0.38	100
N8	Calcareous sandstone	57.14	1.56	12.28	9.86	2.23	4.13	9.29	1.59	0.92	0.42	0.04	0.54	100
N9	Greywacke	56.31	2.62	10.34	15.04	0.07	7.89	2.85	2.16	2.18	0.17	0.06	0.31	100
N10	Calcareous sandstone	57.58	1.38	11.25	10.66	0.06	6.61	2.63	2.43	2.24	0.11	0.04	5.01	100
N11	Calcareous sandstone	54.96	2.36	11.09	14.16	1.61	4.91	6.43	1.72	2.00	0.25	0.05	0.46	100
N12	Calcareous sandstone	50.68	2.91	9.59	17.09	1.45	4.43	9.43	1.56	2.04	0.32	0.06	0.44	100
N13	Greywacke	59.63	1.99	10.08	15.47	0.05	5.90	2.12	1.87	2.41	0.12	0.05	0.31	100
N14	Calcareous sandstone	55.54	1.68	10.14	15.31	1.60	4.09	7.45	1.53	1.73	0.41	0.05	0.47	100
N15	Calcareous sandstone	49.63	2.19	7.45	13.86	0.12	2.40	5.74	1.45	1.85	0.44	0.05	14.82	100
N16	Calcareous sandstone	62.28	2.23	9.13	12.49	0.14	3.01	6.72	1.55	1.92	0.13	0.05	0.35	100
N17	Calcareous sandstone	55.00	1.81	10.88	14.81	0.19	11.88	1.53	1.91	1.41	0.15	0.05	0.39	100
N18	Calcareous sandstone	55.62	2.32	11.69	15.45	2.22	3.80	4.76	1.80	1.51	0.27	0.06	0.50	100
N19	Calcareous sandstone	45.21	1.66	8.90	17.12	0.15	4.40	4.57	1.63	1.35	0.11	0.05	14.86	100
N20	Calcareous sandstone	56.18	1.57	11.46	16.59	0.14	4.57	5.16	2.06	1.78	0.14	0.05	0.31	100
N21	Calcareous sandstone	58.22	1.59	12.11	14.98	0.11	4.05	4.61	2.04	1.80	0.13	0.05	0.31	100
N22	Calcareous sandstone	50.77	3.20	8.84	18.01	0.14	4.55	10.41	1.73	1.81	0.15	0.07	0.31	100
N23	Coquina limestone	8.05	0.11	1.28	2.56	0.20	1.20	58.73	0.22	0.24	0.10	0.00	27.31	100
N24	Beachrock	41.04	0.62	7.91	10.19	0.13	7.58	29.21	1.32	1.44	0.22	0.01	0.32	100
N25	Calcareous sandstone	71.89	0.65	9.49	6.81	0.17	1.20	5.49	1.72	1.88	0.29	0.01	0.40	100
N26	Calcareous sandstone	72.77	0.88	11.78	5.48	0.33	2.60	1.61	1.96	1.84	0.26	0.01	0.47	100
N27	Calcareous sandstone	64.54	1.21	13.43	9.38	0.06	2.86	3.44	2.39	2.22	0.15	0.02	0.31	100
N28	Beachrock	46.92	1.00	8.91	9.58	0.30	1.92	28.15	1.61	1.15	0.12	0.02	0.33	100
N29	Calcareous sandstone	64.22	1.93	12.78	7.47	0.53	1.75	6.95	1.97	1.73	0.19	0.03	0.44	100
N30	Calcareous sandstone	42.84	1.68	8.94	6.21	0.42	1.46	4.54	2.00	1.51	0.12	0.04	30.23	100
N31	Calcareous sandstone	54.69	0.73	7.45	8.30	0.12	2.16	2.68	1.55	1.08	0.10	0.03	21.11	100
N32	Calcareous sandstone	74.47	0.64	8.59	8.31	0.16	2.15	2.39	1.42	1.37	0.12	0.01	0.38	100
N33	Lapilli-tuff	81.56	0.25	10.09	0.80	0.01	0.29	0.63	2.53	3.48	0.04	0.01	0.31	100
N34	Lapilli-tuff	57.54	0.23	12.29	8.51	0.33	0.84	1.51	3.90	2.65	0.07	<0.001	12.13	100
N35	Lapilli-stone	75.34	0.33	13.42	1.90	0.01	0.56	0.91	3.92	3.27	0.04	0.00	0.31	100
N36	Tuff-breccia	73.40	0.78	12.66	2.75	0.01	0.37	1.61	3.23	4.75	0.13	0.00	0.31	100
N37	Lapilli-stone	75.12	0.24	13.82	1.24	0.01	0.62	1.00	4.69	2.90	0.06	0.00	0.31	100
N38	Lapilli-stone	75.06	0.33	13.46	1.64	0.02	0.61	0.93	4.25	3.34	0.05	0.00	0.31	100
N39	Lapilli-stone	66.75	0.30	12.19	2.41	0.07	0.80	1.44	4.36	3.31	0.06	<0.001	8.31	100
N40	Tuff	79.91	0.35	11.04	1.19	0.00	0.41	0.60	3.05	3.10	0.05	0.00	0.31	100

Ti-bearing clay minerals such as fine-grained smectites are rare in the pyroclastic rocks of the NZA drill core evidenced by low TiO_2 values of ca. 0.3 wt-%. P_2O_5 content is also less abundant in pyroclastic rocks compared to Zululand Group rocks of the NZA drill core which contain phosphate-bearing fossils. Typically, MnO content is also extremely low ca. 0.02 wt-% because Mn-bearing minerals are rare in the pyroclastic rocks of the NZA drill core. However, MnO content of 0.33 wt-%, for sample N34 is attributed to the presence of Mn-bearing siderite; thought to have formed by hydrothermal alteration processes. LOI of ca. 12 wt-% for sample N34 is attributed to the release of CO_2 from burning of siderite present in the rock sample.

4.4 Spectral imaging results

Spectral data of the core trays indicate the presence of selected minerals, conveniently processed using *IntelliCore* software provided by the *GeoSpectral Imaging Company*. The lithological borehole log compiled for the NZA drill core is consistent with the mineralogical and chemical data extracted from *IntelliCore* in Figure 16. In the following paragraphs a summary of mineral features detected in a single core tray are highlighted using the SWIR image.

Carbonates are easily detected and are used to highlight chemical and mineralogical features identified between core logging and spectral imaging in the following example. The core tray at ca. 327-367 m depth comprises coquina limestone and carbonate-rich beachrock lithofacies with a reddish appearance identified during hand specimen descriptions. During petrographic study several body fossils of bivalves, gastropods and fragments of echinoid spines and coral sponges were identified. These fossils and carbonate cements were identified collectively as carbonates during spectral imaging. Calcite cements the body fossils, while Al-smectite matrix is irregularly distributed throughout the coquina beds. The lithological borehole log compiled for the NZA drill core is compared with the detection of carbonate mineral species during spectral imaging in Figure 16 indicating the correlation of carbonate minerals where coquina limestones occur in the NZA drill core.

Three minerals are analysed via *IntelliCore* software and show the distribution for coquina limestone core tray in Figure 17. To enhance visibility the presence of carbonates is marked in blue, illite in orange and Al-smectite in yellow. Each mineral group was detected due to unique spectral signatures due to adsorption characteristics of the molecules and cations and anions bonded. The advantage of spectral imaging of drill core is the fast, complete and non-destructive identification of minerals compared to petrographic studies which can only investigate selectively. The minerals identified throughout the NZA drill core by spectral imaging are presented in the figures and paragraphs that follow.

In the following paragraphs the abundance of mineral phases are plotted alongside the NZA borehole log to indicate their variation with depth. The percentage of Al-smectite detected during spectral imaging in Figure 18 varies with depth in the NZA drill core, and correlates well with petrographic and XRD findings. Glauconite is both chemically and structurally analogous to aluminous illite-smectite (Thompson, 1975) hence the detection of Al-smectite and Mg-smectite throughout the siliciclastic glauconite bearing rocks of the NZA drill core in Figure 18. The percentage of Al-smectite detected for pyroclastic rocks is low with distinct spikes correlating with weathered volcanic lithoclasts hosted in the pyroclastic rocks ca. 571-521 m. The level of Al-smectite increases drastically at ca. 521 m where

siliciclastic rocks of the NZA drill core are intercepted in Figure 18. The weathered volcanic clasts hosted in the calcareous sandstones, observed during petrographic study, contribute to increased Al-smectite content. Low Al-smectite percentage correlate well with limestone beds at ca. 326 m and 486 m depth consistent with lower amount of Al-smectite observed during petrographic study.

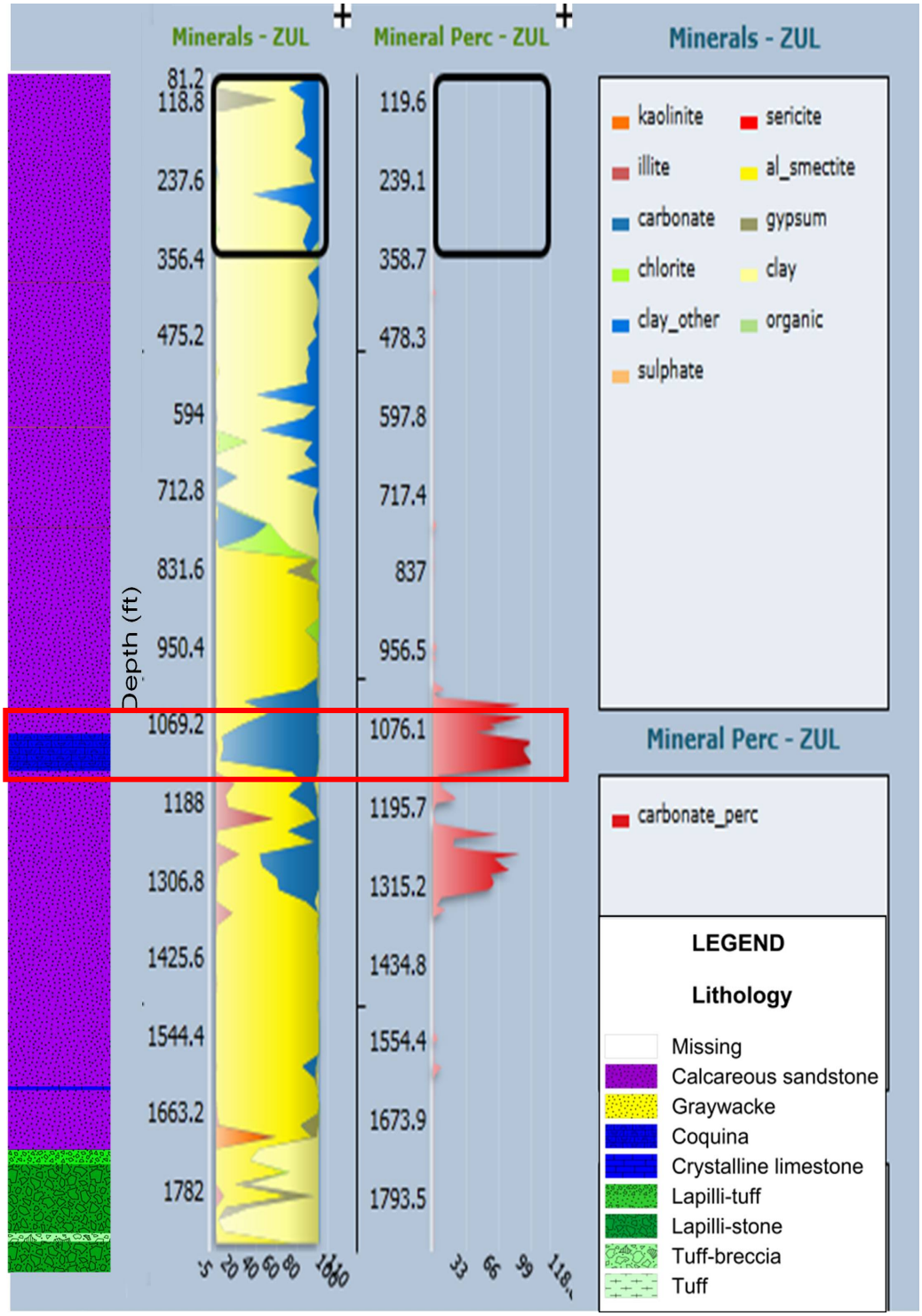

Figure 16. **Spectral log of the NZA drill core compiled in *IntelliCore* indicating the abundance of carbonate for the core tray containing the coquina limestone unit, highlighted in the red box correlating with the NZA borehole log.**

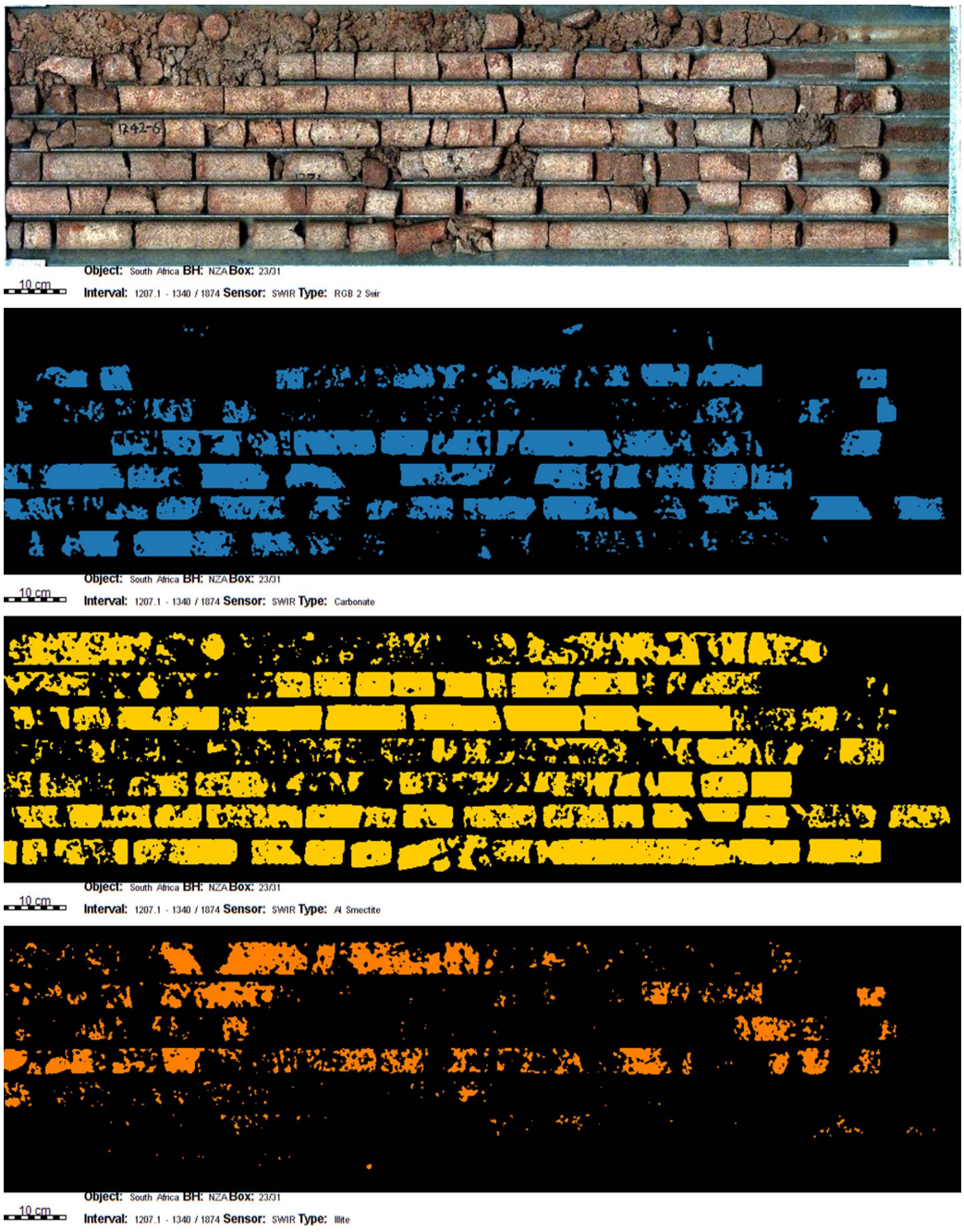

Figure 17. **The core tray comprising coquina limestone and beachrock is indicated in the uppermost RGB image. The distribution of carbonate in blue, Al-smectite in yellow and illite in orange is overlayed on the RGB image to highlight the distribution of various minerals across the same drill core.**

The different composition of smectites are noted with changing depth for the NZA drill core and linked to differences in the chemistry of source rock, as well as degree of diagenesis (Środoń, 1984). Mg-smectite occurs at shallow depths of the NZA drill core ca. 106-219 m and could possibly reflect a lower degree of diagenesis compared to older Al-smectite occurring at greater depths, ca. 255-571 m, which are more prone to alteration. Sharp increases in Mg-smectite percentage observed in the NZA drill core in Figure 18 are consistent with greywacke beds at ca. 118 m, 182 m, and 200 m depth. These findings are consistent with abundant smectite detected by XRD analysis for the greywackes as well as well distributed smectite matrix observed during petrographic study.

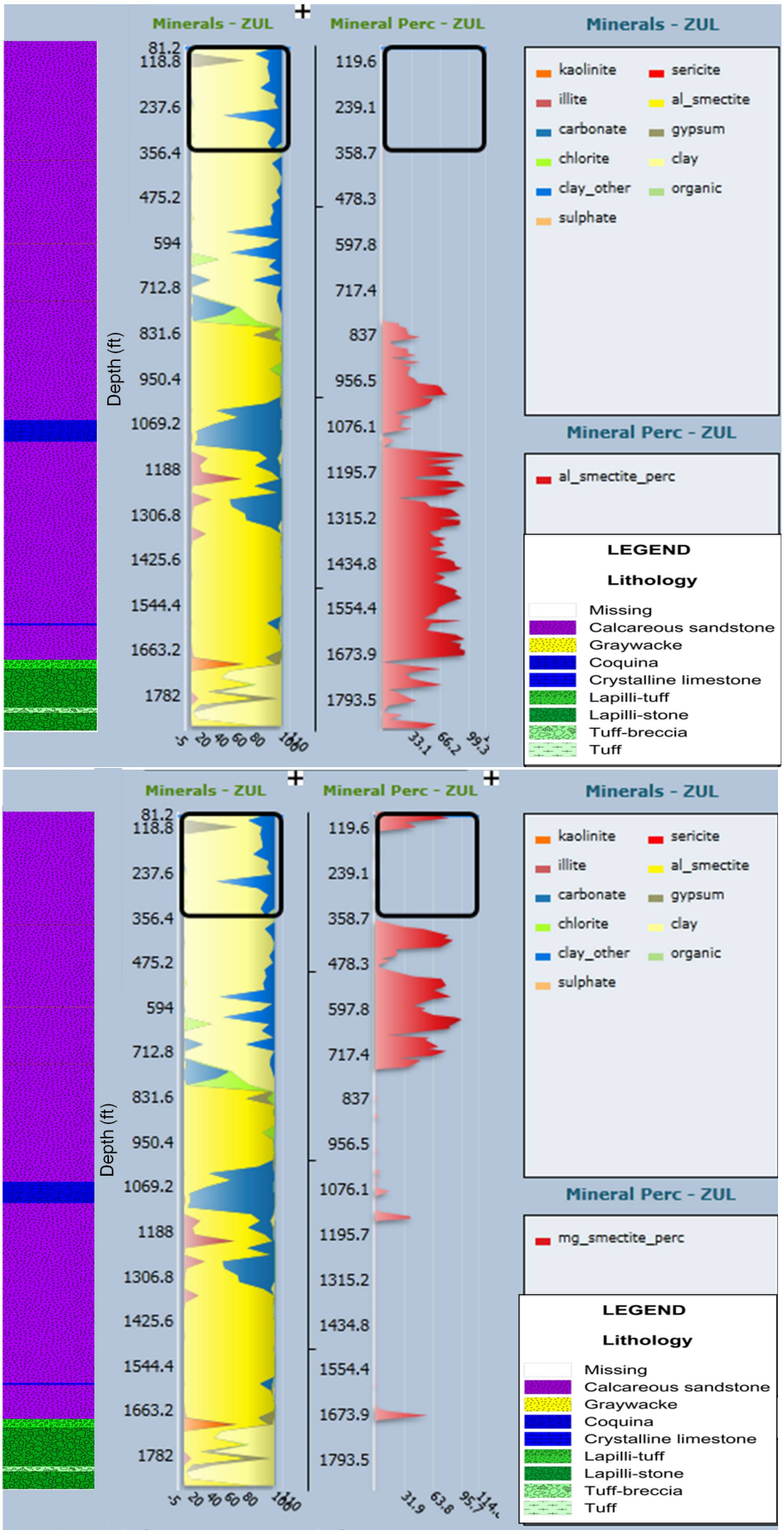

Figure 18. **Spectral logs indicating the mineral percentage abundance of Al-smectite and Mg-smectite detected throughout the NZA drill core.**

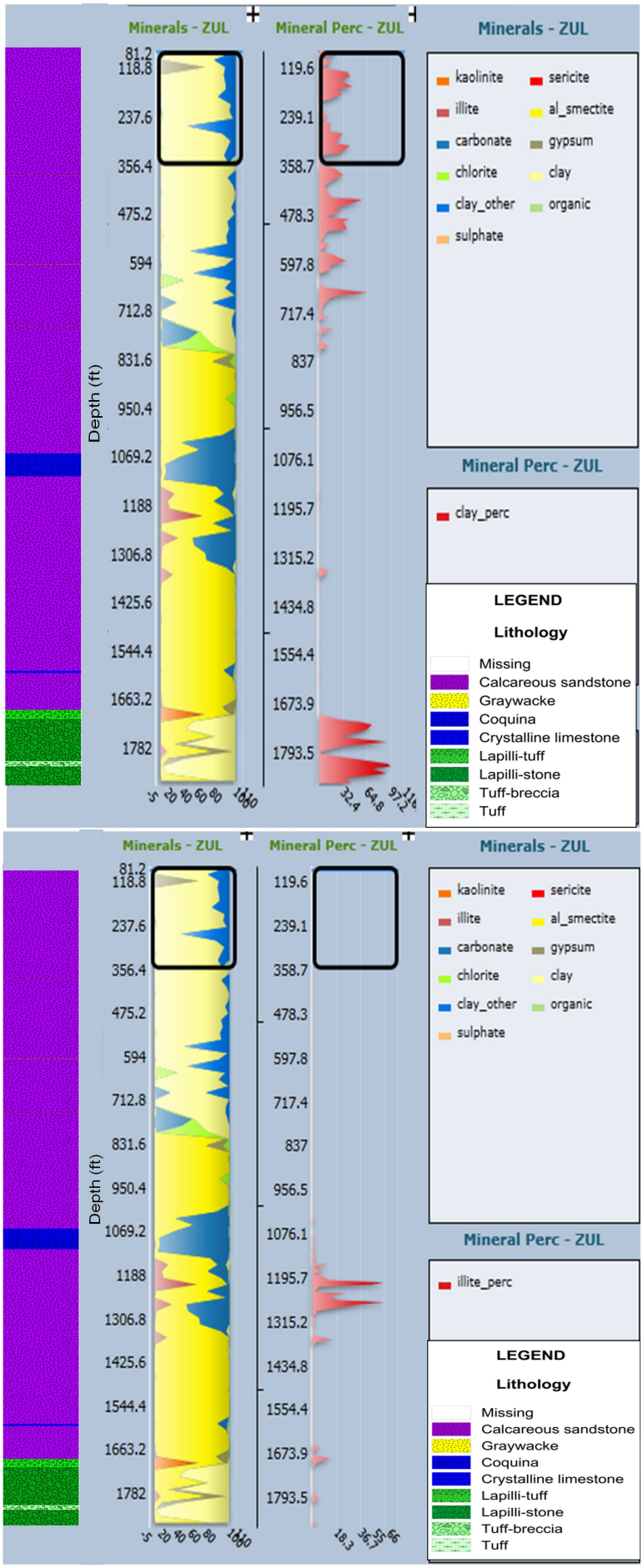

Figure 19. **Spectral logs indicating the mineral percentage abundance of clay and illite detected throughout the NZA drill core.**

Undifferentiated clay minerals are detected during spectral imaging and provide an unclear signature of exactly which mineral is detected in Figure 19. However, clay minerals detected via spectral imaging correlate well with the occurrence of Al and Mg-smectite detected by XRD analysis and observed during petrographic study. This variety of clay minerals is consistent with eroded and weathered volcanic rocks, readily weathering to clay minerals, as well as glauconite present in siliciclastic rocks of the NZA drill core. For the pyroclastic rocks underling the Zululand Group, undifferentiated clay minerals are also detected and are presumably derived from alteration products of unstable volcanic glass.

Detectable illite is rare in the XRD results for the NZA drill core and is inferred to be the weathering product of volcanic material (Pettijohn *et al.,* 1972; Thompson, 1975). Glauconite also comprises illite, in varying abundance, and is detected sporadically in the NZA drill core. Although illite was identified rarely by spectral imaging and XRD analysis, in the NZA drill core, the highest percentage detected, ca. 50%, correlates with a beachrock unit at ca. 386 m depth constituting well distributed clay matrix and glauconite grains. Illite was also detected at ca. 400 m depth and is consistent with fine-grained calcareous sandstones in Figure 19 which comprise weathered volcanic clasts and glauconite grains.

Detectable kaolinite occurs rarely in the NZA drill core in Figure 20 and is also attributed to hydrothermal activity associated with the pyroclastic debris. The only occurrence of kaolinite, ca. 64%, detected for the NZA drill core at ca. 525 m depth at which highly altered pyroclastic rocks were recorded during core logging. Kaolinite parent minerals are typically K-feldspars and micas which were likely to occur in fresh felsic pyroclastic rocks. Kaolinite was not observed during petrographic study and was not detected by XRD analysis, thus highlighting the advantage of spectral imaging as a mineral identification technique.

Chlorite also occurs rarely in the NZA drill core in Figure 20 and was not commonly detected by spectral imaging and XRD analysis. The presence of chlorite is attributed to hydrothermal activity and alteration of volcanic minerals. Chlorite was not observed during core logging and petrographic study. However, percentages of ca. 40 % are detected at a depth of ca. 272 m through spectral imaging. XRD analysis only detected chlorite at a core depth of ca. 100 m, thus highlighting the disadvantage of spectral imaging as a non-penetrative technique.

Although spectral imaging is a non-penetrative, surface technique it provided a means of correlating minerals observed during core logging, petrographic study and XRD analysis in the NZA drill core. The majority of clay minerals detected in the NZA drill core are Al-smectites and Mg-smectites which are analogous to glauconite and less common, fine-grained, well distributed matrix material. Thus, the technique was particularly useful for identifying clay minerals that could not be identified by other techniques used in this study. It was also integral in fortifying the vertical stratigraphic continuity of the collected data, which would have been impossible to obtain by sampling and laboratory analytical methods.

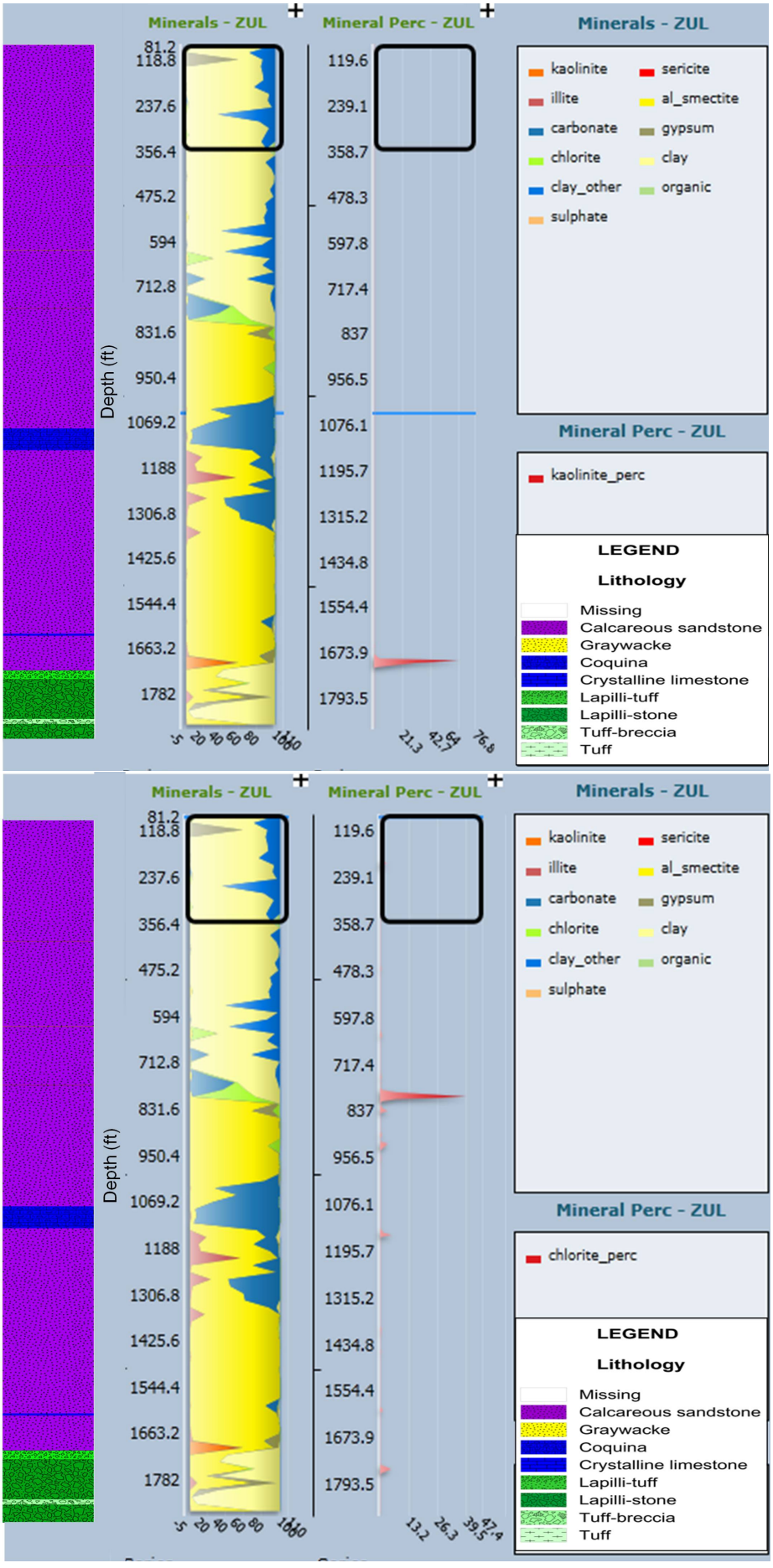

Figure 20. **Spectral logs indicating the mineral percentage abundance of kaolinite and chlorite detected throughout the NZA drill core.**

4.5 Similarities and differences of techniques used in study

The techniques used in this study to obtain representative data from the selected samples and NZA drill core provide overlapping information, however gaps in the information exist due to inherent errors and inhomogenous samples. Although spectral imaging is a non-penetrative surface technique, it consistently provided similar results to major element analysis, mineralogical composition analysis and observations made during petrography. The spectral imaging technique further aided in identifying fine-grained clay minerals that were below the detection limit and not identified by XRD analysis. Clay minerals detected by XRD analysis were chlorite, mica and smectite. However, spectral imaging provided better resolution of the clay minerals present in the NZA drill core by positively identifying Mg-smectite, Al-smectite, illite, kaolinite and chlorite.

Petrographic study provided the main source of mineralogical data for rock samples taken from the NZA drill core. The mineralogical and chemical results acquired from the aforementioned analyses were similar to petrographic findings, although discrepancies were observed between XRD analysis and petrographic observations. However, the advantage of XRD analysis in the identification of minerals which cannot be discerned by petrography provided invaluably towards studying the mineralogy of the NZA drill core's rocks.

4.6 Geochemical interpretation

4.6.1 Siliciclastic rocks

Geochemical classification of the NZA siliciclastic rocks utilises major element results to compare petrographic interpretations with several geochemical approaches for classifying the NZA sandstones, ascertaining their provenance, and determining the degree of weathering and identifying the tectonic setting. Although chemical bulk rock analysis does not discriminate cements and matrix from detritus, major element analyses were recalculated to exclude calcite cement and shelly fossils to more accurately present the chemistry of the allochthonous detritus. This recalculation contributed to meaningful geochemical interpretation of terrigenous detritus of the NZA calcareous sandstones. The paragraphs that follow detail the results and interpretation of various geochemical techniques employed in this study.

Detritus of the calcareous sandstones and greywackes of the NZA drill core were classified according to Herron (1988), who classified calcareous and non-calcareous sandstones based on percentages of SiO_2/Al_2O_3 to separate silica-rich sandstones from clay-rich sandstones (Herron, 1988). The Fe_2O_3/K_2O ratio used in the SandClass Scheme in Figure 21 is used as a stability indicator according to (Herron, 1988), and further aims to distinguish lithic fragments from feldspars in sandstones. The NZA sandstones plot mostly within the "Fe-sand" field and border the "Wacke" and "Litharenite" fields. These findings are consistent with the presence of fine-grained siderite, closely associated with organic matter, throughout the calcareous sandstones. Rare haematite and goethite also contribute to Fe-content in the NZA sandstones. Furthermore, abundant glauconite grains, up to 30 % in some cases, observed during petrography also contribute to elevated Fe-content throughout

the sandstones. Seed (1965) found that glauconite grains may comprise ca. 16 wt-% iron content in their mineral lattices. The presence of volcanic clasts, plagioclase grains, orthoclase grains and smectite-rich greywackes observed agrees with petrographic findings and the sandstones plotting in the “Wacke” and “Litharenite” field.

The Pettijohn Scheme in Figure 22 utilises the Na_2O/K_2O ratio to distinguish greywackes from arkoses (Pettijohn *et al.,* 1972; Herron, 1988). Plotting sandstones in the Pettijohn Scheme in Figure 22 indicates NZA sandstones occur within the “Greywacke” and “Litharenite” field. The NZA sandstones comprise chemically immature detritus including plagioclase grains, orthoclase grains and numerous volcanic clasts. These findings are consistent with the low degree of chemical maturity observed in the detritus of the NZA sandstones in Figure 26.

Geochemistry also provides a means of discriminating tectonic settings of sedimentary rocks. According to Pettijohn *et al.* (1972), Bhatia (1983), Roser and Korsch (1986) and Herron (1988), tectonic setting is the single most important control on provenance and thus composition of sandstones. Tectonism can create relief influencing rate and depth of erosion, which affects the type and quantity of detritus deposited in a basin (Pettijohn *et al.,* 1972) affecting sandstone composition.

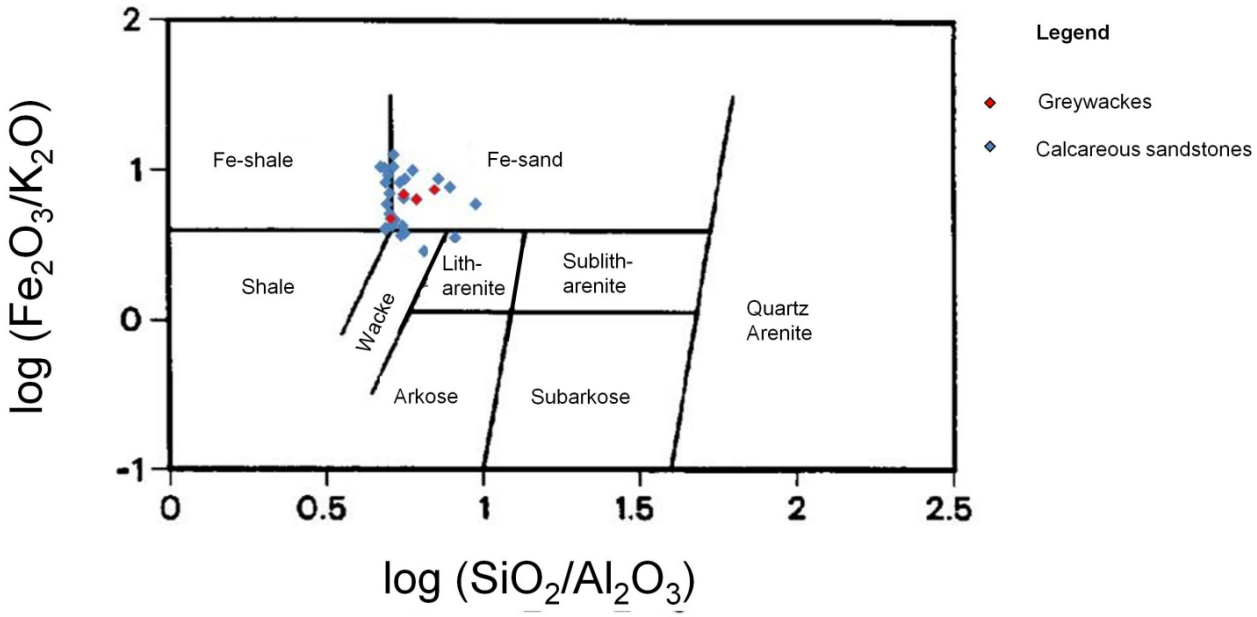

Figure 21. **Geochemical classification of the provenance of NZA calcareous sandstones and greywackes utilising the SandClass Scheme adapted from Herron (1988). The greywackes and calcareous sandstones plot mostly in the “Fe-sand” field due to the presence of Fe-bearing minerals such as siderite and glauconite.**

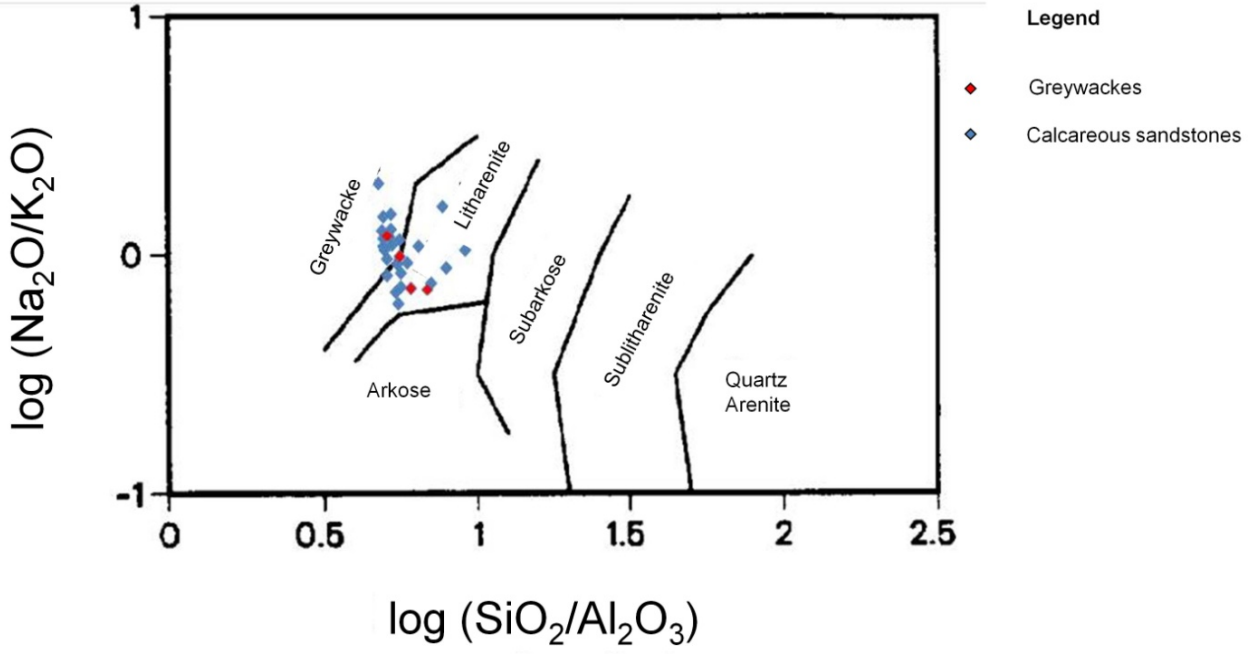

Figure 22. **Geochemical classification of NZA sandstones utilising the Pettijohn scheme adapted from Herron (1988) and Pettijohn *et al.* (1972). The NZA sandstones and greywacke plot in the "Litharenite" and "Greywacke" fields due to volcanic clasts, plagioclase and orthoclase detritus indicating low chemical maturity.**

The high Fe-content due to siderite and glauconite present in the NZA sandstones was problematic for determining the tectonic setting using plots proposed by Bhatia (1983). Recently, Verma and Armstrong-Altrin (2013) showed that new multi-dimensional diagrams can be used to accurately discriminate three major tectonic settings for the source of siliciclastic sediments. These multi-dimensional diagrams account for analytical errors due to changes in chemistry caused by weathering, recycling and post-depositional processes. Verma and Armstrong (2013), also tailored their approach for various tectonic settings by separating siliciclastic rocks into low-silica rocks containing 35-63 % SiO_2, in Figure 23 and high-silica rocks containing 64-95 % SiO_2, in Figure 24. Their tectonic settings include island or continental arc, continental rift and continental collision. The tectonic evolution of the east coast of South Africa is the product of continental rifting (Watkeys, 2002), thus most of the NZA sandstones plot in the expected continental rift field as the detritus was sourced from the continental craton. In total, nine calcareous sandstones plotted in the collision field, while six calcareous sandstones plotted in the arc field. These slight deviations from the expected rift field are explained by quantitative errors during analysis. The presence of volcanic and metamorphic lithoclasts within the sandstones providing misleading results could likely be sourced from the Natal Belt, however further investigation is required.

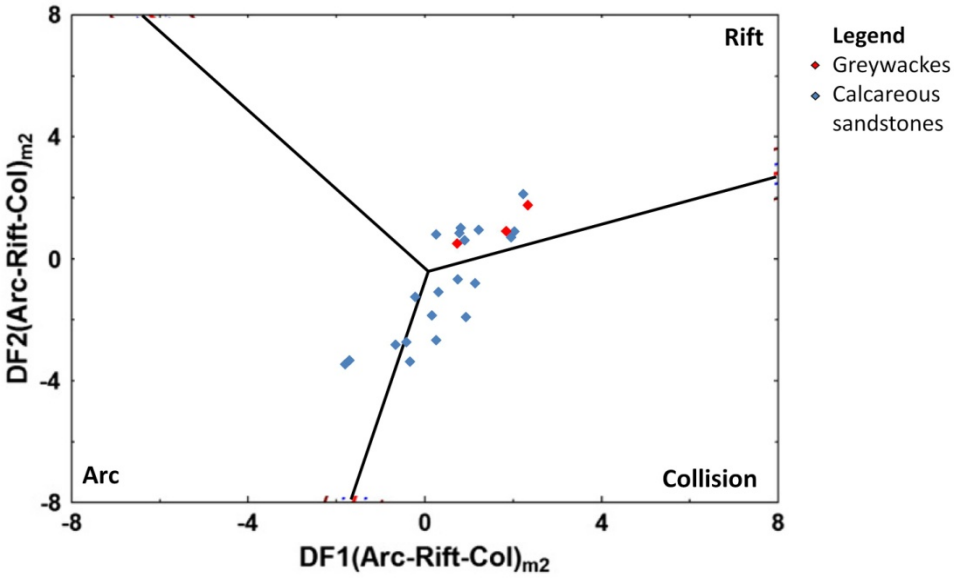

Figure 23. **Results of low-silica calcareous sandstones and low-silica greywackes from borehole NZA plotted on the revised discriminant-function multi-dimensional diagram after (Verma and Armstrong-Altrin, 2013), indicating detritus was mostly sourced from continental rocks related to rifting.**

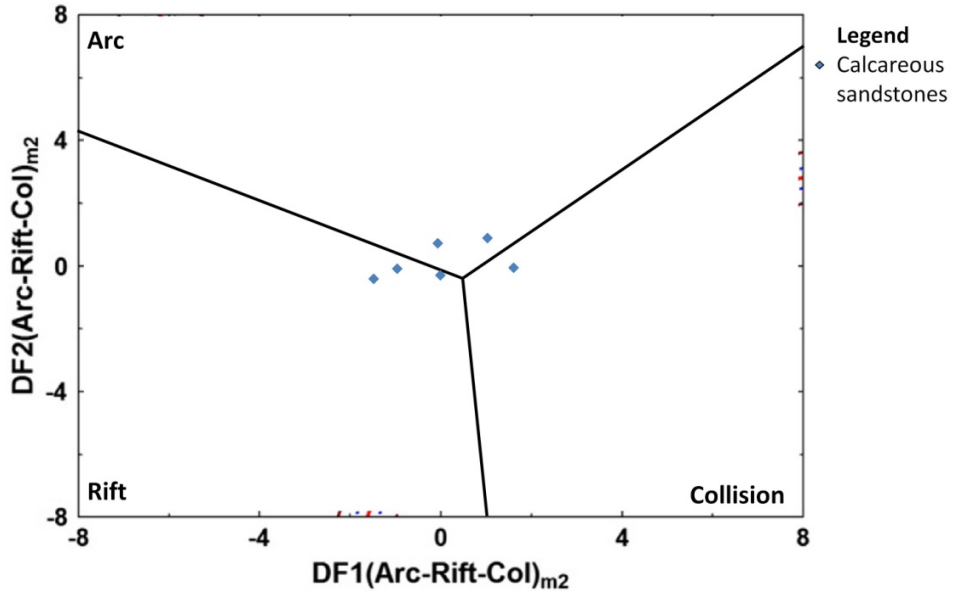

Figure 24. **Results of high-silica calcareous sandstones from borehole NZA plotted on the revised discriminant-function multi-dimensional diagram after (Verma and Armstrong-Altrin, 2013), indicating detritus was mostly sourced from continental rocks related to rifting.**

Chemical weathering contributes largely to changes in major element geochemistry as well as mineralogy of siliciclastic sediments (Fedo, 1995). Chemical weathering causes loss of Ca^{2+}, K^{+} and Na^{+} ions from silicate minerals such as plagioclase and orthoclase transforming minerals into stable mineral phases such as clay minerals (Fedo *et al.,* 1995). The degree of weathering is important to ascertain the reliability of the results for geotectonic and provenance analysis. Four variables are assessed for the degree of chemical alteration, namely Al_2O_3, K_2O, CaO and Na_2O and are expressed as molar proportions in Figure 25. The Chemical Index of Alteration (CIA) proposed by (Nesbitt and Young, 1982) is a widely

established means of deducing the degree of chemical weathering of source rock. However, the effects of K-metasomatism a common post depositional phenomenon, is typically overlooked (Fedo *et al.,* 1995). K-metasomatism occurs due to the conversion of kaolin to illite, during burial metamorphism, as well as replacement of plagioclase by K-feldspars (Fedo *et al.,* 1995). For this reason, the A, C-N, K diagram proposed by (Fedo *et al.,* 1995) is utilised to discern the degree of weathering and alteration of the NZA sandstones. Calcareous sandstone and greywacke detritus trend subparallel to "A-CN" join, due to the abundance of Al-smectite attributed to glauconite and matrix. The data also plot close to plagioclase, on the feldspar join line, consistent with plagioclase grains observed during petrography. The presence of felsic volcanic clasts and anorthite in sandstones cause data to trend towards the "CN" vertex. The sandstones indicate a low degree of weathering, because data do not trend towards the "K" vertex. A low degree of weathering indicates that major element analysis is relatively close to their original source rock composition, inherently providing a higher degree of confidence when employing geochemical discrimination.

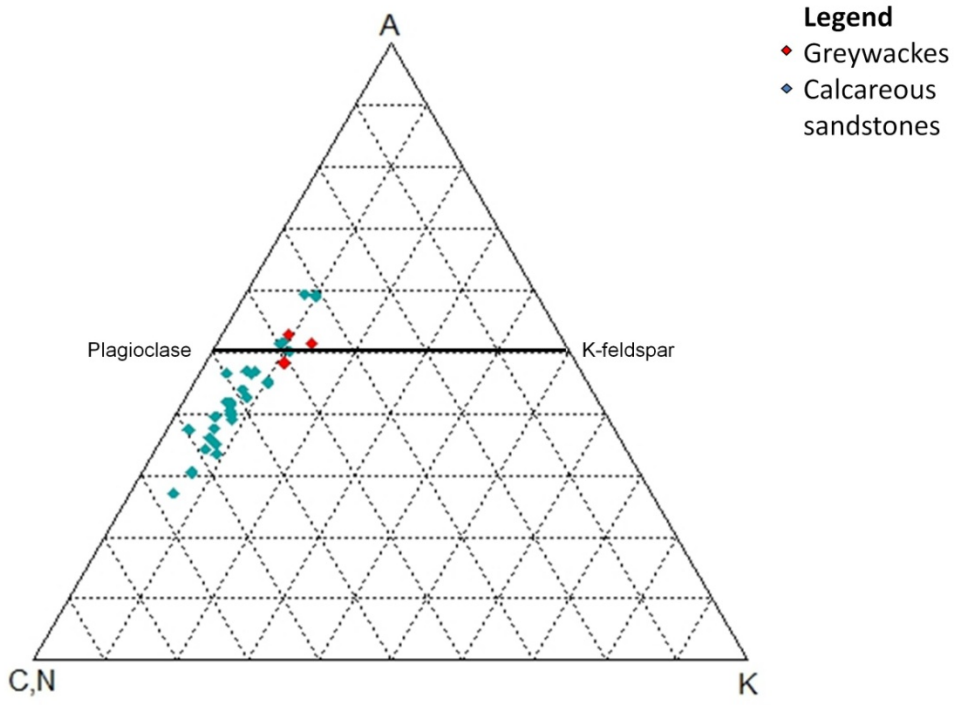

Figure 25. Calcareous sandstones and greywackes of NZA drill core plotted on an A-CN-K diagram after Fedo *et al.* (1995), data plot close to "Plagioclase" due to the abundance of plagioclase detritus and trend towards the "C,N" vertex due to volcanic detritus and anorthite grains.

The geochemical approaches utilised in this study permitted interpretation of the tectonic setting and provenance of sandstones to compliment understanding of the tectonic formation of the onshore Zululand Basin. The provenance of the NZA sandstones is determined by interpreting the NZA sandstone mineralogy, chemistry and textures as discussed in the following paragraphs.

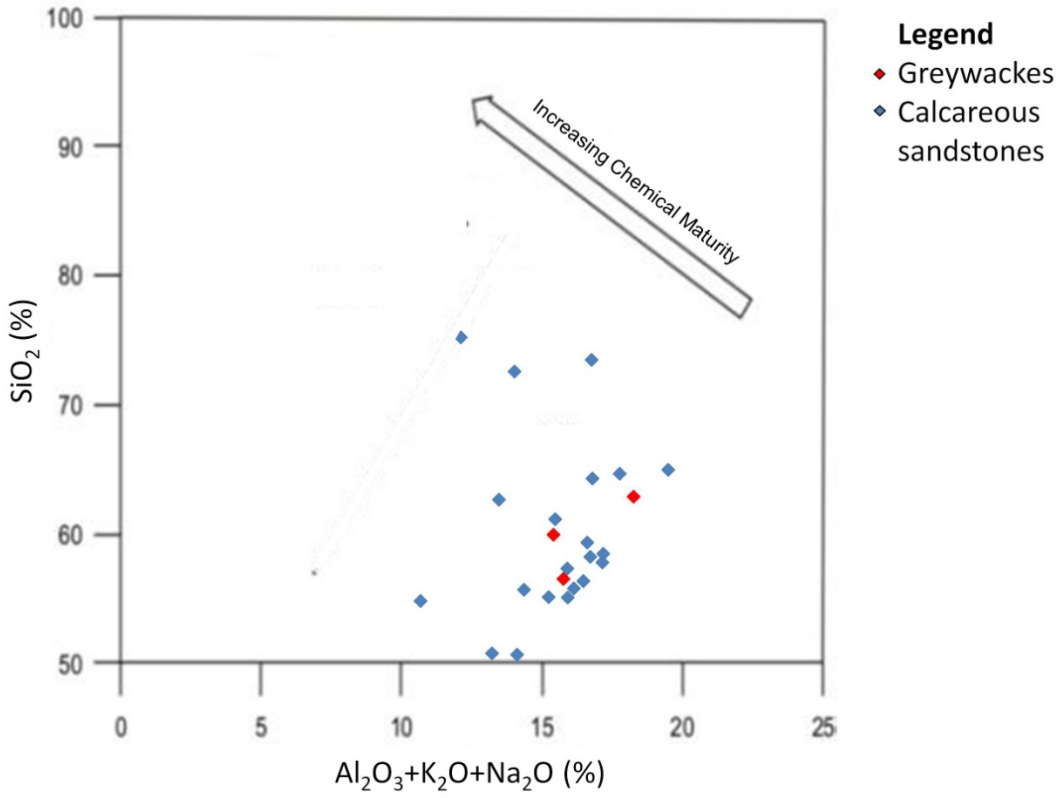

Figure 26. **Chemical maturity diagram of the calcareous sandstones and greywackes of the NZA drill core after Suttner and Dutta (1986), indicating the low degree of chemical maturity of the studied detritus.**

Unique textures in certain minerals present in sandstones allow the inference of their provenance. For example, undulose extinction and polycrystallinity of quartz grains provides insight into the source rock. The monocrystallinity of the quartz grains indicate the sediments were derived from felsic source rock (Basu *et al.,* 1975). However, slight undulose extinction in the monocrystalline quartz grains of the NZA sandstones indicates a slight metamorphic influence on the felsic source rock. Further evidence for metamorphic origin is indicated by the rare presence of fine-grained polycrystalline quartz grains. The overburden of the pre-erosional volcanic rock units possibly strained quartz grains creating undulose extinction. These findings are consistent with the proximal Lebombo Mountain source rocks which are comprised of felsic and mafic rocks (Melluso *et al.,* 2008).

The presence of unweathered subangular to subrounded plagioclase, large subrounded orthoclase and large subrounded volcanic clasts observed during petrographic study indicate rapid erosion of a proximal volcanic source. Volcanic clasts include rare weathered granite lithoclasts ca. 0.5 mm in diameter. Rare lithoclasts of schist ca. 0.5 mm diameter width are also included in the sandstones and provide evidence for a proximal metamorphic source rock, possibly the Natal Belt.

The chemical and textural maturity of the sandstones is considered low because of the predominantly subangular feldspar and volcanic components, as well as the predominantly poorly sorted nature of the sandstones. The low chemical maturity interpreted from petrographic observations is consistent with geochemical interpretation of low chemical maturity for the NZA greywackes and calcareous sandstones in Figure 26. Although low

chemical maturity is inferred to derive from an arid environment, the opposite is most likely true for the NZA detritus, due to the presence of large plant fossils resembling bark from trees. Modern arid environments indicate the presence of large plant fossils is highly unlikely.

Initial bedload transport of coarse-grained detritus is followed by suspension transport which commonly carries detritus less than 0.1 mm such as smectite affording limited abrasion to detritus. Saltation transport and subsequent abrasion of 0.1-1 mm detritus resulted in rounding (Reineck and Singh, 1980) as observed in fine and medium-grained detritus of NZA sandstones. Mg and Al-smectite are typically of detrital origin (Hillier, 1995) and probably formed by abrasion of unstable volcanic detritus during transport prior to deposition in the onshore Zululand Basin. However, smectites are also likely derived from complex dissolution-precipitation mechanisms during burial diagenesis (Hillier, 1995).

The tectonic discrimination diagrams and sandstone classification schemes correlated with the findings from petrographic study for siliciclastic rocks of the NZA drill core. Due to continental rifting starting at ca. 160 Ma (Watkeys, 2002) separating East Gondwana from West Gondwana, a repository was created in which sediments were deposited between ca. 130- 65Ma (Kennedy and Klinger, 1972). The source rock of these terrigenous sediments are predominantly felsic rocks and rare metamorphic rocks, sourced from proximal, steep sided horsts formed during continental rifting. Thus, river systems transported detritus eastwards towards the low lying Zululand Basin, as studied by Tankard *et al.* (1982). Furthermore, the presence of volcanic clasts throughout the sandstones indicates a continuous supply of detritus from adjacent Lebombo Mountains. The rapid transportation and proximal deposition of terrigenous sediments resulted in rocks which are chemically immature and not highly weathered.

4.6.2 Pyroclastic rocks

Due to the extrusive, altered and consolidated nature of the pyroclastic rocks; classification by modal parameters is impractical and not used in this study. Furthermore, the NZA drill core is over forty years old resulting in further alteration of unstable minerals. The abundance of zeolites comprising fine-grained ash as well as pumice renders the NZA pyroclastic rocks susceptible to misleading analyses as zeolites readily exchange ions of major and trace elements. Thus, water free major oxide results of the pyroclastic rock samples were recalculated using *Petromodeler* (Ersoy, 2013), to account for formation of weathering products formed since the core was drilled.

The MFW diagram was used to not only ascertain the composition of pyroclastic rocks but also characterise the degree of weathering in Figure 27. This weathering index is based on eight major oxides and is thus sensitive to chemical changes (Ohta and Arai, 2007), compared to conventional indices typically using four oxides. The “M” and “F” vertices characterise mafic and felsic source rock respectively while the “W” vertex identifies the degree of weathering, independent of unweathered parent rock chemistry (Ohta and Arai, 2007).

The eight pyroclastic rock samples taken from the NZA drill core plot close to the “F” vertex as expected for rocks derived from typically silica-rich, explosive volcanic eruptions.

Furthermore, the chemistry of the Lebombo Group rocks ranges from mafic to felsic (Melluso *et al.,* 2008), which is consistent with the predominantly felsic rock encountered for the NZA pyroclastic rocks.

The data also plots with an indistinct trend towards the "W" vertex indicating the rocks are not severely weathered and altered, possibly due to recalculation of the major element results. The extent of weathering is typically determined by the abundance of secondary weathering-related minerals (Ohta and Arai, 2007). Petrographic study and XRD analysis of the pyroclastic rocks indicates the NZA drill core is altered because of the presence of zeolite, from pre-existing glass transformed to minerals such as clinoptillolite and heulandites. The limited assessment of the chemistry of these highly altered rocks could be improved by obtaining fresh samples from outcrops.

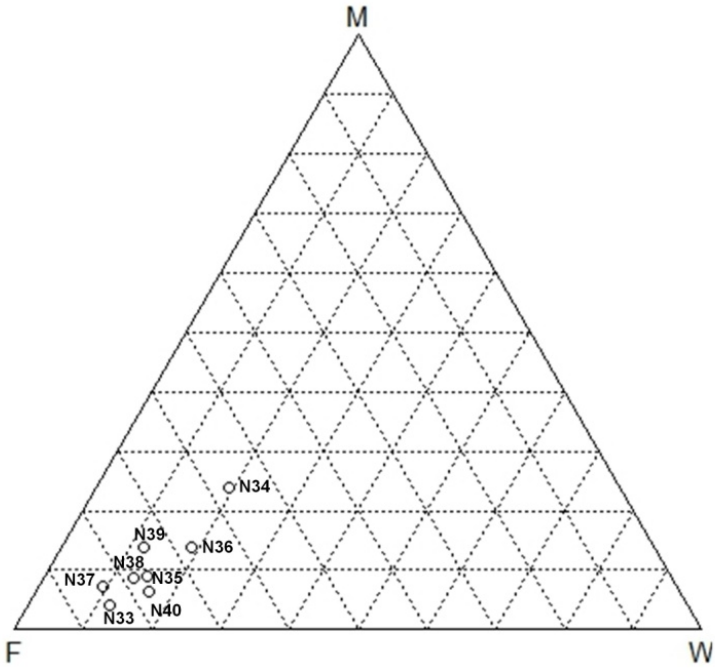

Figure 27. **MFW diagram indicating the chemistry, mafic "M", felsic "F", as well as degree of weathering "W" of the NZA pyroclastic rocks after Ohta and Arai (2007), indicating the predominantly felsic composition and weathered nature of the NZA pyroclastic rocks.**

5. CO_2 reaction experiments

Autoclave experiments on selected samples were conducted at the Martin-Luther Universität of Halle-Wittenberg in Germany. Two calcareous sandstones from the NZA drill core were selected for reaction with $scCO_2$ and pore water at reservoir temperatures and pressures, following a similar methodology to Marbler *et al.* (2013). Comparative observations of geochemical changes in sandstone samples before and after reaction with $scCO_2$ were carried out using thin section microscopy and scanning electron microscopy (SEM). The properties of CO_2 as well as the potential reaction paths that occur when rock samples are subjected to $scCO_2$ are outlined in the following paragraphs.

5.1 Properties of CO_2

CO_2 is a colourless, odourless inert gas, immiscible in water and liquefying under pressure. Above 31.1 °C and 7.38 MPa (73.8 bar) CO_2 occurs in supercritical phase in Figure 28 with a density of 150-850 kg/m^3 behaving both as a gas, by diffusing through solids and as a liquid, as it is completely miscible in water and capable of dissolving materials. The IPCC (2005) suggest a minimum burial depth of at least 800 m to achieve adequate temperature and pressure to maintain CO_2 in a supercritical phase.

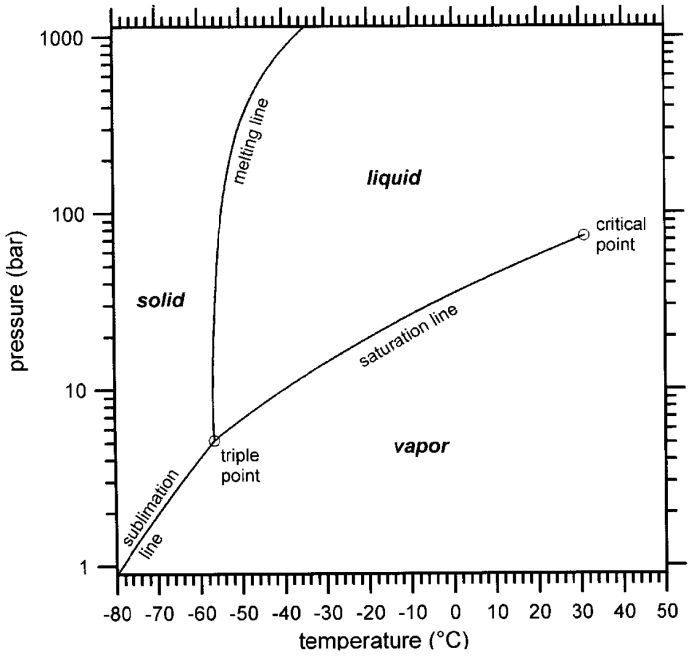

Figure 28. Phase diagram indicating pressure and temperature ranges for various phases of CO_2 (Marini, 2007 after Span and Wagner, 1996).

Several geochemical reactions ensue once CO_2 is dissolved into formation water creating chemical disequilibria (Czernichowski-Lauriol *et al.,* 2006). Currently, it is poorly understood to what extent the NZA rock units would chemically react with $scCO_2$. It is inferred that new carbonate minerals could form from Ca, Mg and Fe-bearing minerals and/or the $scCO_2$ could potentially dissolve mineral species, increasing porosity and permeability of the rock and assist migration of CO_2 fluids (Rochelle *et al.,* 2004). However, geochemical reactions are site specific depending on mineralogy, fluid chemistry, pressure, temperature and time. Thus, both dissolution and precipitation can take place to varying extents. From

limited observations of a representative NZA calcareous sandstone reacting with $scCO_2$ in a closed system, possible reactions based on a multitude of assumptions are described in the equations that follow. Due to the abundance of carbonates within most of the NZA drill core rocks, it is important to explain the effects of dissolution of carbonate.

Equation 1 represents the closed system equilibrium involving injected CO_2 reacting with formation water of rock units. Consequently, pH is dramatically lowered with release of H^+ ions causing dissolution of $CaCO_3$ seen in Equation 2 (Rochelle *et al.,* 2004). Dissolution of carbonates is rapid near the point of injection increasing carbon in solution while decreasing the amount of carbon hosted in mineral species.

$$CO_2 + H_2O <> HCO_3^- + H^+ \quad (1)$$

$$CaCO_3 + CO_2 + H_2O <> Ca^{2+} + 2HCO_3^- \quad (2)$$

$$NaAlSi_3O_8 + CO_2 + H_2O = NaAl(CO_3)(OH)_2 + 3SiO_2 \quad (3)$$

Steady state is likely obtained only after thousands of years once equilibrium is reached between CO_2 concentration and pH (Johnson *et al.,* 2004; Czernichowski-Lauriol *et al.,* 2006). According to these authors, due to slow migration of fluids in the rock and the time span before pH buffering causes reprecipitation of stable carbonates, the reservoir rock is significantly weakened due to dissolution of cement. This can potentially cause rock failure and collapse. CO_2 storage can however lead to formation of dawsonite after reaction with abundant albite in Equation 3, from (Marini, 2007). pH buffering causes dissolution of Al-silicates such as chlorite, illite, albite and K-feldspar, while mineral phases such as dawsonite and siderite could form, depending on chemistry of formation water, which effectively traps CO_2 in the solid phase.

5.2 Sample preparation for autoclave experiments

Assessing the geochemical, geomechanical and mineralogical effects of $scCO_2$ in host rock formations is important for assuring safe storage of CO_2 in the future (Marbler *et al.,* 2013). The reaction of single grains including smectite, chlorite, feldspars, quartz and calcite with $scCO_2$ as well as the reaction of calcitic cements with $scCO_2$ were studied to assess suitability of host rocks for CO_2 storage. Studying the dissolution of carbonates and changes in mineral surface morphology also contributed to estimating porosity of sandstones. Rock porosity is important for estimating the storage potential and to support decision making regarding the feasibility of the rock units for injection of CO_2.

Samples N25 and N32 are both calcareous sandstones from the NZA drill core, which are representative of the predominant lithofacies documented for the NZA drill core. Prior to the static batch autoclave experiments, thin sections for samples, N25 and N32, were prepared before reaction with $scCO_2$ utilizing a dyed blue adhesive to make pore space in the rock visible. Small blocks of the rock samples, ca. 1 cm by 2 cm cut for the two week autoclave experiments were saturated with distilled water for two days because *in situ* rocks are expected to contain pore water. Once the blocks were saturated with water, the density of each sample was measured in Figure 29. Using the block density the required mass of CO_2, to create a pressure of 100 bar within the autoclave, is calculated using Equation 4.

The autoclave experiments were run at 100 °C and 100 bar to ensure $scCO_2$ conditions so as to simulate *in situ* reservoir conditions. The rocks were placed in the autoclaves over a two week period (336 hr) to obtain results concerning possible variations in mineralogy and mineral surface morphology.

The Peng-Robinson equation (Peng and Robinson, 1976), was used to determine the correct mass of CO_2 required for creating 100 bars of pressure within the autoclave placed in an oven at 100 °C using Equation 4. Variables of Equation 4 are included in Equation 5, 6 and 7. After inserting each block and adding dry ice, autoclaves were sealed to prevent the escape of any CO_2 during the experiment before being placed in the oven for two weeks. However, only N25 was studied before and after reaction with $scCO_2$ because sample N32 disintegrated, probably due to dissolution of cements, after saturation with distilled water for 48 hours, rendering it unusable for the autoclave experiments. Although the chemistry and mineralogy of N32 is almost identical to N25, the disintegration of this sample is thought to be a result of lower induration or dissolvable minerals present in the cements.

$$P = \frac{R*T}{V_m - b} - \frac{a}{V_m^2 + 2b*V_m - b^2} \quad (4)$$

$$a = \frac{0.457236\ \alpha\ R^2\ T_c^2}{P_c} \quad (5)$$

$$b = \frac{0.0777961\ R\ T_c}{P_c} \quad (6)$$

$$\alpha = [1+ (0.37464 + 1.54226\omega - 0.26992\omega^2)(1- \sqrt{\frac{T}{T_c}})]^2 \quad (7)$$

P pressure

V_m relative volume

T temperature

T_c critical temperature

P_c critical pressure

ω acentric factor

α Peng-Robinson constant a

b Peng-Robinson constant b

R molar gas constant

Following the two week autoclave experiment with $scCO_2$, a thin section was prepared from sample N25 with a similar blue dyed adhesive to make porosity of the rock visible. Furthermore, changes in mineral surface morphology especially of carbonate cements and single minerals were observed by SEM providing insights of rock structure after reaction with $scCO_2$.

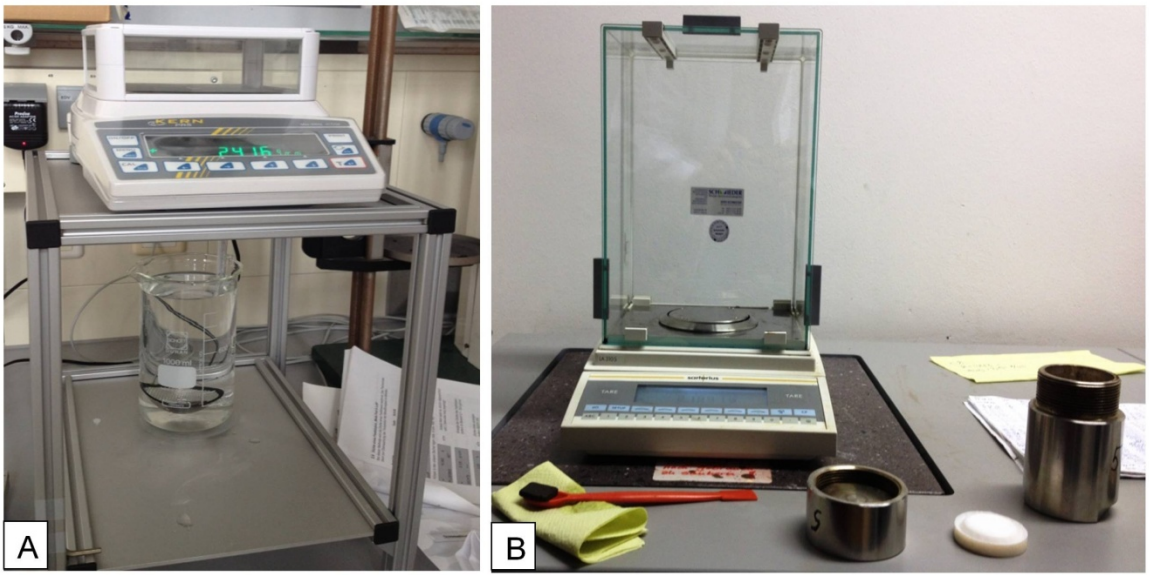

Figure 29. **Preparation of rock samples before autoclave experiments. (A) The density of each water saturated block is calculated to determine the mass of CO_2 required to create pressure of 100 bar and temperatures of 100 °C in the autoclave. (B) A water saturated block prior to placement in an autoclave with the relevant mass of solid carbon dioxide (dry ice).**

5.3 Results from autoclave experiments

The rock sample, N25, used in the static batch autoclave experiment is a fine-grained calcareous sandstone and was assessed for its suitability as a host rock for injected CO_2. The fine-grained sandstone is moderately sorted and comprises monocrystalline quartz, plagioclase, volcanic clasts, orthoclase, glauconite and shelly fossils hosted in a poikilotopic fabric of calcite cement in Table 9. The sandstone displays indistinct bedding and signs of bioturbation.

Table 9. **Mineralogical and chemical characterisation of sample N25, before reaction with CO_2.**

Sample ID	Depth		Lithofacies	Mineralogy (Thin section and XRD)	Geochemistry wt-% (XRF)	Observations
N25	From (m)	To (m)	Calcareous sandstone	Subrounded monocrystalline quartz (30%), subrounded plagioclase (10%), subrounded orthoclase (5%), volcanic clasts (10%), invertebrate fossils (5%), organic matter (10%), subrounded glauconite (5%) and calcite cement (25%).	71.89 SiO_2; 9.49 Al_2O_3; 6.81 Fe_2O_3; 1.20 MgO; 5.49 CaO; 1.72 Na_2O; 1.88 K_2O; 0.65 TiO_2; 0.29 P_2O_5; 0.17 MnO; 0.01 Cr_2O_3; 0.40 LOI	Indistinctly bedded sandstone comprising moderately sorted fine-grained detritus. Namely, subangular to subrounded quartz grains, similarly sized twinned plagioclase and cross-hatched orthoclase scattered bivalve fossils and uncommon rounded glauconite. Organic matter is evenly distributed throughout the detritus hosted in calcite cement.
	408.05	408.36				

Rock porosity cannot be estimated with a high degree of certainty, ca. 1-2 % and is indistinctly seen within the calcite cement in Figure 30b and Figure 31b as blue void spaces. Prior to reaction with $scCO_2$ the calcite cement appears relatively smooth with no sign of pitting and etching. The expected changes in rock mineralogy include dissolution of carbonate cement and reaction of feldspars with $scCO_2$ (Marbler *et al.,* 2013).

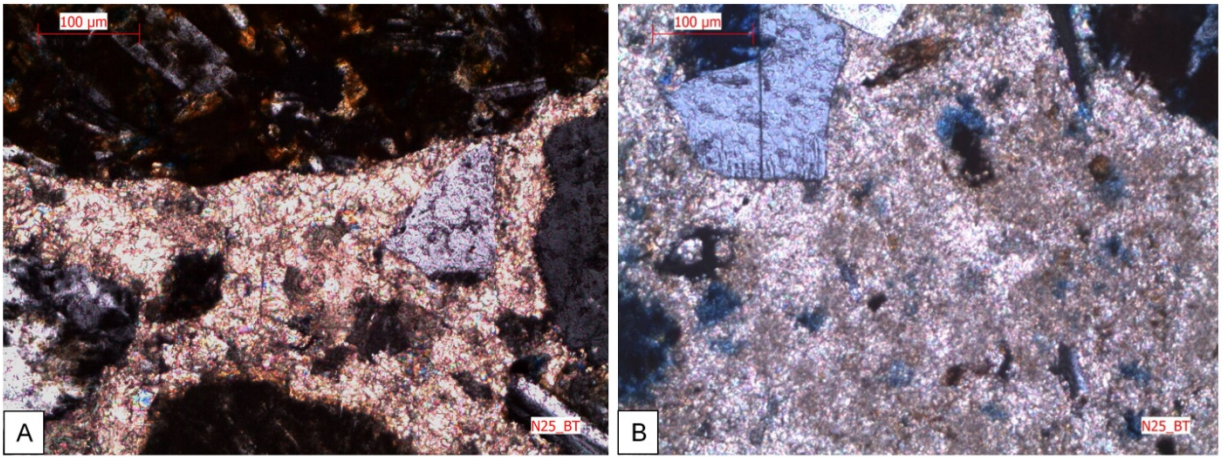

Figure 30. **Photomicrographs of sample N25 before autoclave experiments. (A) XPL photomicrograph before treatment with $scCO_2$ during static batch autoclave experiments. Note the large, black volcanic clast and subangular quartz hosted in calcite cement. (B) XPL photomicrograph indicating minute blue spots in the calcite cement indicate porosity present in the cement.**

XPL photomicrographs of N25 in Figure 31 after reaction with $scCO_2$ are consistent with findings by Marbler *et al.* (2013). Faint, blue dye is observed where dissolution of the calcite cement created new void space in Figure 31b; furthermore the calcite cement appears pitted and rough due to dissolution. Single mineral grains are seemingly unaffected by the reaction of $scCO_2$. However, mineral grains such as orthoclase have been found to react in similar experiments conducted by Marbler *et al.* (2013). The porosity increase ca. 2% cannot be estimated with a high degree of certainty. However, porosity is certainly created during dissolution of carbonate cement and carbonate coatings around grains. In this way secondary porosity is created in the rock, allowing better dispersion and diffusion of $scCO_2$ and pore water through the rock at a microscopic scale. Marbler *et al.* (2013) also noted that clay fines can potentially block pore throats which ultimately reduce porosity created after reaction with $scCO_2$.

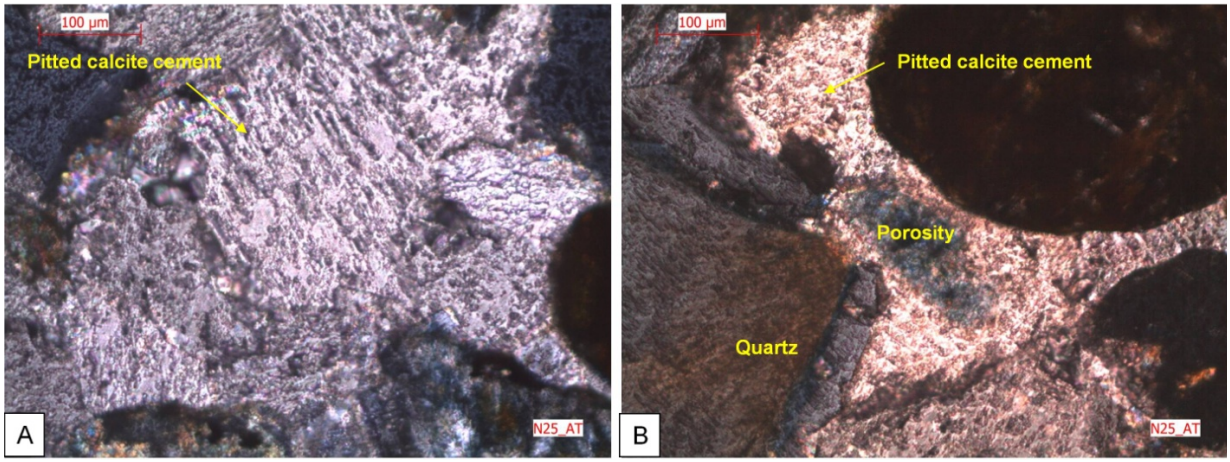

Figure 31. **Photomicrographs of N25 after autoclave experiments. (A) XPL photomicrograph of highly pitted calcite cement after $scCO_2$ experiment resulting in dissolution of the mineral surface. (B) XPL photomicrograph of sandstone 25 after $scCO_2$ experiment indicating dissolution of calcite cement creating void space indicated by blue dye. The porosity can be estimated to have risen from ca. 2 % to ca. 4% after $scCO_2$ reaction.**

It remains not entirely understood how significantly such migration of fine clay grains will affect the permeability by blocking pore throats. Furthermore, if steady state is achieved silicate minerals are expected to dissolve, at a slower rate, further adding to the unsuitability of these rock units for geological storage of CO_2. Although a potential caprock was not identified in the NZA drill core, caprock should be highly impermeable, and mineralogically stable, such as shales which are typically investigated for containing injected CO_2 (Cloete, 2010). Minerals such as illite, smectite and kaolinite typically found in shales are found to be less reactive with CO_2 than carbonates (Marini, 2007). The reaction of CO_2 with caprock is dependent on reservoir pressure, temperature, time and mineralogy (Marini, 2007).

Although, the porosity cannot be estimated with a high degree of certainty, similar studies performed by Marbler *et al.* (2013) found that porosity increased by ca. 2 % due to dissolution of calcite cement under similar temperatures and pressures. The reaction of $scCO_2$ with carbonate-bearing rocks indicates that porosity of the rocks increases over a short period of time and leads to identifiable changes in a sandstone's granular structure (Marbler *et al.,* 2013) likely reducing rock strength. Storage of $scCO_2$ over geological time could dissolve a considerable amount of calcite leading to displacement of framework grains resulting in rock instability. The autoclave experiments in this study were limited to a two week reaction period, with noticeable mineral surface dissolution of calcite cement observed in Figure 31a. Single mineral grains such as quartz were not visibly affected by $scCO_2$, possibly because of the short reaction time of two weeks in Figure 31b.

5.4 SEM of rock samples before and after reaction with $scCO_2$

SEM analysis of mineral surface topography and mineralogy was also conducted at the Martin-Luther Universität of Halle-Wittenberg in Germany. SEM-micrographs as well as mineral identification using energy dispersive X-ray (EDX) analysis are included for sample N25 before reaction with $scCO_2$ and after reaction with $scCO_2$ during the aforementioned static batch autoclave experiments. These analyses provided insights into microscopic changes in mineralogy and chemistry which ultimately affect the rock quality.

5.4.1 Sample preparation for SEM analysis

A representative, untreated, flat ca. 5 mm in diameter broken portion of sample N25 was mounted on a glass disc in Figure 32a using adhesive strips followed by a carbon coating for better conductivity, to provide a better image during analysis. A similarly sized portion of treated N25 sample was prepared in a similar manner after the two week static batch autoclave experiment, to compare mineral surface morphology as well as changes in mineralogy and geochemistry. The samples were then analysed using the JOEL JSM 6300 scanning electron microscope.

Figure 32. SEM preparation and analysis of sample N25. (A) Mounting of a sandstone sample onto a glass disc before SEM analysis. (B) Observing surface morphology of samples and mapping their mineralogy utilising EDX.

The most prominent features such as grain surface topography, textures and structures were studied and recorded during SEM analysis in Figure 32b using secondary electron (SE) and back scattered electron (BSE) images, following methods used by Marbler *et al.* (2013). The investigation showed that calcite cement was significantly altered by dissolution; however marked changes in resistant mineral grains such as quartz and orthoclase were not observed in Figure 34a. This is possibly due to the short experimental time and relatively low temperature and pressure experiment conditions. Dissolution of calcite cement observed in Figure 34b probably leads to increased pore space and greater permeability of fluids and matrix material as already observed in thin section. Dissolution was observed in different grain surfaces of calcite before and after treatment. Before treatment the calcite surfaces mostly appear smooth, but after treatment with $scCO_2$ the surface appeared rough in Figure 34a. Continued reaction between $scCO_2$, pore water and calcite can thus probably lead to drastic dissolution of calcite, possibly affecting rock quality.

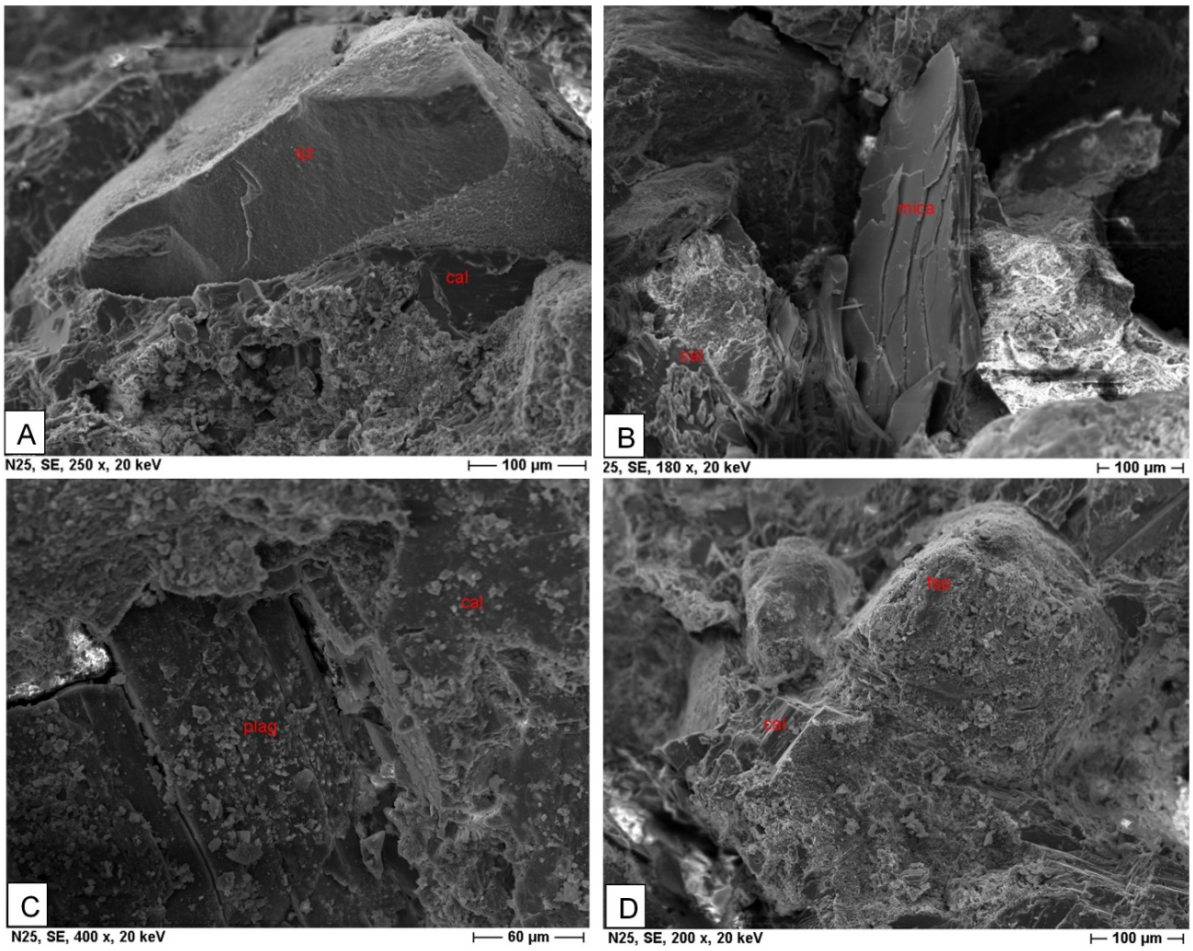

Figure 33. **SEM photomicrographs of N25 before autoclave experiments. (A) A quartz grain embedded in smooth calcite cement prior to reaction with $scCO_2$. Note the fine unidentifiable clay minerals on the rough surface of calcite cement, surrounding the quartz grain. (B) A mica grain displays perfect cleavage, surrounded by smooth calcite cement and unidentifiable minerals before reaction with $scCO_2$. (C) Plagioclase lamellae are visible, with the mineral surfaces coated in fine-grained clay mineral and calcite. Adjacent calcite cement surfaces are smooth and also covered in fine-grained clay minerals. (D) Feldspar grain coated in calcite cement and fine-grained clay minerals.**

Reactions leading to secondary mineral precipitation were not observed in the experiments although Marbler *et al.* (2013), observed such precipitation in kaolinite where considerable decomposition of anorthite and albite occurs. Undifferentiated clay minerals were commonly observed on the surfaces of quartz and plagioclase grains as well as on calcite cement before reaction with $scCO_2$ in Figure 33a and Figure 33b. After the rock reacted with $scCO_2$ these clay minerals were not observed on mineral surfaces in Figure 34a and Figure 34b. The sample size and reaction time in the experiments are insufficient to produce precipitates in detectable quantities.

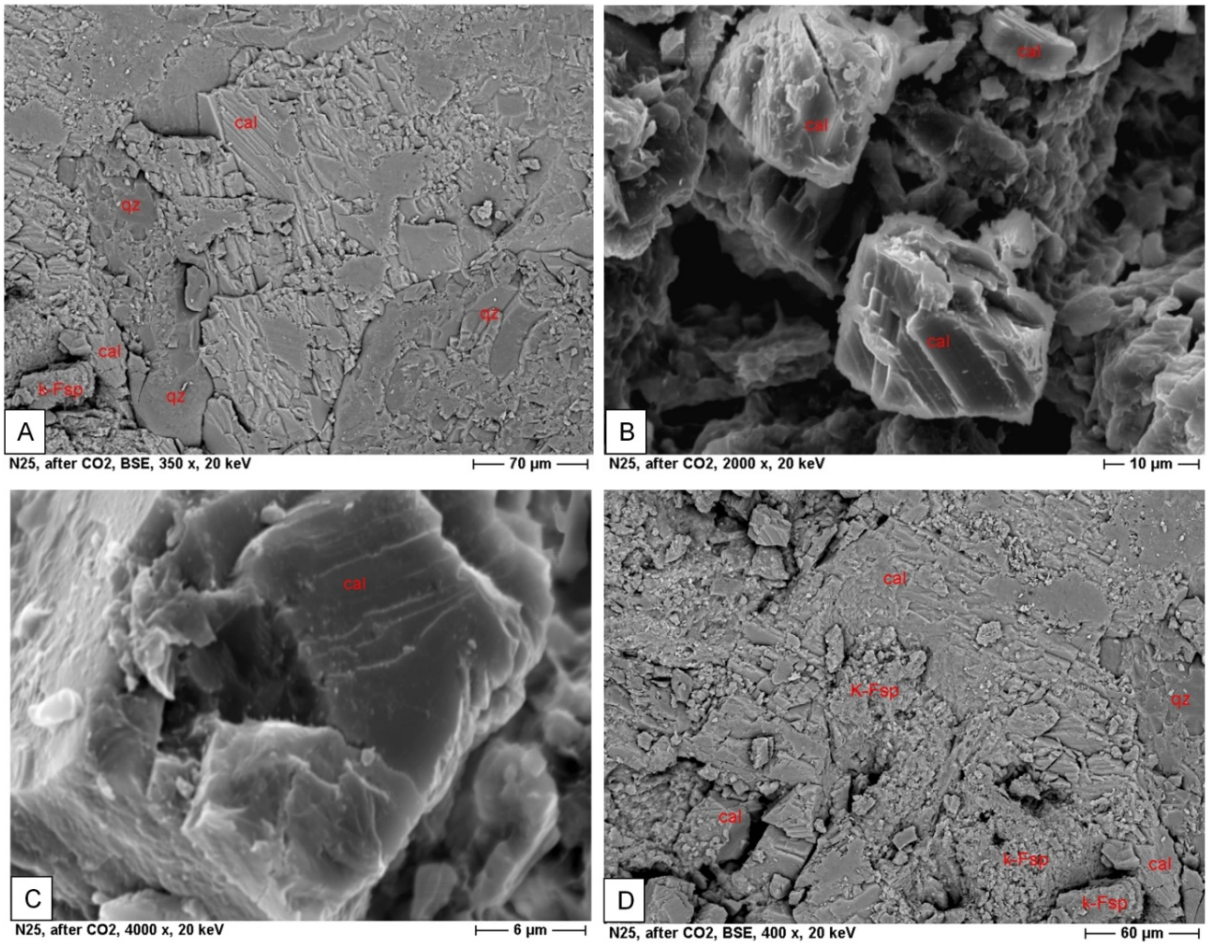

Figure 34. **SEM photomicrographs of N25 after autoclave experiments. (A) After reaction with $scCO_2$, calcite surfaces are rough and expose cleavage due to slight dissolution of calcite. Mineral grain surfaces appear smooth, and have no traces of clay minerals because they have migrated during the experiment, or were dissolved. (B) Enlarged calcite grain exposing cleavage, with surface devoid of traces of minerals at the surface after reaction with $scCO_2$. Pockets have formed in the calcite cement increasing porosity and permeability, while allowing movement of clay fines. (C) Calcite grain clearly displaying cleavage due to differential dissolution. (D) K-feldspar grains have a rough surface, presumably due to reaction with $scCO_2$ and surrounding calcite appears rough and pitted.**

6. Discussion and conclusions

The paragraphs that follow summarise the findings and observations of the NZA drill core that were characterised in this study as well as the suitability of potential host rocks and caprocks for CO_2 storage. Formations of the Zululand Group identified in the NZA drill core are described according to their similarity to literature data as well as inferred changes of relative sea-level. The inferred depositional environment is discussed for the rock packages of the NZA drill core. Lastly, a tentative lithostratigraphic correlation between adjacent Zululand Basin boreholes provides an overview of the lateral continuity and thickness of rock packages.

A generally shallow marine environment such as a continental shelf is identified for the accumulation of rock packages in the Zululand Basin (Kennedy and Klinger, 1972; Dingle and Scrutton, 1974) due to presence of bivalves and gastropods fossils, siliciclastic rocks interbedded with limestone as well as the presence of authigenic glauconite grains (Pettijohn *et al.,* 1972; Johnson and Baldwin, 1996). Open shelf areas, such as the Zululand Basin, facing the ocean are typically affected by both tidal regimes and ocean storms in varying degrees transporting sediment along the shelf (Nichols, 2009). Primary sedimentary structures observed in the NZA sandstones include cross-laminations, horizontal laminations and bedding. However, the preservation of primary sedimentary structures is often obscured by extensive bioturbation structures due to activity of benthic organisms such as bivalves and gastropods. Inferring palaeocurrents and direction of sedimentation along the continental shelf from the predominantly massive sandstones of the NZA drill could not be determined due to the lack of oriented core. However, Tankard *et al.* (1982) recorded an easterly palaeocurrent direction based on outcrop studies of the Zululand Group, consistent with sediment transported from the high lying hinterland including the Lebombo Mountains to low lying coastal areas. A seaward thickening shelf prism commonly forms on passive margins, such as southeast Africa, supplied with sediment from continental drainage systems (Johnson and Baldwin, 1996) extending into the thicker offshore component of the Zululand Basin.

Shallow marine environments are also sensitive to changes in sea-level which are recorded within the sedimentary sequence. Deposition of sediment in the onshore Zululand Basin was accommodated by several events of basin subsidence noted by (McMillian, 2003). Marine transgressions, induced by basin subsidence, across the onshore Zululand Basin are linked to fine-grained siliciclastic rocks typically forming successions over 100 m thick. However, irregular basin morphology due to extensive down faulting of the crust, and unequal sedimentation rates resulted in poor correlation of the NZA drill core with adjacent borehole lithologies from the onshore Zululand Basin in Figure 36.

The presence of glauconite is also linked to a marine shelf environment (Pettijohn *et al.,* 1972) and slow rates of sedimentation (Brett, 1995) which is conclusive for the Makatini, Mzinene and St Lucia Formations as found in NZA drill core. Glauconite grains occur in varying abundances in all Zululand Group rocks of NZA drill core and formed under reducing conditions during marine authigenesis when Fe^{2+}, Fe^{3+} and K^{+} are introduced to the faecal pellets of benthic herbivorous animals such as bivalves and gastropods (Williams *et al.,*

1954; Pettijohn *et al.,* 1972; Flügel, 2004). Newly formed glauconite is bright green but oxidation of iron radically alters glauconite to brownish yellow limonitic aggregates.

Glauconite grains are typically subrounded indicating reworking along the continental shelf, by currents and storms, while vermicular glauconites indicate *in situ* formation of glauconite (Seed, 1965). Petrographic studies indicate glauconite content dramatically increases in the Mzinene and St. Lucia Formations, comprising ca. 30 % of some calcareous sandstones. The increased sea-level and ongoing marine transgression with decreased input of longshore movement probably lead to increased glauconite content. Furthermore, marine transgressions caused by extensive basin subsidence allowed widespread upwelling of deep nutrient rich water causing increased glauconite formation. The presence of plant fossils and preserved organic material in varying quantities further indicate pervasive reducing conditions of proximally sourced terrestrial material.

6.1 Fenda Formation of the Bumbeni Complex

The porosity of the NZA drill core's pyroclastic rocks was not studied but is inferred to be low because of the prominent clay and zeolite matrix. Pyroclastic rocks of NZA drill core would make an unsuitable repository for CO_2 injection because the thickness and morphology of the rocks is unsuitable. However, the stratigraphy and formation of the pyroclastic rocks are briefly summarised in the following paragraphs.

6.1.1 Nxwala Member

The Nxwala Member's pyroclastic rocks were described by Bristow (1984), and McMillian (2003), as the uppermost member of the Fenda Formation, forming part of the Bumbeni Complex. These rocks are the basement to the Zululand Basin sedimentary deposits in the NZA drill core. Proximal and intermediate-source facies were identified for the poorly sorted lapilli-tuffs, tuff-breccia and lapilli-stones comprising various blocks and volcanic ash, deposited in a subaerial volcanic environment. Inferred Plinian eruptions, as described by Bristow (1984), probably contributed repetitive cycles of pumice-rich breccias and air-fall deposits, which were identified between 521-571 m depth of the NZA drill core. Bristow (1984), attributed these repetitive cycles to successive explosion of vent blockages and dome collapses. A thin basal layer of fine-grained ash, formed by settling of a Plinian eruption column represents distal-source facies. Overlying the tuff are near-source and intermediate-source facies of poorly sorted pyroclastic rocks comprising coarse pumice and lithic fragments formed by surge and pyroclastic flows sourced from chemically similar magma (Bristow, 1984). The unwelded nature of the majority of the pyroclastic rocks is consistent with distal deposition of ash flows (Fisher and Schminke, 1984). Ash flow deposits proximal to the eruption site are characteristically thicker and partially welded due to higher density and slower cooling rates (Pettijohn *et al.,* 1972). Furthermore, individual pulses of sedimentation were observed because of differing grain sizes, density and colour differences of the units of pyroclastic rocks.

The basal pyroclastic rocks of NZA drill core are eroded at the top and overlain by Zululand Group sedimentary rocks. Slow, steady subsidence of the basin throughout the

Barremian to Maastrichtian created space for sediment accommodation (McMillian, 2003), and influx of the proto-Indian Ocean (Tankard *et al.,* 1982). The high energy environment during early Barremian transgression is responsible for erosion of pyroclastic rocks of the NZA drill core forming a ravinement surface and commencing deposition of the Zululand Group rocks in Figure 35.

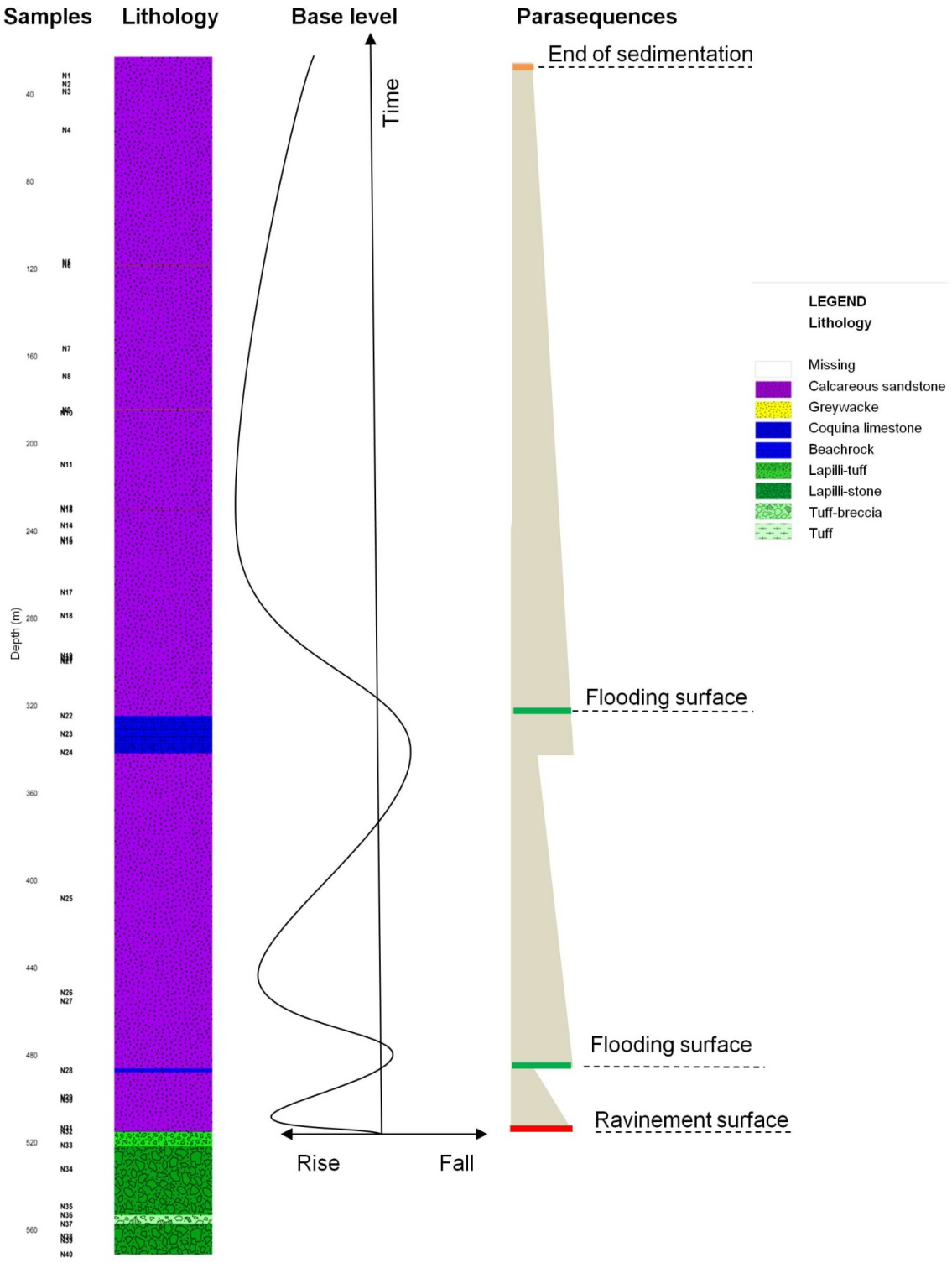

Figure 35. **Relative rise and fall of base level as well as bounding surfaces observed in the NZA drill core are correlated with formations of the Zululand Group rocks.**

6.2 Zululand Group

The NZA borehole was drilled on the northeast trending basement ridge, Bumbeni Ridge therefore the Zululand Group rock units of NZA drill core are characteristically thinner compared to adjacent Zululand Basin drill cores which were drilled in palaeotopographic low areas such as grabens. The Zululand Basin is the only Mesozoic Basin on the South African coast that experienced appreciable marine transgressions (McMillian, 2003), linked to all three formations of the Zululand Group. The Zululand Basin is the southernmost extent of the larger Mozambique Basin where the rock successions were also deposited in a shelf environment (McMillian, 2003), fed by river systems such as the Mkuze, Msunduze, Limpopo and Tugela river systems. Summarised in Dingle and Scrutton (1974), the sedimentation history of the onshore Zululand Basin is controlled by factors including basin morphology, vertical movement of the base related to disassembly of Gondwana and changing volume of sediments from respective source areas. Tankard *et al.* (1982), further reiterate that unequal subsidence rates and sedimentation rates across the faulted Zululand Basin affected morphology of the Zululand Group rock units.

6.2.1 Makatini Formation

The Makatini Formation is a thin package of rocks in the NZA drill core; ca. 35 m thick deposited during Barremian marine transgression and terminated by an inferred drop in relative sea-level due to the Aptian regression recorded in the Zululand Basin by McMillian (2003). The oldest Zululand Group sedimentary rocks in the NZA drill core are encountered at ca. 513-521 m depth and comprise ca. 8 m thick well sorted, faintly cross-laminated and indistinctly bedded, medium-grained calcareous sandstones. These shoreface deposits are comprised of monocrystalline quartz grains, plagioclase grains, orthoclase grains and volcanic detritus cemented in calcite cement, often displaying poikilotopic fabric. Pervasive calcite cement creates low porosity ca. 2%. Thus, a low storage potential for CO_2 is inferred.

A basal lag of gravel is not observed in the NZA drill core which is usually present in shoreface facies of shelf environments, identified by Tankard *et al.* (1982), at the base of the Makatini Formation. Wave action within the shore facies sorted sediment and contributed to rounding and sorting with low preservation of wave-ripple cross-lamination evident in the drill core. As the fair weather wave base is approached, with increasing water depth during continued Barremian transgression, cross-laminations are less common and deposition of fine-grained sandstones is observed creating an upward fining sequence illustrated in Figure 35. At ca. 487-513 m depth the ca. 30 m thick series of massive and poorly bedded, poorly sorted, fine-grained calcareous sandstone is consistent with sedimentary and mineralogical characteristics of offshore transition zone facies (Brett, 1995; McMillian, 2003). Fragments of thick and thin shelled bivalve and gastropod fragments in the fine-grained calcareous sandstones indicate proximal shoreface facies existed.

Capping the fine-grained sandstones is a ca. 1 m thick pinkish, heavily recrystallised beachrock at ca. 486 m depth marking a distinct change in facies in Figure 35 and termination of the Makatini Formation in the NZA drill core. In subtropical environments, such as the onshore Zululand Basin, rapid calcite precipitation cements detritus and creates

characteristic seaward tilting beachrocks (Vousdoukas *et al.,* 2007). This beachrock unit comprises mostly recrystallised, idiomorphic calcite grains forming a crystalline mosaic with scattered subrounded volcanic clasts, fine to medium-grained quartz grains, similarly sized feldspar grains, fragments of thick ca. 0.3 mm shell fragments as well as a clay and haematite matrix. Heavy recrystallisation has obliterated pre-existing structures of the beachrock.

The reliability of beachrock as an indicator of sea-level is questionable (Killitat, 2006) and thus two possibilities for their formation in Zululand Basin are proposed. During the Albian regression (Kennedy and Klinger, 1972, McMillian, 2003) decreased sea-level caused a facies shift to higher energy shoreface environments such as the intertidal zone. The mixing of seawater with freshwater is a possible cause for calcite cementation in this zone (Kelletat, 2006). Alternatively, the accumulation of similar detritus in the supratidal zone due to sporadic storm surges creates storm ridges which precipitate calcite in the upper beach due to evapouration of seawater (Kelletat, 2006). Formation of beachrock from standing water also provides an alternative explanation for the presence of dolomite, in sample N24, which is known to precipitate from evapouration of supersaturated water (Flügel, 2004). Among the cemented invertebrate fossils a thin coating of reddish haematite is observed imparting a pinkish colour to the beachrock, possibly formed by subaerial exposure. The termination of the Makatini Formation is evidenced by hardround (Shone, 2006). Although not observed in the NZA drill core, falling sea level is evidenced by the presence of high energy facies for the termination of the Makatini Formation.

6.2.2 Mzinene Formation

The increased spreading rate of South America from South Africa caused further basin subsidence and renewed marine transgression in the Albian, during which fine-grained sandstones were deposited creating the second upward fining sequence in the NZA drill core, illustrated in Figure 35. The Mzinene Formation rocks overlay the Makatini Formation rocks in the NZA drill core between depths of ca. 342-486 m depth forming ca. 144 m thick monotonous, massive, moderately sorted, fine-grained calcareous sandstones with distinctively higher glauconite content compared to Makatini Formation sandstones. Increased sea level not only resulted in deposition of fine-grained sandstone, typical of offshore transition zone and offshore facies, but also accommodated upwelling of deep, nutrient rich water leading to increased glauconite content (Dingle and Scrutton, 1974). The sandstones comprise rare sedimentary bedding and are dominated by bioturbation structures. The Early Albian-Cenomanian transgression across the Zululand Basin was terminated by regional Turonian marine regression (Kennedy and Klinger, 1972; Watkeys *et al.,* 1993).

A drop in sea level is inferred from a ca. 1 m thick whitish beachrock and coquina limestone marking the termination of the Mzinene Formation. This beachrock is similar to the aforementioned pinkish beachrock, and likely formed under similar environmental conditions due to their striking similarity. The ca. 15 m thick, well sorted coquina limestone deposit, overlying the thin beachrock indicates a shift of facies to high energy conditions leading to extensive reworking of older, ca. 30 mm bivalves that were previously deposited in deeper

water. Calcite cement precipitated among pore spaces created between shell fragments during shallow, burial diagenesis. Haematite occurs in isolated pockets among the shell fragments and is thought to have formed from subaerial exposure. The presence of glauconite indicates shallow marine conditions attributed to renewed rise in sea-level. Fine-grained detritus includes subrounded quartz and feldspar grains which occur rarely in the coquina limestone due to extensive reworking of coarser, shelly detritus, in a high energy environment. The termination of the Mzinene Formation is identified as an angular unconformity as well as hardground horizons after basin-wide regression (Shone, 2006). While neither an angular unconformity nor hardground horizons were identified for the termination of the Mzinene Formation, falling sea level is evidenced by high energy facies.

6.2.3 St Lucia Formation

Succeeding the high energy facies of the Turonian regression are lower energy facies, of the offshore-transition zone and offshore zone, related to subsidence of the Zululand Basin inducing the final marine transgression associated with deposition of the St Lucia Formation spanning the Coniacian to Maastrichtian (Dingle and Scrutton, 1974). Terrigenous sediments deposited in offshore-transition zone and offshore facies on the continental shelf include fine-grained, calcareous sandstones and thin greywackes creating the final upward fining sequence observed in the NZA drill core, illustrated in Figure 35. Similarity in the detritus, sedimentary structures and morphology between siliciclastic lithofacies of the Mzinene Formation and St Lucia Formation encountered in NZA drill core are consistent with the findings of Tankard *et al.* (1982).

However, thin greywacke beds, muddy horizons and indurated horizons less than ca. 30 cm thick are sporadically interbedded in the fine-grained calcareous sandstones of the NZA drill core belonging to the St Lucia formation. Although these horizons have an inferred low permeability, they are extremely thin and will not make a suitable cap rock for CO_2 storage. Greywackes are typically deposited from turbidity fans displaying characteristic grading and turbulent flow structures (Pettijohn *et al.,* 1972). Only three samples were studied and due to poor sorting and no grading observed they are interpreted to have formed during periods of quiet weather during which significant quantities of mud accumulated in offshore facies of the continental shelf. The indurated horizons comprise clusters of dissolved shelly fragments, possibly aiding in cementing the sediments with calcite.

The St Lucia Formation terminates in poorly consolidated fine-grained calcareous sandstones comprising significant plant fossils, organic matter and invertebrate fossils. The upper 22 m of core is missing from borehole NZA as the core trays do not record any rocks to a shallower depth. The missing section of core is interpreted to comprise unconsolidated sediments of the Maputaland Group which could not be recovered during drilling.

6.3 Tentative lithostratigraphic correlation with adjacent Zululand Basin boreholes

Lithofacies of the NZA drill core are similar with adjacent boreholes ZA, ZB and ZC of the onshore Zululand Basin, located ca. 30 km, 25km and 40km northeast of borehole NZA.

Identifying sequence stratigraphic correlation of the onshore Zululand Basin rock units is important for accurately calculating storage potential and predicting behaviour of CO_2 throughout host rock formations. Sequence boundaries in the NZA drill core are not directly correlated with adjacent ZA, ZB and ZC rock units in Figure 36. Limestone beds across the boreholes provided limited correlation. Locally, the position of borehole NZA astride the Bumbeni Complex palaeohigh accounts for large variations in rock unit morphology between the Kosi Trough and St Lucia Trough. Thus, the stratigraphy sequence of NZA is much thinner because sedimentation commenced later in the history of deposition in the Zululand Basin. This lack of lateral stratigraphic continuity across the rock units of the NZA borehole with adjacent boreholes provides a low level of confidence for injecting CO_2 into the sandstone units.

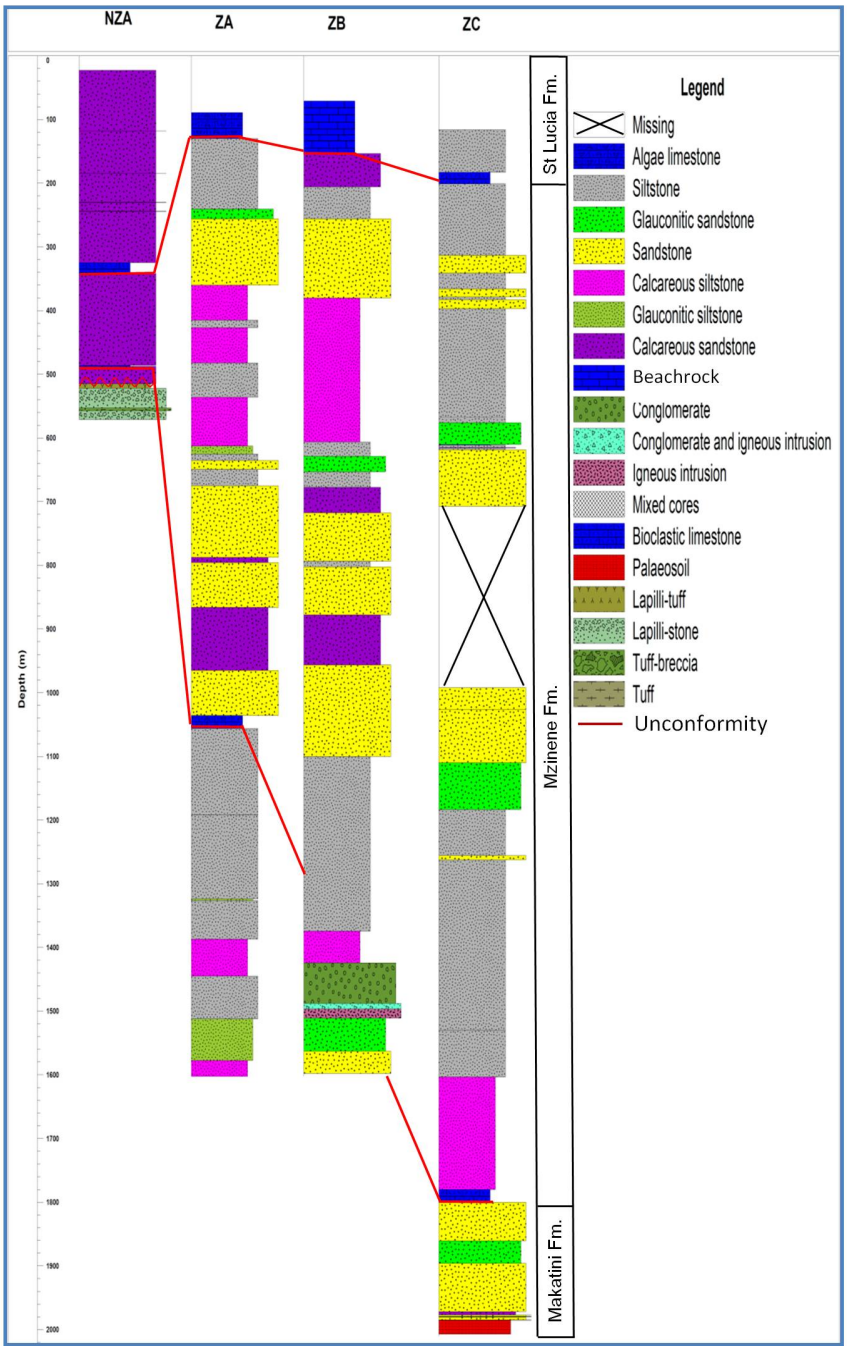

Figure 36. **Tentative lithostratigraphic correlation of rock packages of the NZA, ZA, ZB and ZC drill cores from the onshore Zululand Basin.**

The chemistry, mineralogy and physical properties of the NZA rock units indicate a low confidence for safe CO_2 storage. Highly impermeable rock packages such as shales of considerable thickness as potential caprocks were not identified within the NZA drill core. The prominent calcareous sandstones of the NZA drill core for potential host rocks have an inferred low porosity, but are highly susceptible to widespread dissolution of carbonate cement and detritus. Experiments reacting NZA sandstones with $scCO_2$ under reservoir conditions as performed at the University of Halle, Germany in pressurized autoclaves indicate that porosity could be created by carbonate dissolution. Increase in porosity is expected to assist with dispersion and diffusion of $scCO_2$ throughout the rock due to increased storage potential.

However, pH buffering will lead to precipitation of the solutes and depending on the migration path; precipitates could significantly reduce porosity and permeability in some formations. The extent of carbonate dissolution and the effect of the granular structure on the host rocks strength are yet poorly understood.

The mineralogy and geochemistry of the Zululand Group rocks is consistent with detritus derived from a proximal felsic source rock, transported in river systems and deposited in shallow marine environment. Shelf environments are typically laterally extensive; however, the lack of lateral continuity of rock packages across the onshore Zululand Basin indicates that complex tectonic controls have shifted rock packages presumably during basin subsidence. The correlation of rock packages of borehole NZA with boreholes ZA, ZB and ZC indicates basin-wide continuity of deep sandstone packages, to act as reservoir rock, is poor in the onshore Zululand Basin.

Furthermore, the shallow depth of the NZA borehole, less than 800 m, makes this site, as well as the entire Bumbeni Ridge area unsuitable for safe storage of CO_2. Nevertheless, in the Kosi Trough and St Lucia Trough the Zululand Group formations attain a total thickness exceeding 2000 m and thus CO_2 storage would theoretically be possible if the chemical and physical properties of the rocks are suitable. For these reasons, rock packages of the NZA drill core provide a low level of confidence for geological storage of CO_2 storage. Therefore, research efforts should be directed at new and adjacent boreholes in the onshore Zululand Basin.

7. Recommendations

The onshore Zululand Basin drill core studied in this project is extremely old, weathered and altered. For this reason the chemistry, appearance and reliability of results is somewhat questionable. In order to gain meaningful insights into the physical, geochemical and mineralogical properties of the onshore Zululand Basin further investigation is required. This should include the following aspects:

1. Acquire fresh drill core to ensure better quality results for assessing the suitability of the onshore Zululand Basin and should not be drilled on the Bumbeni Ridge but in the northeast corner of the Zululand Basin.

2. Acquire pore water samples during drilling to precisely characterise host formation fluids to predict outcomes of rock and formation water reacting with $scCO_2$ (Czernichowski-Lauriol *et al.,* 2006).

3. Acquire accurate data on expected geothermal gradients across all boreholes of the onshore Zululand Basin to better understand reservoir conditions for accurately modelling *in situ* temperatures of the onshore Zululand Basin.

4. Conduct autoclave experiments for longer periods of time, under reservoir conditions of the Zululand Basin to establish how chemistry and mineralogy of the Zululand Basin rocks are affected by $scCO_2$.

5. Reservoir models should be used to simulate the suitability and potential of selected formations for storing captured CO_2 as studied by Hatzignatiou *et al.* (2008).

6. Correlate rock units between boreholes of the onshore Zululand Basin using biostratigraphy, facies analysis and sequence stratigraphy to gain an understanding of the lateral continuity of rock packages across the entire onshore Zululand Basin.

7. Commence investigation of other onshore Mesozoic basins such as the Algoa Basin reservoir rocks and caprocks to evaluate their suitability for geological storage of CO_2.

8. Acknowledgements

The lessons learned from the people who have been part of this journey cannot be adequately made mention of. Firstly, I thank Professor Wladyslaw Altermann for greatly assisting me with obtaining financial aid for this study and for granting me generous opportunities to become involved with CCS research. My somewhat informal co-supervisor and travel partner Mr Victor Tibane is thanked for providing constructive advice throughout this study. My generous bursary through SACCCS (South African Centre for Carbon Capture and Storage) is thanked many times over for their financial aid, especially Dr Tony Surridge and Mr Brendan Beck, and for sponsorship to attend CAG25. Members of the Council for Geoscience, especially Dr Thinus Cloete, and University of Pretoria's Stoneman analytical team, especially Mrs Wiebke Grote and Mrs Jeanette Dykstra, are thanked for their assistance and for teaching me how to prepare samples correctly. The National Research Fund is thanked for their financial assistance through the Thuthuka programme and for allowing me to travel to Germany with Mr Victor Tibane. The Department of Mineralogy at Martin-Luther Universität of Halle are thanked, particularly Professor Pöllman, for making laboratories, equipment and experienced staff available for my research. My colleagues, Mr Fillsmith Ndongani and Mr Daniel Hugo are thanked for assisting me with data compilation, software utilisation and ultimately making a great team. Mr Sello Baloyi, the geology department's library assistant, is thanked for tirelessly making inaccessible journals articles and books available to me. My parents and sister are thanked for constantly being supportive and believing in me. Thank you to my friends for providing necessary distractions and being part of the many adventures along the way.

9. References

Allsopp, H.L., Manton, W.I., Bristow, J.W., Erlank, A.J. (1984). Rb-Sr geochronology of Karoo felsic volcanics. *Special Publication of Geological Society of South Africa.* **13:** 273-280.

Bachu, S. (2000). Sequestration of CO_2 in geological media: criteria and approach for site selection in response to climate change. *Energy Conversion and Management.* **41:** 953-970.

Bala, G. (2013). Digesting 400 ppm for global mean CO_2 concentration. *Current Science.* **104(11):** 1471-1472.

Barr, J.L., Humphries, S.D., Nehrir, A.R., Repasky, K.S., Dobeck, L.M., Carlsten, J.L., Spangler, L.H. (2011). Laser-based carbon dioxide monitoring instrument testing during a 30-day controlled underground carbon release field experiment. *International Journal of Greenhouse Gas Control.* **5:** 138-145.

Basu A., Young S., Suttner L.J., James W.C., Mack C.H. (1975). Re-evaluation of the use of undulatory extinction and polycrystallinity in detrital quartz for provenance interpretation. Journal of Sedimentary Petrology. **45:** 873-882.

Blatt, H., Middleton, G., Murray, R. (1980). *Origin of Sedimentary Rocks*. 2nd Ed. Prentice-Hall, New Jersey. -782pp.

Bhatia, M. (1983). Plate tectonics and geochemical composition of sandstones. *The Journal of Geology*. **91(6):** 611-627.

Botha, G.A. (1992). Written communication. *In:* Watkeys, M.K., Mason, T.R., Goodman, P.S. (1993). The role of geology in the development of Maputaland, South Africa. *Journal of African Earth Sciences.* **16(1-2):** 205-221.

Branney, M.J., Kokelaar, P. (2002). Pyroclastic Density Currents and the Sedimentation of Ignimbrites. *Geological Society*, London, Memoirs. -143pp.

Brett, C.E. (1995). Sequence Stratigraphy, Biostratigraphy, and Taphonomy in Shallow Marine Environments. *Palaios.* **10(6):** 597-616.

Bristow, J.W. 1984. Plinian air-fall activity and rhyolitic dome building in the Bumbeni Complex, Southern Lebombo. *Geological Society of South Africa*. 20th Geological Congress of the Geological Society of South Africa; 1984 Jul 9-13; Potchefstroom, South Africa: GSSA; 1984, pp. 11-13.

Broad, D.S., Jungslager, E.H.A., McLachlan, I.R., Roux, J. (2006). *Offshore Mesozoic Basins*. *In:* Johnson, M.R., Anhaeusser, C.R. and Thomas R.J. (Eds.). *The Geology of South Africa*. Geological Society of South Africa, Johannesburg/Council for Geoscience, Pretoria. pp. 553-571.

Chabangu, N., Beck, B., Hicks, N., Botha, G.A., Viljoen, J.H.A., Davids, S., Cloete, M. (2014). The investigation of CO_2 storage potential in the Zululand Basin in South Africa. *Energy Procedia*. **63:** 2789-2799.

Cloete, M. (2010). *Atlas on geological storage of carbon dioxide in South Africa.* Prepared for the Council of Geoscience. (Compiler M., Cloete). -59pp.

Curtis, C.D., Pearson, M.J., Somogy, V.A. (1975). Mineralogy, chemistry, and origin of a concretionary sheet (clay-ironstone band) in the Westphalian of Yorkshire. *Mineralogical Magazine*. **40:** 385-393.

Czernichowski-Lauriol, I., Rochelle, C., Gaus, I., Azaroual, M., Pearce, J., Durst, P. (2006). Geochemical interactions between CO_2, pore-waters and reservoir rocks. Lessons learned from laboratory experiments, field studies and computer simulations. *In:* Lombardi, S. Altunina, L.K. Beaubien, S.E. (Eds.). Advances in the Geological Storage of Carbon Dioxide. Springer, Netherlands. pp. 157-174.

[DEA] Department of Environmental Affairs (RSA) (2014). GHG National Inventory Report South Africa 2000-2010. Prepared for the Department of Environmental Affairs. November 2014. Available from https://www.environment.gov.za/sites/default/files/docs/greenhousegas_invetorysouthafrica.pdf

Dingle, R.V., Scrutton, R.A. (1974). Continental breakup and the development of Post-Palaeozoic sedimentary basins around southern Africa. *Geological Society of America Bulletin.***85:** 1467-1474.

Ersoy, E.Y. (2013). PETROMODELER (Petrological Modeller): a Microsoft® Excel© spreadsheet program for modelling melting, mixing, crystallization and assimilation processes in magmatic systems. *Turkish Journal of Earth Sciences*. **22:** 115-125.

Fedo, C.M., Nesbitt, H.W., Young, G.M. (1995). Unravelling the effects of potassium metasomatism in sedimentary rocks and paleosols, with implications for palaeoweathering conditions and provenance. *Geology.* **23(10):** 921-924.

Fisher, R. V., Schminke, H.U. (1984). *Pyroclastic rocks*. Springer-Verlag. Berlin Heidelberg New York Tokyo. -472pp.

Folk, R.L. (1959). Practical petrographic classification of limestones. *American Association of Petroleum Geologists Bulletin*. **43:** 1-38.

Flügel, E. (2004). *Microfacies of Carbonate Rocks: Analysis, Interpretation and Application.* Springer, Berlin Heidelberg New York. -976pp.

Gillespie, M.R., Styles, M.T. (1999). *BGS Rock Classification Scheme; Volume 1 Classification of igneous rocks*. British Geological Survey Research Report. 2nd Ed. -52pp.

Groenenberg, H., Carpenter, M., Flach, T., Zink-Jørgensen, K., Schröder, P., Christenseng, N.P., Beck, B., Chatwick, A., Lescanne, M, Aimard, N. (2008). Guidelines for licensing CO_2 storage operation around the globe. *Society of Exploration Geophysicists.* **27(4):** 496-501.

Harris, P. (2012). *GeoSpectral Imaging pamphlet*, GeoSpectral Imaging, Johannesburg.

Hatzignatiou, D.G., Riis, F., Berenblyum, R., Hladik, V., Lojka, R., Francu, J. (2008). Screening and evaluation of a saline aquifer for CO_2 storage: Central Bohemian

Basin, Czech Republic. *International Journal of Greenhouse Gas Control.* **5:** 1429-1442.

Herron, M.M. (1988). Geochemical classification of terrigenous sands and shales from core or log data. *Journal of Sedimentary Petrology.* **58(5):** 820-829.

Hillier, S. (1995). *Erosion, Sedimentation and Sedimentary Origin of Clays*. *In:* Velde, B. (Ed.) *Origin and mineralogy of clays*. Springer-Verlag Berlin Heidelberg New York. Pp. 162-219.

IEA (2015). Energy and Climate Change. World Energy Outlook Special Report before COP21.

IPCC (Intergovernmental Panel on Climate Change), 2005. IPCC Special Report on Carbon Dioxide Capture and Storage. Metz, B., Davidson, O., De Coninck, H.C., Loos, M., Mayer, L.A. (Eds.). Cambridge University Press, Cambridge, U.K. and New York, NY, U.S.A., -442pp.

Johnson, H.D., Baldwin, C.T. (1996). Shallow clastic seas. pp. 232-277. Eds. Reading, H.G. 3rd edition. Sedimentary Environments: Processes, Facies and Stratigraphy. Blackwell Science. USA, Canada, Australia.

Johnson, J.W., Nitao, J.J., Knauss, K.G. (2004). Reactive transport modelling of CO_2 storage in saline aquifers to elucidate fundamental processes, trapping mechanisms and sequestration partitioning. *Geological Society of London Special Publication on Carbon Sequestration Technologies.* **23:** 107-128.

Kelletat, D. (2006). Beachrock as Sea-Level Indicator? Remarks from a Geomorphological Point of View. *Journal of Coastal Research*. **22(6):** 1558-1564.

Kennedy, W.J., Klinger, H.C. (1972). Hiatus concretions and hard ground horizons in the Cretaceous of Zululand. *Palaeontology*. **15:** 539-549.

Kennedy, W.J., Klinger, H.C. (1975). Cretaceous faunas from Zululand and Natal, South Africa Introduction, Stratigraphy. *Bulletin of the British Museum of Natural History*. **25(4):** 263-315.

Lotz, M., Brent A.C. (2008). A review of carbon dioxide capture and sequestration and the Kyoto Protocol's clean development mechanism and prospects for Southern Africa. *Journal of Energy in Southern Africa*. **19:** 13-24.

Loubser, M., Verryn, S. (2008). Combining XRF and XRD analyses and sample preparation to solve mineralogical problems. *South African Journal of Geology.* **111(2-3):** 229-238.

Marbler, H., Erickson, K.P., Schmidt, M., Lempp, C., Pöllman, H. (2013). Geomechanical and geochemical effects on sandstones caused by the reaction with supercritical CO_2: an experimental approach to in situ conditions in deep geological reservoirs. *Environmental Earth Sciences*. **69:** 1981-1998.

Marini, L. (2007). Geological sequestration of carbon dioxide: Thermodynamics, kinetics and reaction path modelling. *Developments in Geochemistry.* 1st Ed. Elsevier-Amsterdam.-453pp.

McLachlan, I.R., McMillian, I.K. (1979). Microfaunal biostratigraphy, chronostratigraphy, and history of Mesozoic and Cenozoic deposits on the coastal margin of South Africa. *Geological Society of South Africa Special Publication.* **6:** 161-181.

McMillian, I.K. (2003). Foraminiferally defined biostratigraphic episodes and sedimentation pattern of the Cretaceous drift succession (Early Barremian to Late Maastrichtian) in seven basins on the South African and southern Namibian continental margin. *South African Journal of Science.* **99:** 537-576.

McPhie, J., Doyle, M., Allen, R. (1993). Volcanic Textures: a Guide to the Interpretation of Textures in Volcanic Rocks. University of Tasmania, Centre for Ore Deposits and Exploration Studies, Hobart. -196pp.

Melluso, L., Cucciniello, C., Petrone, C.M., Lustrino, M., Mora, V., Tiepolo, M., Vasconcelos, L. (2008). Petrology of the Karoo volcanic rocks in the southern Lebombo monocline, Mozambique. *Journal of African Earth Sciences.* **52:** 139-151.

Monastersky, R. (2013). Global carbon dioxide levels near worrisome level. *Nature.* **497:** 13-14.

Mwakasonda, S., Winkler, H. (2005). Carbon capture and storage in South Africa. Chapter 6 *In.* Bradley, R., Baumert, K., Pershing, J. (Eds). *Growing in the greenhouse: Protecting the climate by putting development first*. (Washington DC, World Resources Institute) pp. 94-109.

Nesbitt, H.W. and Young, G.M. 1984. Predictiofedon of some weathering trends of plutonic and volcanic rocks based on thermodynamic and kinetic considerations. *Geochimica Cosmochimica Acta.* **48(7):** 1523-1534.

Nichols, G. (2009). *Sedimentology and Stratigraphy*. 2nd Ed. Wiley-Blackwell. -419pp.

Ohta, T., Arai, H. (2007). Statistical empirical index of chemical weathering in igneous rocks: A new tool for evaluating the degree of weathering. *Chemical Geology.* **240:** 280-297.

Peng, D., Robinson, D.B. (1976). A New Two-Constant Equation of State. *Industrial Engineering Chemistry Fundamentals.* **15(1):** 59-64.

Pettijohn, F.J., Potter, P.E., Siever, R. (1972). *Sand and Sandstone*. Springer-Verlang. New York, Heidelberg, Berlin. -618pp.

Reineck, H.E., Singh, I.B. (1980). *Depositional Sedimentary Environments With Reference to Terrigenous Clastics.* 1st Ed. Springer-Verlag, Berlin Heidelberg New York. -549pp.

Roberts, D.L., Botha, G.A., Maud, R.R., Pether, J. (2006). *Coastal Cenozoic Deposits. In:* Johnson, M.R., Anhaeusser, C.R. and Thomas R.J. (Eds.). *The Geology of South Africa*. Geological Society of South Africa, Johannesburg/Council for Geoscience, Pretoria. pp. 605-628.

Rochelle, C.A., Czernichowski-Lauriol, I., Milodowski, A.E. (2004). The impact of chemical reactions on CO_2 storage in geological formations: a brief review. *In:* Baines, S.J. and Worden, R.H. (Eds.). *Geological Storage of Carbon Dioxide*. Special Publication of the Geological Society of London. **233**: 87-106.

Roser, B.P., Korsch, R.J. (1986). Determination of tectonic sandstone-mudstone suites using SiO_2 content and K_2O/Na_2O ratio. *The Journal of Geology.* **94(5):** 635-650.

SACS (South African Handbook of Stratigraphy). Stratigraphy of South Africa. Pt. 1 (Compiler L.E. Kent). Lithostratigraphy of South Africa, South West Africa/Namibia and the Republics of Boputhatswana, Transkei and Venda. Handbook of the Geological Survey South Africa. 8. -690pp.

Seed, D.P. (1965). The formation of vermicular pellets in New Zealand glauconites. *The American Mineralogist.* **50:** 1097-1106.

Shone, R.W. (2006). Onshore *Post-Karoo Mesozoic Deposits*. *In:* Johnson, M.R., Anhaeusser, C.R. and Thomas R.J. (Eds.). *The Geology of South Africa*. Geological Society of South Africa, Johannesburg/Council for Geoscience, Pretoria. pp. 541-552.

Span, P. and Wagner, W. (1996). A new equation of state for carbon dioxide covering the fluid region from triple point temperature to 1100K at pressures up to 800MPa. *Journal of Physical Reference Data.* **25(6)**:1509-1596.

Środoń, J. (1984). Mixed-layer illite-smectite in low-temperature diagenesis: data from Miocene of the Carpathian Foredeep. *Clay Minerals.* **19:** 205-215.

Suttner, L.J., Dutta, P.K. (1986). Aluvial sandstone composition and climate. 1. Framework mineralogy. *The Society of Economic Palaeontologists and Mineralogists.* **56(3):** 329-345.

Tankard, A.J., Jackson, M., Eriksson, K. A., Hobday, D. K., Hunter, D. R., Minter, W. E. L. (1982). *Crustal Evolution of Southern Africa: 3,8 Billion Years of Earth History.* 1st Edition. Springer-Verlag, New York Heidelberg Berlin. pp. 407-423.

Thompson, G.R. (1975). The mineralogy of glauconite. *Clays and Clay Minerals.* **23:** 289-300.

Tucker, M.E., Wright, V.P. (1990). *Carbonate sedimentology.* Blackwell Scientific Publications, Oxford. -482pp.

Van Vuuren, C.J., Broad, D.S., Jungslager, E.H.A., Roux, J. and McLachlan, I.R. (1998). Oil and Gas. *In:* Wilson, M.G.C., Anhaeusser, C.R. (Eds.). *The Mineral Resources of South Africa*, Council for Geoscience, Pretoria. pp. 483−494.

Verma, S.P., Armstrong-Altrin, J.S. (2013). New multi-dimensional diagrams for tectonic discrimination of siliciclastic sediments and their application to Precambrian basins. *Chemical Geology.* **355:** 117-133.

Viljoen, J.H.A., Stapelberg, F.D.J., Cloete, M. (2010). *The technical report on geological storage of carbon dioxide in South Africa*. -238pp.

Viljoen, J.H.A., Hicks, N., Botha, G.A., Davids, S., Musekiwa, C., Singh, R.G. Stapelberg, F.D.J., Cloete, M. (2011). *Towards an effective CO_2 storage capacity assessment of the Zululand Basin, South Africa.* -115pp.

Vousdoukas, M.I., Velegrakis, A.F., Plomaritis, T.A. (2007). Beachrock occurrence, characteristics, formation mechanisms and impacts. *Earth Science Reviews*. **85:** 23-46.

Watkeys, M.K., Mason, T.R., Goodman, P.S. (1993). The role of geology in the development of Maputaland, South Africa. *Journal of African Earth Sciences.* **16(1-2):** 205-221.

Watkeys, M.K. (2002). Development of the Lebombo rifted volcanic margin of southeast Africa. *In:* Menzies, M.A., Klemperer, S.L., Ebinger, C.J., and Baker, J. (Eds.). Volcanic Rifted Margins: Boulder, Colorado, Geological Society of America Special Paper 362. pp. 27-46.

Williams, H., Turner, F.J., Gilbert, C.M. (1954). *Petrography: An introduction to the Study of Rocks in Thin Sections.* In: Gilully, J., Woodford, A.O. (Eds.) PW. H. Freeman and Company. San Francisco. -406pp.

Appendix A

Abbreviations

BSE	Back scattered electron
CCS	Carbon capture and storage
CGS	Council for Geoscience
CH_4	Methane
CIA	Chemical Index of Alteration
CO_2	Carbon dioxide
EDX	Energy dispersive X-Ray
EOR	Enhanced oil recovery
GHG	Greenhouse gas
IEA	International Energy Agency
IPCC	Intergovernmental Panel on Climate Change
INDC	Intended Nationally Determined Contributions
LOI	Loss on ignition
LWIR	Long-wave Infrared
N_2O	Nitrogen dioxide
O_3	Ozone
PPL	Plane polarised light
PVA	Polyvinyl alcohol
RGB	Red, green, blue
SA	South Africa
$scCO_2$	Super critical carbon dioxide
SE	Secondary electron
SEM	Scanning electron microscopy
SOEKOR	South African Exploration Corporation

SWIR	Short-wave Infrared
UNFCCC	United Nations Framework Convention on Climate Change
VNIR	Visible and Near-Infrared
XPL	Cross polarised light

Units of measurement

Å	Ångström
cm	centimetres
g	grams
Gt	giga tonnes
hr	hours
km	kilometres
km^2	square kilometres
m	metres
Ma	million years
mm	millimetres
MPa	mega Pascal
Mt	mega tonnes
nm	nanometre
ppm	parts per million
t	tonnes
wt-%	weight percent
yr	years
µm	micrometres
%	percent
°C	degrees Celsius

Appendix B

Core tray photographs

Core trays containing the NZA drill core were individually photographed. The depths of the drill core in each core tray are displayed on the top right corner of each tray. The depth readings are recorded in feet, for these photographs, not metres. The drill core is also labelled where the forty samples were taken.

Core trays 1 and 2 comprise mostly brownish coloured, fissile and indurated, fine-grained, calcareous sandstones. Indurated, calcareous sandstones comprise clusters of invertebrate body fossils.

Core trays 3 and 4 comprise mostly intact brown coloured, fine-grained, calcareous sandstones with invertebrate body fossils scattered throughout the drill core.

Core trays 5 and 6 comprise brown coloured, indurated, fine-grained, calcareous sandstones with visible invertebrate body fossils and several fissile portions of the drill core.

Core tray 7 and 8 comprise light brown coloured, fine-grained, calcareous sandstones with indurated portions of drill core as well as extremely fissile portions of drill core.

Core trays 9 and 10 comprise light brown coloured, fine-grained, indurated, calcareous sandstones with several thick shelled invertebrate fossils occurring within dense, grey coloured, calcareous sandstone beds.

Core trays 11 and 12 comprise light brown indurated, fine-grained, calcareous sandstones with scattered invertebrate fossils throughout the drill core with scattered grey coloured dense calcareous sandstone beds.

Core trays 13 and 14 comprise dark brown coloured, indurated, fine-grained, calcareous sandstones with several interbedded grey coloured, dense calcareous sandstone beds.

Core tray 15 comprises dark grey-brownish coloured, indurated, fine-grained, calcareous sandstones with scattered, invertebrate body fossils.

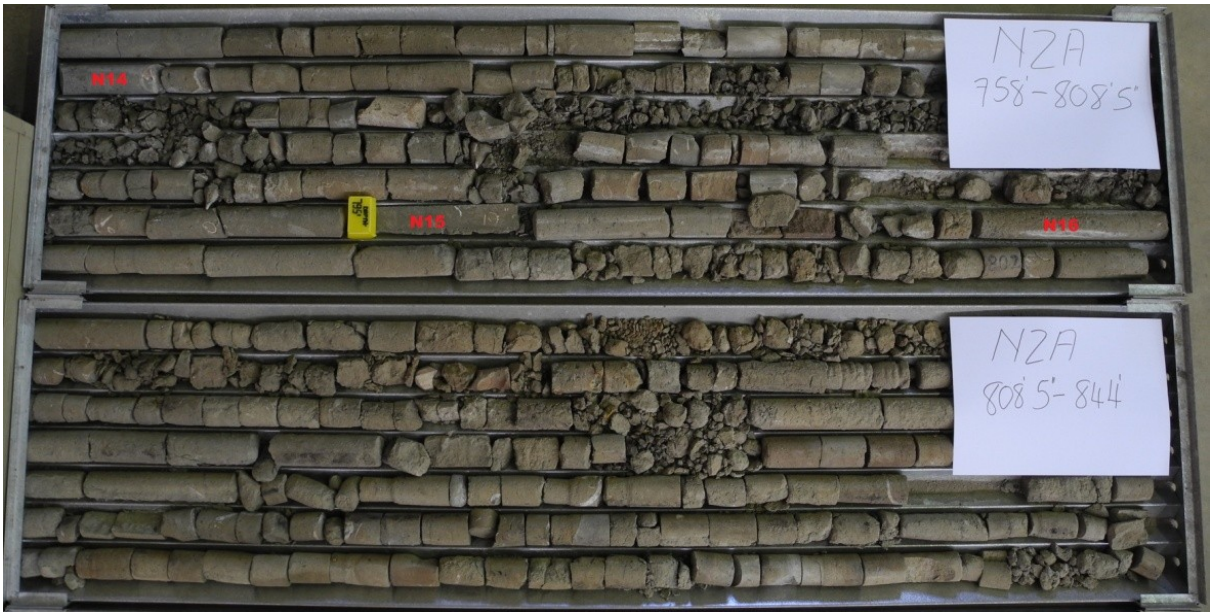

Core trays 16 and 17 comprise dark grey-brownish coloured, indurated, fine-grained, calcareous sandstones as well as fissile portions of calcareous sandstone with scattered, invertebrate body fossils.

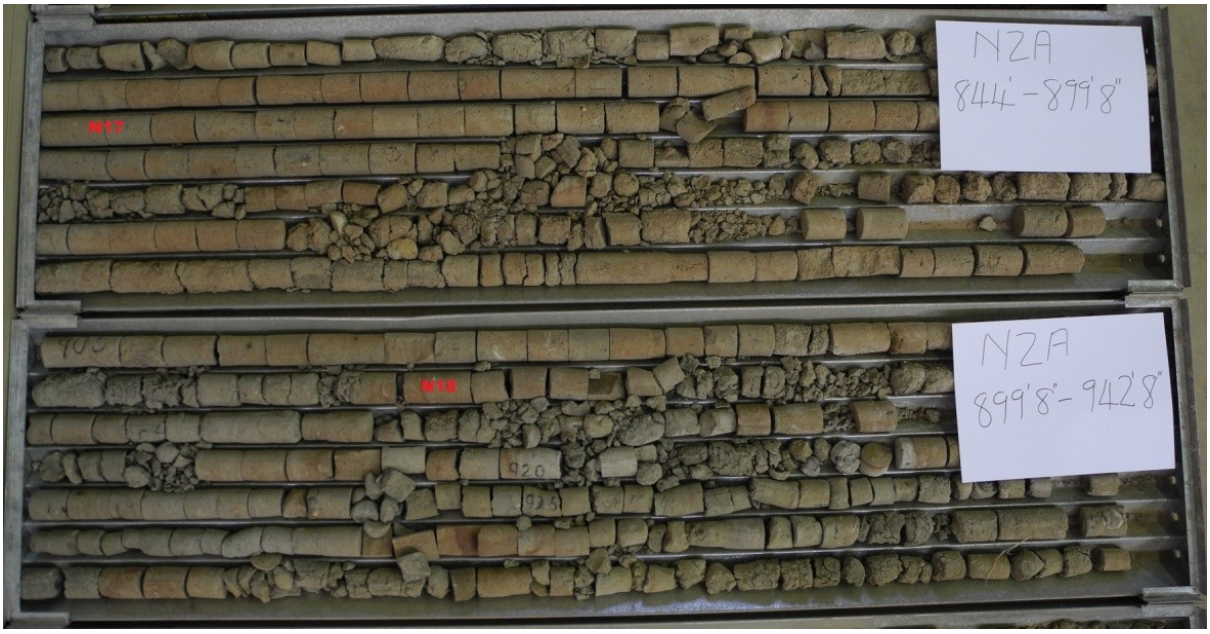

Core trays 18 and 19 comprise light brown and greyish coloured, indurated, fine-grained, calcareous sandstones as well as fissile portions of calcareous sandstone.

Core trays 20 and 21 comprise light brown and greyish coloured, indurated, fine-grained, calcareous sandstones as well as fissile portions of calcareous sandstone.

Core trays 22 and 23 comprise reddish, indurated, fossil-rich beds as well as cream coloured, indurated, fine-grained calcareous sandstones.

Core trays 24 and 25 comprise light grey and cream coloured, indurated and fissile, fine-grained calcareous sandstones with a muddy appearance.

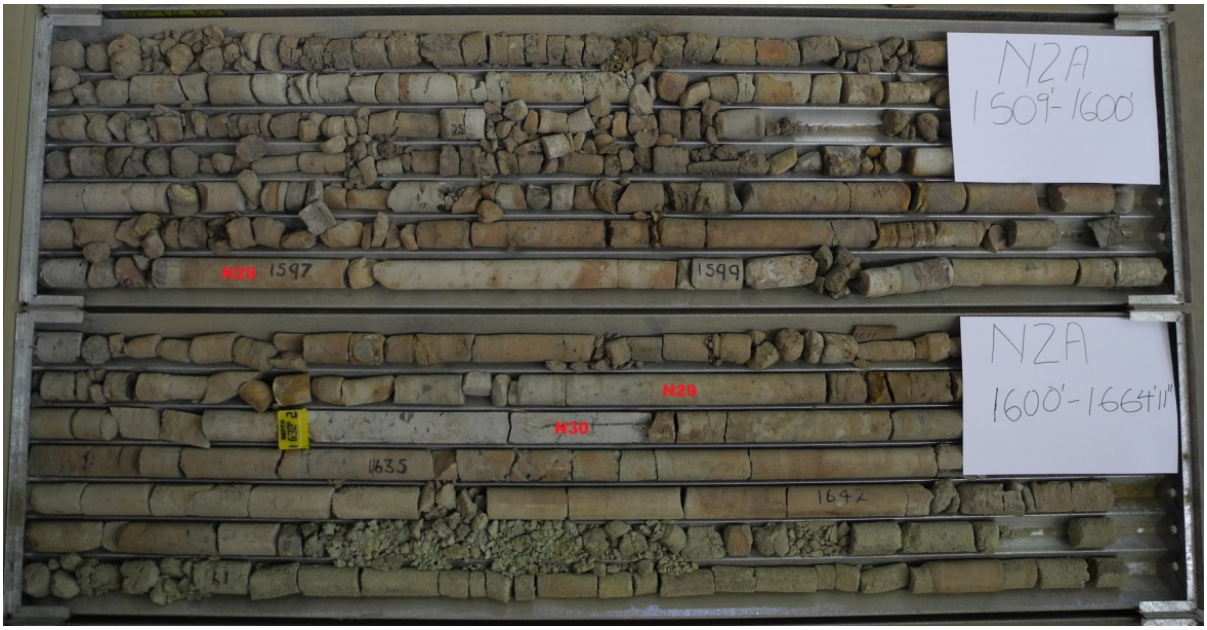

Core trays 26 and 27 comprise greyish and brown coloured, indurated and fissile, fine-grained calcareous sandstones.

Core tray 28 comprises mostly light brown coloured, medium-grained, cross-laminated calcareous sandstones grading into dark grey, poorly sorted pyroclastic rocks. Core tray 29 comprises entirely cream coloured, poorly sorted pyroclastic rocks.

Core trays 30 and 31 comprise several beds of poorly sorted, indurated and fissile pyroclastic rocks varying in colour from pinkish grey to dark grey with yellow staining. A single fine-grained, cream coloured, indurated tuff was also observed at the base of core tray 31.

Appendix C

Drill core samples and photomicrographs

Each hand sample taken from the NZA drill core was photographed prior to cutting for thin sections and milling for XRF and XRD analysis. Presented alongside each hand specimen is a photomicrograph of the sample's thin section.

Sample ID	Depth (m)	Lithology
N1	31.39-31.55	Calcareous sandstone

Macroscopic description: brownish-grey, bioturbated, fine-grained, massive, calcareous sandstone comprised of thin shelled bivalve fossils, organic matter and plant fossils chips.

Petrography: XPL photomicrograph indicating poorly sorted, dominantly fine-grained, subangular, monocrystalline quartz grains, similarly sized, angular and twinned plagioclase grains, elongated plant fossils, fragments of invertebrate fossils and sparse, dark green and brownish, rounded glauconite grains hosted in poikilotopic fabric of calcite cement.

Sample ID	Depth (m)	Lithology
N2	35.33-35.48	Calcareous sandstone

Macroscopic description: brownish-grey, fine-grained, bioturbated, massive, calcareous sandstone with indistinct bedding, a variety of bivalve fossils and black organic matter.

Petrography: XPL photomicrograph displaying poorly to moderately sorted, fine-grained detritus comprising angular monocrystalline quartz grains, twinned plagioclase grains, invertebrate fragments, black organic matter, rare glauconite grains and subrounded cross-hatched orthoclase grains in a poikilotopic fabric of calcite cement.

Sample ID	Depth (m)	Lithology
N3	38.71-38.86	Calcareous sandstone

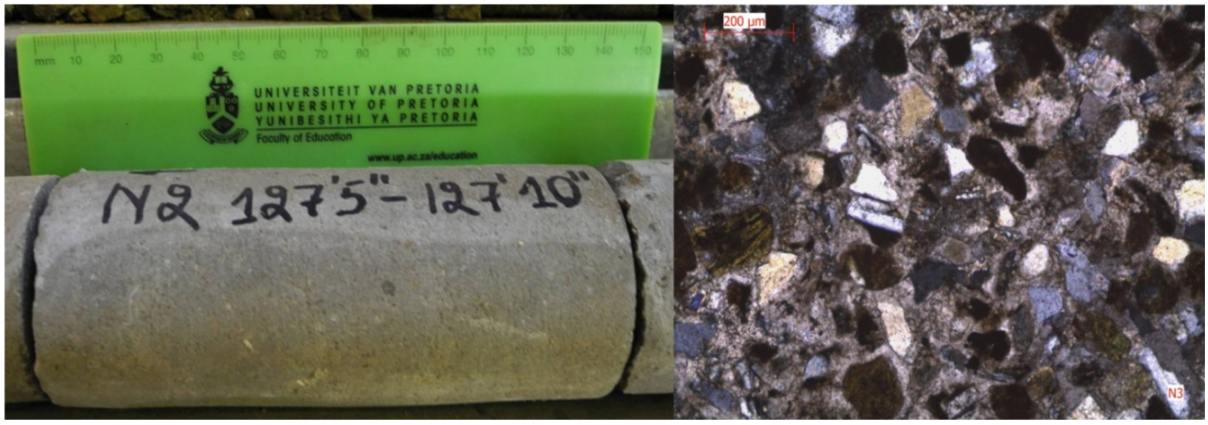

Macroscopic description: brownish-grey, fine-grained, massive, calcareous sandstone with indistinct cross-beds, organic matter, bioturbation and small, calcareous shell fragments.

Petrography: XPL photomicrograph displaying moderately sorted, fine-grained, subrounded to subangular, monocrystalline quartz grains, twinned plagioclase grains, subrounded glauconite grains, black organic matter, plant fossils, thin shelled bivalves and cross-hatched orthoclase grains hosted in calcite cement with minor clay matrix. The first generation of calcite cement surrounds grains followed by slightly darker, irregularly distributed calcite cement.

Sample ID	Depth (m)	Lithology
N4	56.31-56.44	Calcareous sandstone

Macroscopic description: greyish brown, poorly bedded, calcareous sandstone with visible gastropod and bivalve fossils, abundant organic matter as well as bioturbation.

Petrography: XPL photomicrograph displaying poorly to moderately sorted fine-grained, angular detritus including monocrystalline quartz grains, rounded glauconite grains, twinned, subangular plagioclase grains, abundant organic matter and rounded cross-hatched orthoclase grains hosted in calcite cement as well as large gastropod shells with geopetal infill similar to the surrounding detritus but with coarser calcite crystals.

Sample ID	Depth (m)	Lithology
N5	116.69-116.97	Calcareous sandstone

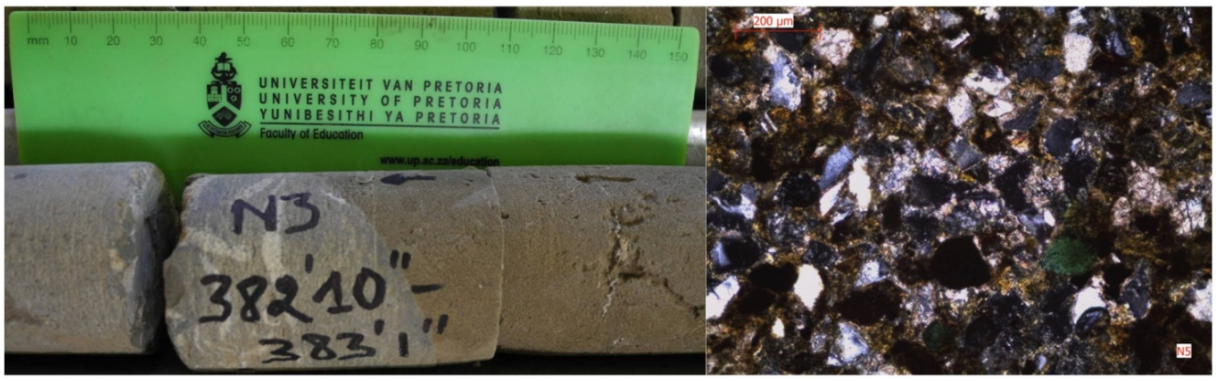

Macroscopic description: monotonous brownish, fine-grained calcareous sandstone grading into greyish brown, poorly bedded, bioturbated, fossiliferous, fine-grained calcareous sandstone, with recrystallised shell fragments and plant debris.

Petrography: XPL photomicrograph displaying moderately sorted, fine-grained detritus comprising angular to subangular, monocrystalline quartz grains, angular, twinned plagioclase grains, tabular chips of plant fossils, rounded glauconite grains, subrounded volcanic clasts and large invertebrate fossils hosted in sparsely distributed clay matrix and calcite cement.

Sample ID	Depth (m)	Lithology
N6	118.11-118.31	Greywacke

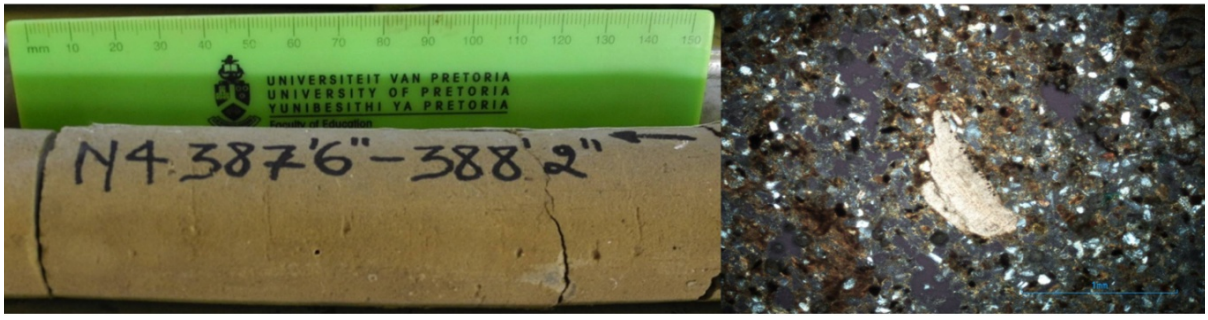

Macroscopic description: light brown, poorly bedded, massive, fine-grained greywacke with rare, thin shelled bivalve fragments and black organic matter.

Petrography: XPL photomicrograph indicating fine-grained, poorly sorted detritus of monocrystalline quartz grains, angular plagioclase grains, organic matter coated in siderite and rounded glauconite grains hosted in predominant clay matrix as well as recrystallised, isolated calcareous skeletal fragments distributed throughout the section.

Sample ID	Depth (m)	Lithology
N7	156.39-156.56	Calcareous sandstone

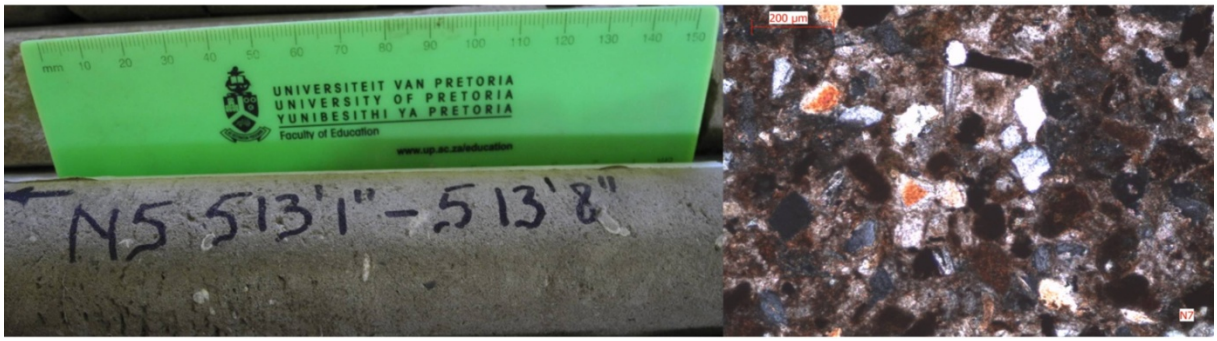

Macroscopic description: brownish-grey, massive, fine-grained, fossiliferous, calcareous sandstone rich in black organic matter displaying thick and thin shelled bivalve fossils, geopetal gastropod fossils and bioturbation.

Petrography: XPL photomicrograph displaying poorly sorted, fine-grained, angular to subangular, monocrystalline quartz grains, subrounded, cross-hatched orthoclase grains, invertebrate fossils, organic matter, subangular, twinned plagioclase, reddish fine-grained siderite and predominant calcite cement.

Sample ID	Depth (m)	Lithology
N8	169.09-169.32	Calcareous sandstone

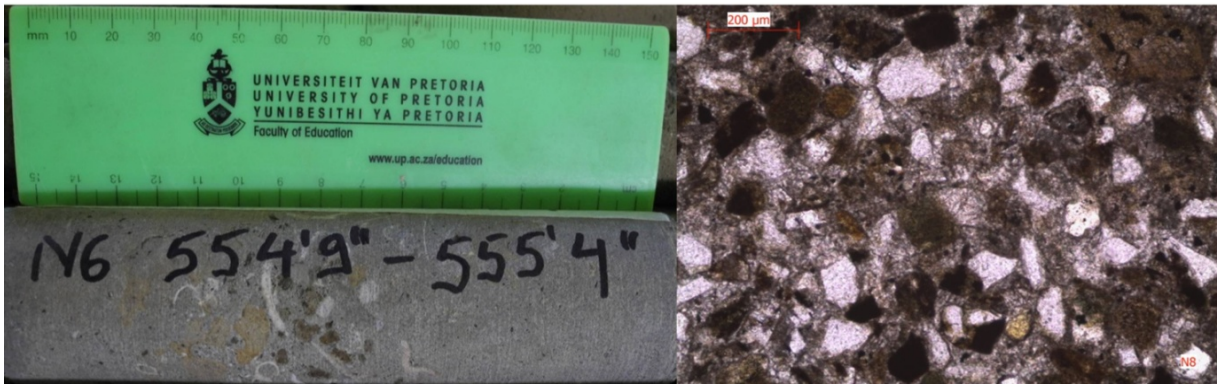

Macroscopic description: brownish-grey, fossiliferous, fine-grained, calcareous sandstone comprising large thick shelled fragments and plant remains.

Petrography: PPL photomicrograph displaying moderately sorted detritus of subangular to subrounded, fine-grained, monocrystalline quartz grains, similarly sized tabular and angular twinned plagioclase grains, large invertebrate fossils, scattered plant fossils, sparse volcanic fragments and angular orthoclase hosted in calcite cement. The first generation of calcite cement surrounds grains followed by slightly darker, irregularly distributed calcite cement.

Sample ID	Depth (m)	Lithology
N9	184.40-184.63	Greywacke

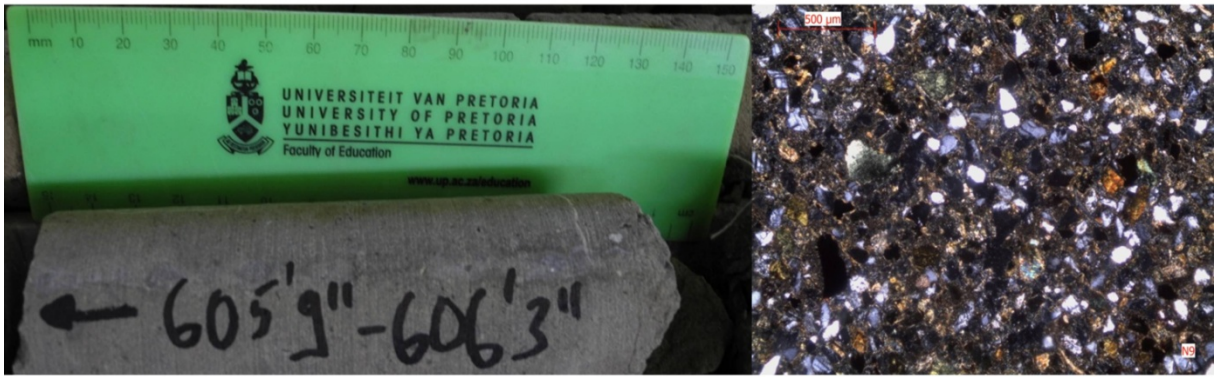

Macroscopic description: brownish-grey, bioturbated, fine-grained, massive greywacke with abundant organic matter and rare calcareous fossil fragments.

Petrography: XPL photomicrograph indicating moderately sorted, fine-grained detritus including subangular and subrounded quartz grains, angular, twinned plagioclase grains, minor orthoclase grains, scattered plant and invertebrate fossils, black organic matter and weathered glauconite grains with an evenly distributed smectite matrix.

Sample ID	Depth (m)	Lithology
N10	184.40-184.63	Calcareous sandstone

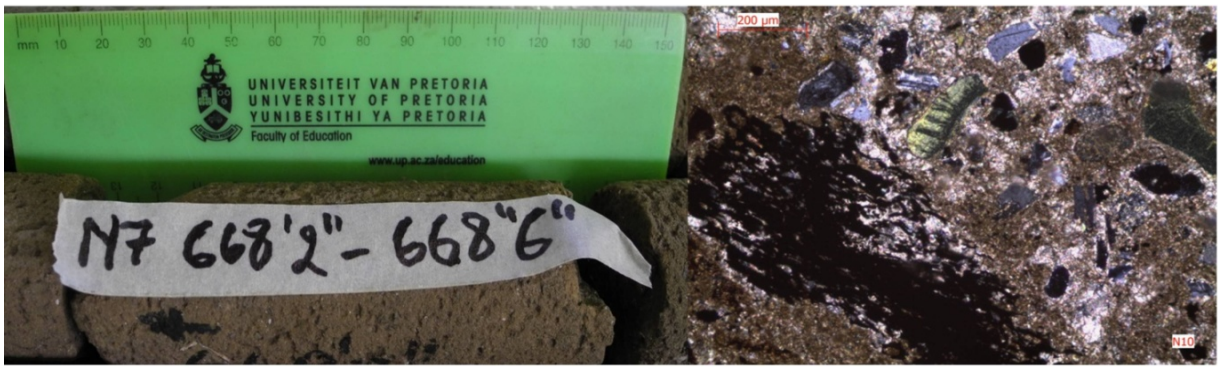

Macroscopic description: light brown, massive, fine-grained calcareous sandstone with plant remains as well as invertebrate fossils displaying a porous and friable texture.

Petrography: XPL photomicrograph comprising large quantities of partially decomposed plant fossils, abundant glauconite replacing mica grains and poorly sorted, fine-grained, subrounded, monocrystalline quartz grains and angular, twinned plagioclase grains. Detritus is hosted in sparse clay matrix and evenly distributed calcite cement. The first generation of calcite cement surrounds grains followed by slightly darker, irregularly distributed calcite cement.

Sample ID	Depth (m)	Lithology
N11	209.40-209.55	Calcareous sandstone

Macroscopic description: brownish-grey, massive, fine-grained calcareous sandstone with rare, thin shelled bivalve fossils and indistinct laminae of black organic matter.

Petrography: XPL photomicrograph displaying poorly sorted section comprising large, subrounded glauconite grains, angular to subangular, fine-grained, twinned plagioclase and quartz grains, invertebrate fossils, small chips of plant fossils, black organic matter hosted in calcite cement. The first generation of calcite cement surrounds grains followed by slightly darker, irregularly distributed second generation of calcite cement.

Sample ID	Depth (m)	Lithology
N12	229.38-229.53	Calcareous sandstone

Macroscopic description: greyish-brown, massive, calcareous sandstone with visible thin shelled bivalves, upward increasing organic content and bioturbation as well as scattered coarse sand sized quartz grains.

Petrography: XPL photomicrograph displaying large, slightly decomposed plant debris, as well as black organic matter; fine-grained detritus includes poorly sorted, subrounded quartz grains, tabular and angular grains of twinned plagioclase and abundant subrounded glauconite hosted in minor clay matrix and evenly distributed calcite cement.

Sample ID	Depth (m)	Lithology
N13	230.12-230.30	Greywacke

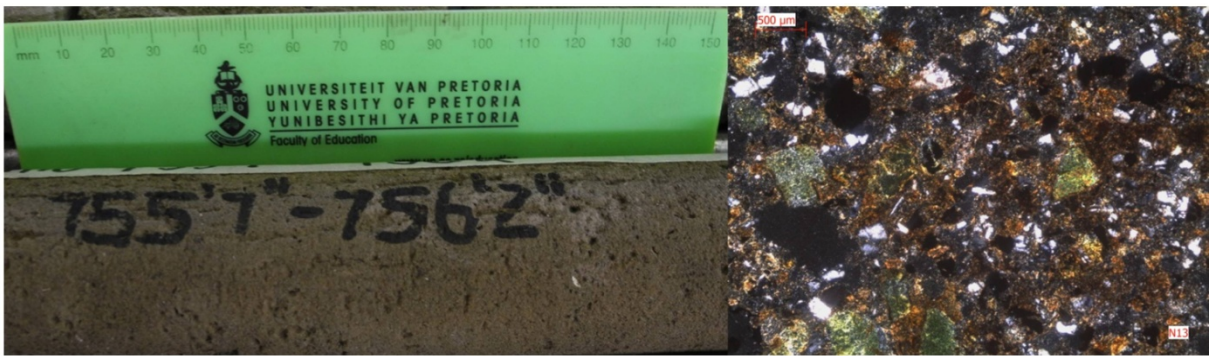

Macroscopic description: dark brown-grey, massive, fine-grained greywacke rich in organic matter displaying indistinct bedding and bioturbation.

Petrography: XPL photomicrograph comprising moderately sorted, fine-grained detritus including subangular to subrounded quartz grains, angular, twinned plagioclase grains, minor cross-hatched orthoclase grains, scattered plant fossils, black organic matter and invertebrate fossils with abundant glauconite grains and an evenly distributed smectite matrix.

Sample ID	Depth (m)	Lithology
N14	237.31-237.46	Calcareous sandstone

Macroscopic description: greyish-brown, massive, fine-grained calcareous sandstone with rare, thin shelled fossil remains and indistinct laminae of organic matter.

Petrography: XPL photomicrograph indicating poorly to moderately sorted section comprising abundant subrounded to rounded, fine-grained glauconite, subangular quartz and twinned plagioclase grains, subrounded, cross-hatched orthoclase, minor volcanic clasts, rare muscovite grains and abundant black organic matter hosted in evenly distributed calcite cement.

Sample ID	Depth (m)	Lithology
N15	243.71-244.09	Calcareous sandstone

Macroscopic description: greyish-brown, fossiliferous, massive, fine-grained calcareous sandstone with large, thick shelled bivalve and gastropod fragments and black organic matter.

Petrography: XPL photomicrograph indicating poorly sorted detritus including medium-grained, subrounded glauconite grains throughout the section, subangular to subrounded, twinned plagioclase, quartz grains and abundant black organic matter and reddish siderite hosted in calcitic cement. Large oyster fragments occur in section with greater proportions of smectite matrix occurring above the shell fragment.

Sample ID	Depth (m)	Lithology
N16	244.60-244.88	Calcareous sandstone

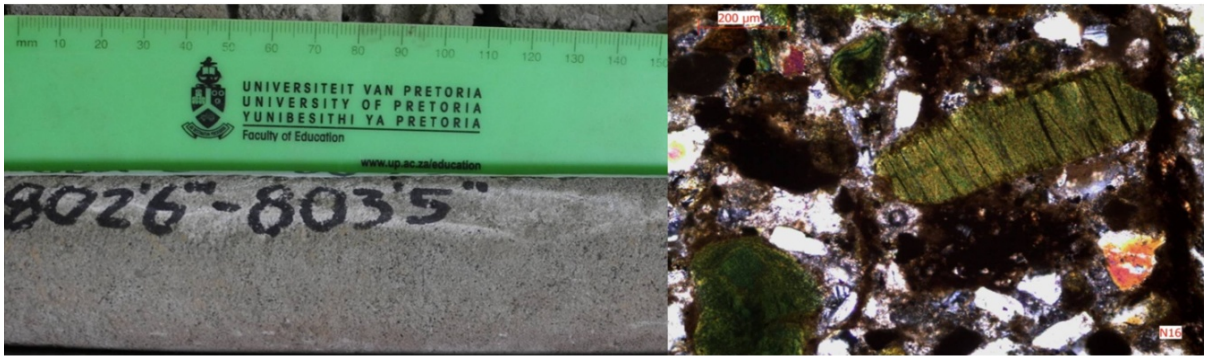

Macroscopic description: brownish-grey, massive, fine-grained calcareous sandstone, with black organic matter and rare fossil fragments.

Petrography: XPL photomicrograph of poorly sorted detritus including abundant rounded and elongated medium-grained glauconite grains replacing mica grains, minor plant fossils and organic material occur scattered throughout the section and coated in siderite, fine-grained monocrystalline quartz grains and angular plagioclase grains are hosted in calcitic cement.

Sample ID	Depth (m)	Lithology
17	267.87-268.15	Calcareous sandstone

Macroscopic description: brownish-grey, fine-grained, massive calcareous sandstone of friable texture containing bivalve fossil fragments and plant remains.

Petrography: XPL photomicrograph exhibiting poorly sorted detritus of scattered, large invertebrate and plant fossils, fine-grained, angular quartz grains, similarly sized minor, twinned plagioclase, cross-hatched orthoclase grains and uncommon fine-grained subrounded glauconite grains hosted in calcite cement.

Sample ID	Depth (m)	Lithology
18	278.64-278.84	Calcareous sandstone

Macroscopic description: light brown-grey, massive, fine-grained calcareous sandstone with scattered, thin shelled bivalves and gastropod fossils, chips of plant fossils and organic matter grading into an organic and mud rich horizon.

Petrography: XPL photomicrograph displaying scattered poorly sorted detritus of fine-grained quartz grains; similarly sized angular, twinned plagioclase, rare, subrounded glauconite grains and scattered invertebrate fossils as well as predominant organic matter hosted in smectite matrix with irregularly distributed calcite cement.

Sample ID	Depth (m)	Lithology
19	296.63-297.13	Calcareous sandstone

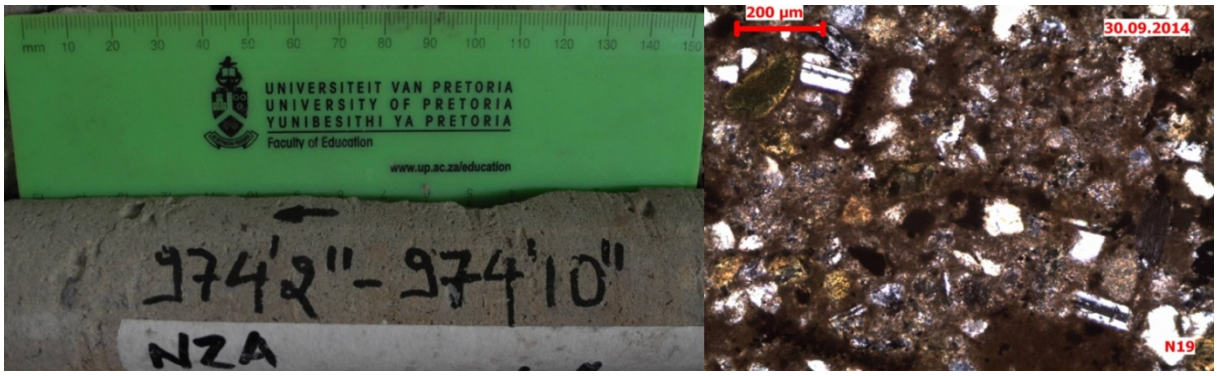

Macroscopic description: brownish-grey, massive, fine-grained, friable calcareous sandstone with some black organic matter and sparse plant and invertebrate fossil remains.

Petrography: XPL photomicrograph comprises poorly to moderately sorted, subangular to subrounded, fine-grained plagioclase grains, similarly sized quartz grains, scattered, large invertebrate and plant fossils as well as abundant glauconite grains hosted in sparse smectite matrix and evenly distributed calcite cement. The first generation of calcite cement surrounds grains followed by slightly darker, irregularly distributed calcite cement.

Sample ID	Depth (m)	Lithology
20	298.37-298.60	Calcareous sandstone

Macroscopic description: brownish-grey, poorly bedded, massive, fine-grained calcareous sandstone with organic matter coated in reddish mineral with organic matter and a pitted surface.

Petrography: PPL photomicrograph comprises moderately sorted, fine-grained detritus of predominantly subangular, monocrystalline quartz grains, similarly sized angular plagioclase grains, rare volcanic clasts, large plant fossils and organic matter coated in abundant reddish siderite and scattered, highly weathered, subrounded glauconite grains hosted in calcitic cement.

Sample ID	Depth (m)	Lithology
21	299.41-299.64	Calcareous sandstone

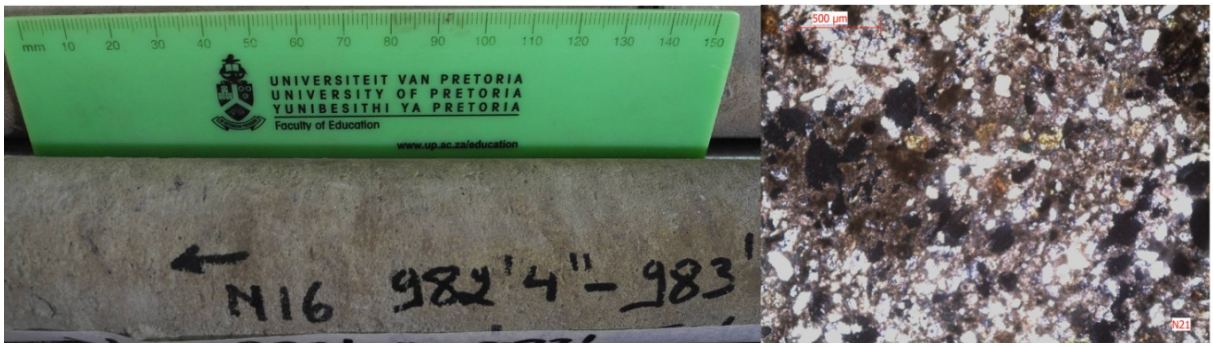

Macroscopic description: greyish-brown, massive, fine-grained calcareous sandstone displaying indistinct cross-laminae and bioturbation containing abundant organic matter and small plant fossils coated in red mineral.

Petrography: PPL photomicrograph of section comprising poorly sorted, fine-grained detritus of dominant angular quartz grains; subrounded, twinned plagioclase grains, rare subrounded volcanic clasts, organic matter and plant debris coated in reddish siderite and scattered rounded grains of glauconite hosted in evenly distributed calcite cement.

Sample ID	Depth (m)	Lithology
22	324.48-324.74	Calcareous sandstone

Macroscopic description: brownish-grey, massive, fine-grained calcareous sandstone with thick shelled and thin shelled unbroken bivalves and gastropod shells. Organic matter and plant fossils are coated in reddish mineral.

Petrography: XPL photomicrograph of section comprises several recrystallised gastropod fossils filled with blocky calcite. Poorly sorted detritus comprises fine-grained, angular to subangular quartz and plagioclase grains, fine-grained glauconite grains, abundant black organic matter and abundant reddish siderite in evenly distributed calcite cement.

Sample ID	Depth (m)	Lithology
23	340.46-340.61	Coquina limestone

Macroscopic description: reddish and whitish, coquina limestone comprised of large, thin and thick shelled bivalves and gastropods. Glauconite grains are visible with the naked eye.

Petrography: XPL photomicrograph of section comprises well sorted ca. 30 mm fragments of bivalves, gastropods, echinoid spines and coral sponges with sparsely distributed smectite matrix and rare fine-grained quartz and plagioclase grains hosted in calcite cement.

Sample ID	Depth (m)	Lithology
24	341.07-341.22	Beachrock

Macroscopic description: greyish brown, fine-grained beachrock with visible glauconite grains.

Petrography: XPL photomicrograph of section comprises heavily recrystallised, fine-grained calcite grains with scattered smectite matrix and calcite cement, rare fossil fragments and abundant fine-grained rounded glauconite grains. Determining the orientation and size of original calcitic material is impossible due to heavy recrystallisation.

Sample ID	Depth (m)	Lithology
25	408.05-408.36	Calcareous sandstone

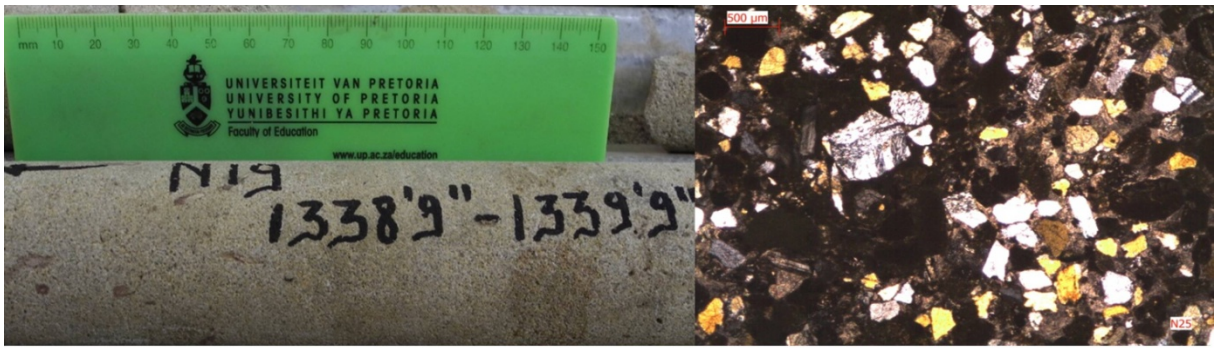

Macroscopic description: brownish-grey, massive, fine-grained calcareous sandstone with indistinct bedding and patches of organic matter.

Petrography: XPL photomicrograph displays moderately sorted, fine-grained detritus of predominantly subangular to subrounded quartz grains, similarly sized, twinned plagioclase and cross-hatched orthoclase, scattered bivalve fossils and uncommon rounded glauconite. Organic matter is evenly distributed throughout the detritus hosted in calcite cement.

Sample ID	Depth (m)	Lithology
26	451.26-451.41	Calcareous sandstone

Macroscopic description: greyish-brown, massive, fine-grained calcareous sandstone with abundant fine-grained organic matter showing signs of bioturbation.

Petrography: XPL photomicrograph displaying moderately to poorly sorted, fine-grained detritus of subrounded, monocrystalline quartz grains, lesser subangular, twinned plagioclase grains, subrounded volcanic clasts, rare cross-hatched orthoclase grains, scattered subrounded glauconite grains and invertebrate fossils all hosted in abundant poikilotopic fabric of calcite cement.

Sample ID	Depth (m)	Lithology
27	455.12-455.27	Calcareous sandstone

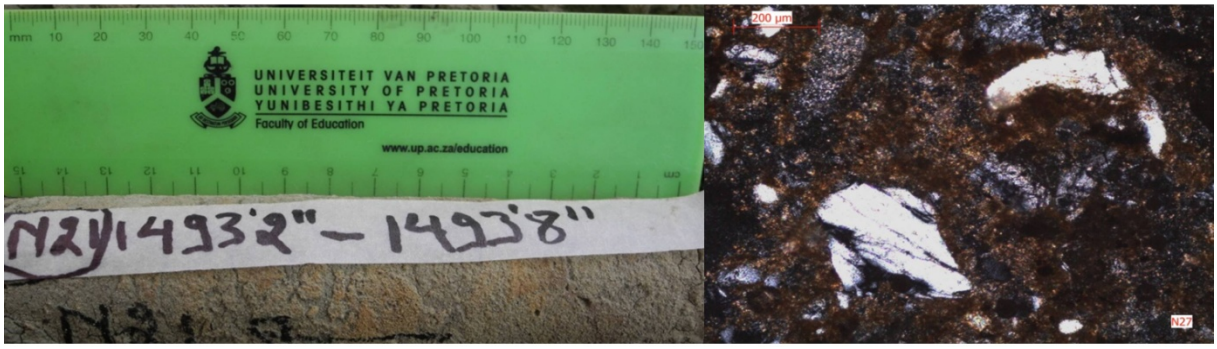

Macroscopic description: brownish, fine-grained, massive calcareous sandstone with small plant fossils, organic matter and friable surface appearance.

Petrography: XPL photomicrograph comprising poorly sorted, fine-grained detritus of dominant, angular quartz grains, twinned plagioclase grains, rare rounded glauconite grains, and black organic matter as well as evenly distributed, reddish, fine-grained minerals, presumably haematite hosted in calcite cement.

Sample ID	Depth (m)	Lithology
28	486.16-486.46	Beachrock

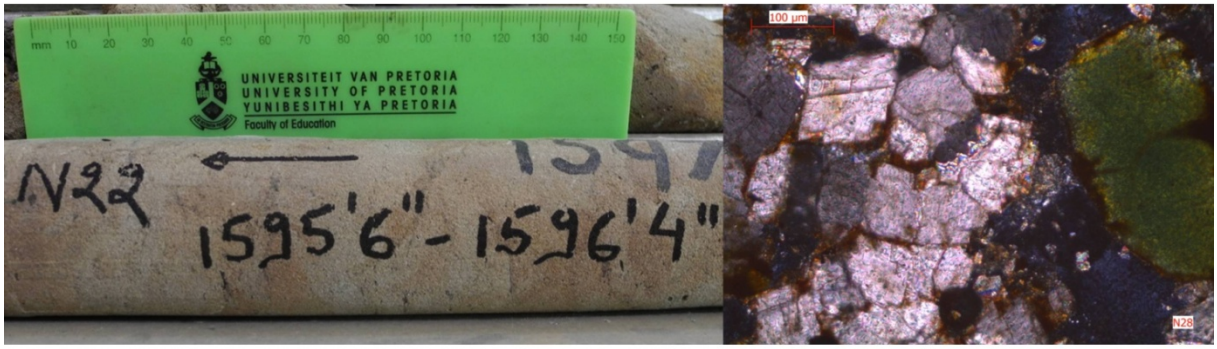

Macroscopic description: pinkish-reddish coloured, fine-grained beachrock containing some organic material and reddish staining imparting a mottled surface appearance.

Petrography: XPL photomicrograph displaying heavily recrystallised, fine-grained calcite grains with scattered smectite matrix, rare thick shelled bivalve fragments and abundant fine-grained rounded glauconite grains.

Sample ID	Depth (m)	Lithology
29	499.01-499.44	Calcareous sandstone

Macroscopic description: light brown to grey coloured, massive, fine-grained calcareous sandstone with indistinct laminae of plant fossils coated in reddish minerals and rare, thin shelled bivalve fossils.

Petrography: XPL photomicrograph displaying moderately to poorly sorted, fine-grained detritus of subangular monocrystalline quartz grains, angular, twinned plagioclase grains, scattered organic matter coated in siderite, subrounded volcanic clasts, rare cross-hatched orthoclase grains, scattered subrounded glauconite grains and invertebrate fossils all hosted in a well distributed poikilotopic fabric of calcite cement. The first generation of calcite cement surrounds grains followed by slightly darker, irregularly distributed calcite cement.

Sample ID	Depth	Lithology
30	500.18-500.66	Calcareous sandstone

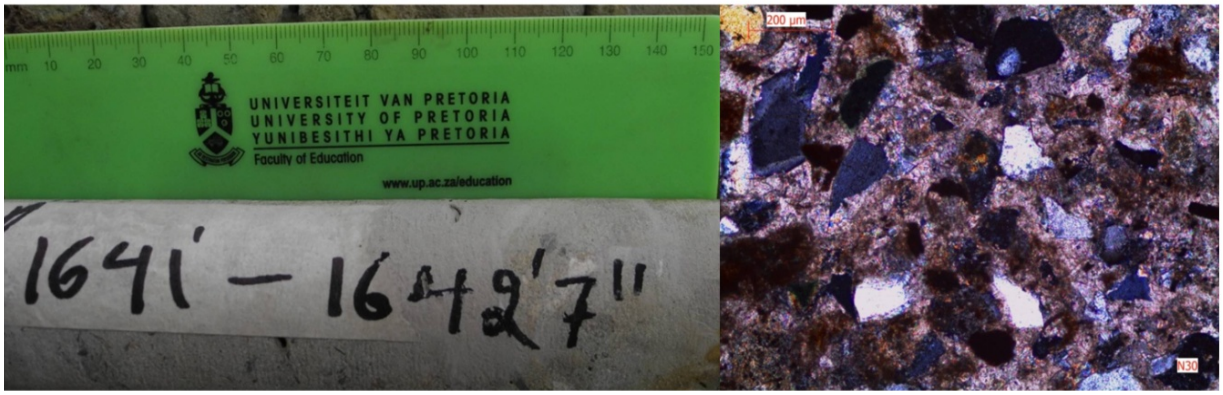

Macroscopic description: light brown to grey coloured, massive, fine-grained calcareous sandstone displaying indistinct bedding and bioturbation, coarse-grained volcanic clasts, poorly laminated plant fossils and rare, thick shelled bivalve fossils.

Petrography: XPL photomicrograph displaying poorly sorted fine-grained detritus of dominant angular quartz grains, twinned plagioclase grains, scattered thin shelled bivalves, rare rounded glauconite grains and scattered smectite matrix hosted in poikilotopic fabric of calcite cement. The first generation of calcite cement surrounds grains followed by slightly darker, irregularly distributed calcite cement.

Sample ID	Depth (m)	Lithology
31	513.23-513.41	Calcareous sandstone

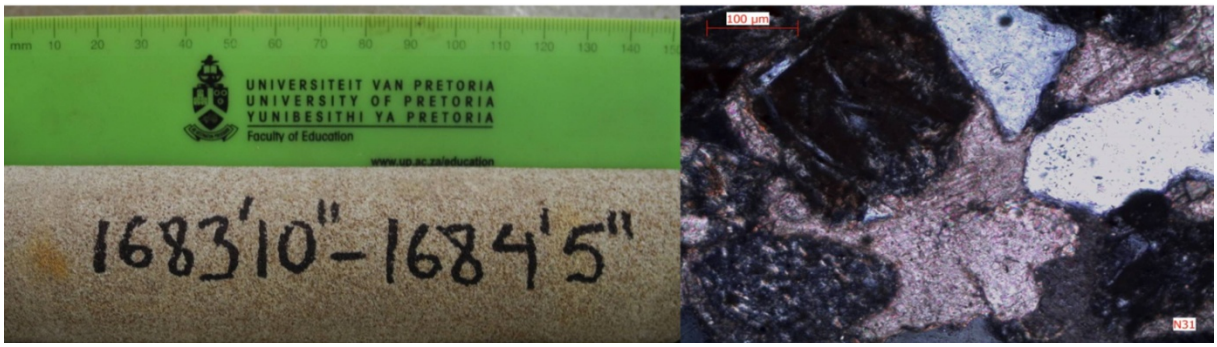

Macroscopic description: greyish-brown, medium-grained, indistinctly cross-laminated calcareous sandstone with reddish clasts and black organic matter.

Petrography: XPL photomicrograph of a moderately sorted calcareous sandstone comprising dominant, subrounded to rounded fine-grained quartz grains, similarly sized, twinned plagioclase grains, volcanic clasts and cross-hatched orthoclase grains also occur. Sparse glauconite grains and small thick shelled bivalve fragments are scattered throughout the section. The detritus is hosted in evenly distributed, poikilotopic calcite cement.

Sample ID	Depth (m)	Lithology
32	514.71-514.96	Calcareous sandstone

Macroscopic description: greyish-brown, well indurated, medium-grained, indistinctly cross-laminated, calcareous sandstone comprised of reddish clasts, and black organic matter.

Petrography: XPL photomicrograph of moderately sorted sandstone comprising dominant, subrounded to rounded, fine-grained quartz grains. Similarly sized, twinned plagioclase grains, volcanic clasts and cross-hatched orthoclase grains also occur. Sparse glauconite grains occur scattered throughout the section. The detritus is hosted in evenly distributed calcite cement.

Sample ID	Depth (m)	Lithology
33	521.06-521.31	Lapilli-tuff

Macroscopic description: grey-black coloured, poorly sorted lapilli-tuff with visible, white pumice displaying upward coarsening then upward fining trend hosted in fine-grained volcanic ash matrix.

Petrography: XPL photomicrograph displaying lapilli-grade pumice, crystals of fine-grained cross-hatched orthoclase, twinned plagioclase and monocrystalline quartz hosted in a very fine-grained matrix of dark volcanic ash.

Sample ID	Depth (m)	Lithology
34	532.05-532.18	Lapilli-tuff

Macroscopic description: creamish-pink coloured, fine-grained lapilli-tuff with several large pumice fragments and lithic fragments hosted in fine-grained creamish volcanic ash matrix.

Petrography: XPL photomicrograph indicating predominant, very fine-grained ash matrix hosting lapilli-sized pumice, fine-grained crystals of monocrystalline quartz and plagioclase. Chalcedony filled veins and voids are common throughout the rock.

Sample ID	Depth (m)	Lithology
35	549.15-549.27	Lapilli-stone

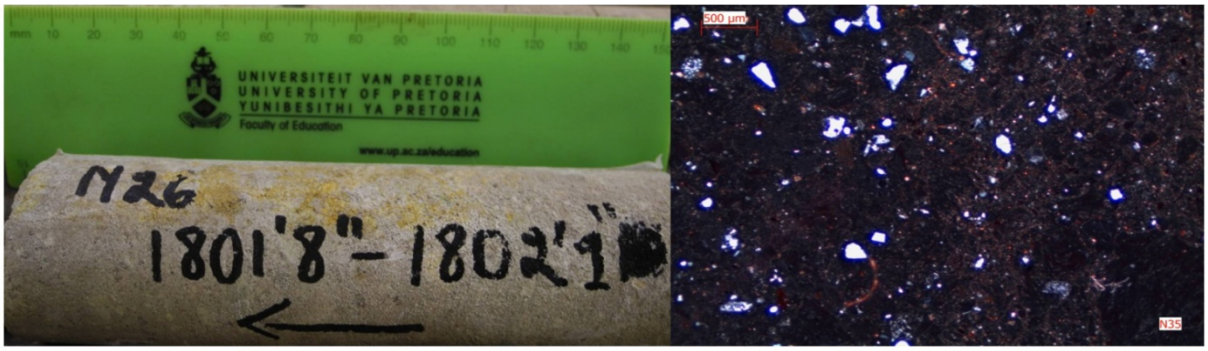

Macroscopic description: creamish-brown coloured, poorly sorted lapilli-stone comprised of lapilli-sized whitish to greenish pumice, surface exhibits yellow weathered appearance.

Petrography: XPL photomicrograph displaying dominant, very fine-grained volcanic ash matrix hosting fine-grained crystals of monocrystalline quartz and twinned plagioclase. Lapilli-grade pumice is scattered throughout the rock.

Sample ID	Depth (m)	Lithology
36	553.06-553.29	Tuff-breccia

Macroscopic description: grey-black, poorly sorted tuff-breccia with weathered green appearance.

Petrography: XPL photomicrograph of dark brown smectite and plagioclase needle matrix with scattered blocks of volcanic fragments, angular pumice, tabular crystals of plagioclase and fine-grained quartz crystals.

Sample ID	Depth (m)	Lithology
37	557.12-557.35	Lapilli-stone

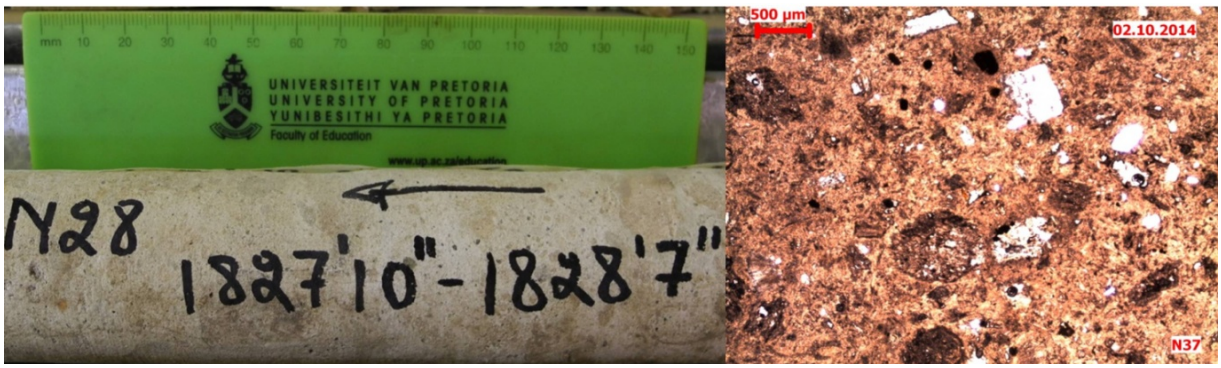

Macroscopic description: cream coloured, lapilli-stone comprising angular pumice and volcanic clasts in a whitish coloured fine-grained volcanic ash matrix.

Petrography: PPL photomicrograph of predominantly fine-grained volcanic ash matrix hosting poorly sorted angular crystals of quartz and plagioclase as well as angular pumice and volcanic clasts.

Sample ID	Depth (m)	Lithology
38	562.89-563.07	Lapilli-stone

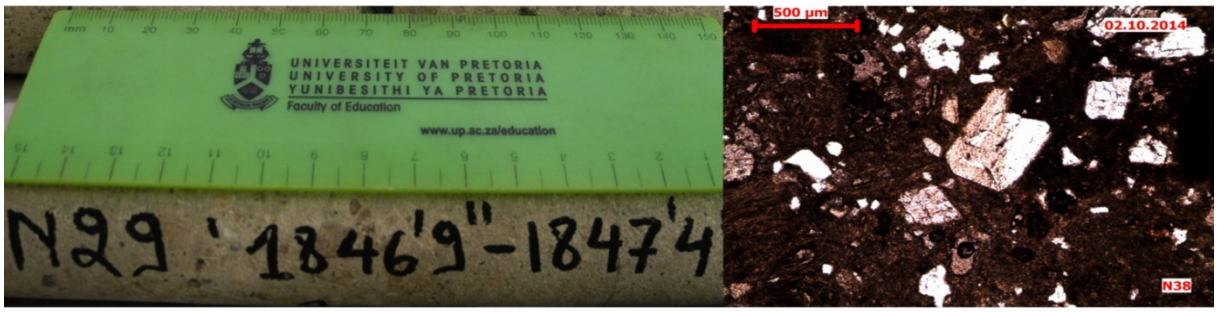

Macroscopic description: cream-grey coloured lapilli-stone comprising angular pumice and volcanic clasts in a whitish-greenish coloured, fine-grained volcanic ash.

Petrography: XPL photomicrograph of predominantly fine-grained volcanic ash matrix hosting poorly sorted angular crystals of quartz and plagioclase as well as angular pumice and volcanic clasts.

Sample ID	Depth (m)	Lithology
39	564.62-564.79	Lapilli-stone

Macroscopic description: cream coloured, poorly sorted lapilli-stone comprising lapilli-grade pumice and volcanic clasts crystals hosted in a whitish-greenish volcanic ash matrix.

Petrography: XPL photomicrograph of subrounded volcanic clasts, angular quartz and plagioclase crystals and subangular pumice and scattered spherultic glass hosted in an evenly distributed matrix of fine-grained volcanic ash.

Sample ID	Depth (m)	Lithology
40	571.09-571.20	Tuff

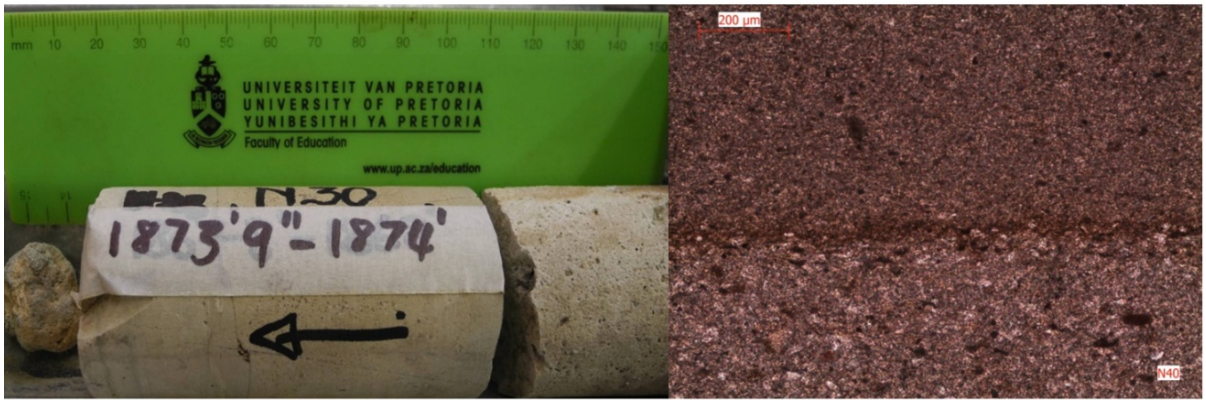

Macroscopic description: fine to very fine-grained, cream coloured tuff coarsening and then fining upward with indistinct laminae.

Petrography: XPL photomicrograph displaying upward fining sequence of very fine-grained volcanic ash separated by a sharp contact in which dolomite rhombs formed. Common, small black bodies, thought to be organic matter are scattered throughout the rock forming indistinct laminae.

Appendix D

Geochemical approaches used in study

Several geochemical approaches were utilised during the herein investigation of the NZA drill core. The equations and formulae utilised in each approach are presented in the following paragraphs. Recalculated major element analyses in Table 8 were utilised in the following geochemical approaches:

SandClass Scheme and Pettijohn Scheme after Herron (1988):

Sample	$\log(Na_2O/K_2O)$	$\log(Fe_2O_3/K_2O)$	$\log(SiO_2/Al_2O_3)$
N1	0.05	1.93	0.73
N2	-0.16	1.56	0.73
N3	-0.10	2.01	0.74
N4	-0.03	1.94	0.73
N5	0.24	2.05	0.67
N6	0.06	2.31	0.70
N7	-0.01	2.08	0.69
N8	0.02	2.02	0.69
N9	-0.01	2.09	0.74
N10	0.04	2.27	0.71
N11	-0.07	1.95	0.69
N12	-0.12	1.90	0.72
N13	-0.11	2.07	0.77
N14	-0.05	1.86	0.74
N15	-0.11	1.68	0.82
N16	-0.09	1.70	0.83
N17	0.13	2.37	0.70
N18	0.08	1.78	0.68
N19	0.08	1.96	0.71
N20	0.06	1.99	0.69
N21	0.06	1.93	0.68
N22	-0.02	1.79	0.76
N25	-0.04	2.20	0.88
N26	0.03	2.30	0.79
N27	0.03	2.07	0.68
N29	0.06	1.72	0.70
N30	0.12	1.56	0.68
N31	0.16	1.93	0.87
N32	0.02	2.22	0.94

Multi-variate discrimant-function analysis for low silica siliciclastic rocks after Verma and Armstrong-Altrin (2013):

$$DF\ 1 = (0.608 * \ln(TiO_2/SiO_2) + (-1.854 * \ln(Al_2O_3/SiO_2) + (0.299 * \ln(Fe_2O_3/SiO_2) + (-0.550 * \ln(MnO/SiO_2) + (0.120 * \ln(MgO/SiO_2) + (0.194 * \ln(CaO/SiO_2) + (-1.510 * \ln(Na_2O/SiO_2) + (1.941 * \ln(K_2O/SiO_2) + (0.003 * \ln(P_2O_5/SiO_2) - 0.294$$

$$DF\ 2 = (-0.554 * \ln(TiO_2/SiO_2) + (-0.995 * \ln(Al_2O_3/SiO_2) + (1.765 * \ln(Fe_2O_3/SiO_2) + (-1.391 * \ln(MnO/SiO_2) + (-1.034 * \ln(MgO/SiO_2) + (0.225 * \ln(CaO/SiO_2) + (0.713 * \ln(Na_2O/SiO_2) + (0.330 * \ln(K_2O/SiO_2) + (0.637 * \ln(P_2O_5/SiO_2) - 3.631$$

Sample	DF 1	DF 2
N1	-0.23	-2.72356
N2	1.28	-0.85009
N4	0.87	-0.71424
N5	-1.55	-3.30365
N6	0.86	0.484931
N7	-0.25	-3.47633
N8	-0.18	-2.30711
N9	2.02	0.89227
N10	1.37	0.938861
N11	0.49	-2.61937
N12	1.07	-1.98891
N13	2.52	1.764177
N14	0.40	-1.77012
N15	2.58	1.395551
N16	2.31	1.333158
N17	0.42	-1.14487
N18	-0.40	-2.69421
N19	1.04	0.597801
N20	0.91	0.840167
N21	0.94	1.006008
N22	2.20	0.886605
N30	-0.12	-1.30455
N31	0.37	0.794834

Multi-variate discrimant-function analysis for high-silica siliciclastic rocks after Verma and Armstrong-Altrin (2013):

DF 1 = (-0.263 * ln(TiO_2/SiO_2) + (0.604 * ln(Al_2O_3/SiO_2) + (-1.725 * ln(Fe_2O_3/SiO_2) + (0.660 * ln(MnO/SiO_2) + (2.191 * ln(MgO/SiO_2) + (0.144 * ln(CaO/SiO_2) + (-1.304 * ln(Na_2O/SiO_2) + (0.054 * ln(K_2O/SiO_2) + (-0.330 * ln(P_2O_5/SiO_2) + 1.588

DF 2 = (-1.196 * ln(TiO_2/SiO_2) + (1.064 * ln(Al_2O_3/SiO_2) + (0.303 * ln(Fe_2O_3/SiO_2) + (0.436 * ln(MnO/SiO_2) + (0.838 * ln(MgO/SiO_2) + (-0.407 * ln(CaO/SiO_2) + (1.021 * ln(Na_2O/SiO_2) + (-1.706 * ln(K_2O/SiO_2) + (-0.126 * ln(P_2O_5/SiO_2) – 1.068

Sample	DF1	DF2
N3	1.600865	0.160292
N25	-1.17615	-0.23033
N26	1.080054	1.197789
N27	-0.7115	0.130845
N29	0.145999	-0.10708
N32	0.096986	1.016884

MFW diagram used to discriminate chemistry and degree of weathering in volcanic rocks after Ohta and Arai (2007):

Step 1

M = $-0.395\times\ln(SiO_2) + 0.206\times\ln(TiO_2) - 0.316\times\ln(Al_2O_3) + 0.160\times\ln(Fe_2O_3) + 0.246\times\ln(MgO) + 0.368\times\ln(CaO) + 0.073\times\ln(Na_2O) - 0.342\times\ln(K_2O) + 2.266$

F = $0.191\times\ln(SiO_2) - 0.397\times\ln(TiO_2) + 0.020\times\ln(Al_2O_3) - 0.375\times\ln(Fe_2O_3) - 0.243\times\ln(MgO) + 0.079\times\ln(CaO) + 0.392\times\ln(Na_2O) + 0.333\times\ln(K_2O) - 0.892$

W = $0.203\times\ln(SiO_2) + 0.191\times\ln(TiO_2) + 0.296\times\ln(Al_2O_3) + 0.215\times\ln(Fe_2O_3) - 0.002\times\ln(MgO) - 0.448\times\ln(CaO) - 0.464\times\ln(Na_2O) + 0.008\times\ln(K_2O) - 1.374$

Step 2

Closure operation at: C100 [exp(M), exp(F), exp(W)]

Recalculate to 100%.

Sample	M	F	W
N33	4.13	84.26	11.61
N34	24.00	56.85	19.15
N35	9.07	76.22	14.71
N36	13.72	67.56	18.73
N37	7.30	83.44	9.27
N38	8.71	78.23	13.06
N39	13.89	74.14	11.98
N40	6.52	77.33	16.15

The amount of chemical weathering of rock samples was assessed using the A-CN-K diagram (Fedo *et al.,* 1995):

Sample	Al_2O_3/101.96	CaO/56.08+Na_2O/61.98	K_2O/94.2
N1	0.11	0.22	0.02
N2	0.08	0.08	0.02
N3	0.11	0.13	0.02
N4	0.09	0.15	0.02
N5	0.11	0.30	0.01
N6	0.12	0.09	0.02
N7	0.12	0.17	0.02
N8	0.11	0.37	0.02
N9	0.10	0.09	0.02
N10	0.11	0.09	0.02
N11	0.10	0.22	0.02
N12	0.09	0.19	0.02
N13	0.10	0.07	0.03
N14	0.09	0.26	0.02
N15	0.07	0.24	0.02
N16	0.08	0.20	0.02
N17	0.11	0.06	0.01
N18	0.11	0.23	0.01
N19	0.09	0.11	0.01
N20	0.11	0.13	0.02
N21	0.12	0.12	0.02
N22	0.09	0.21	0.02
N25	0.09	0.13	0.02
N26	0.12	0.06	0.02
N27	0.13	0.10	0.02
N29	0.13	0.16	0.02
N30	0.09	0.11	0.02
N31	0.07	0.07	0.01
N32	0.08	0.07	0.01

Appendix E

Autoclave experiments and SEM photomicrographs

Photomicrographs of sample N25 before and after reaction with $scCO_2$ using a polarising microscope followed by SEM-photomicrographs of sample N25 before and after reaction with $scCO_2$ after SEM analysis.

Autoclave experiment photomicrographs of N25

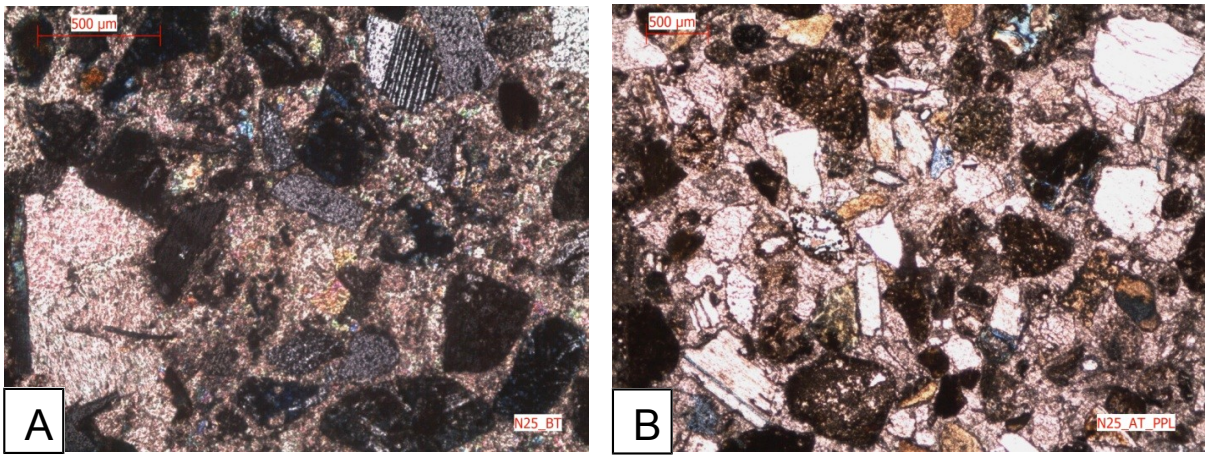

(A) XPL photomicrograph of poorly sorted sandstone comprising angular to subangular plagioclase grains, monocrystalline quartz grains and orthoclase grains cemented in a poikilotopic fabric of calcite cement before treatment with $scCO_2$. Note, the blue dye is not clearly visible in cement. (B) PPL photomicrograph of sandstone N25 after treatment with $scCO_2$ indicating dissolution of calcite cement contributing to an increase in porosity from ca. 1 % to ca. 3 %.

SEM photos of N25

Before reaction with $scCO_2$

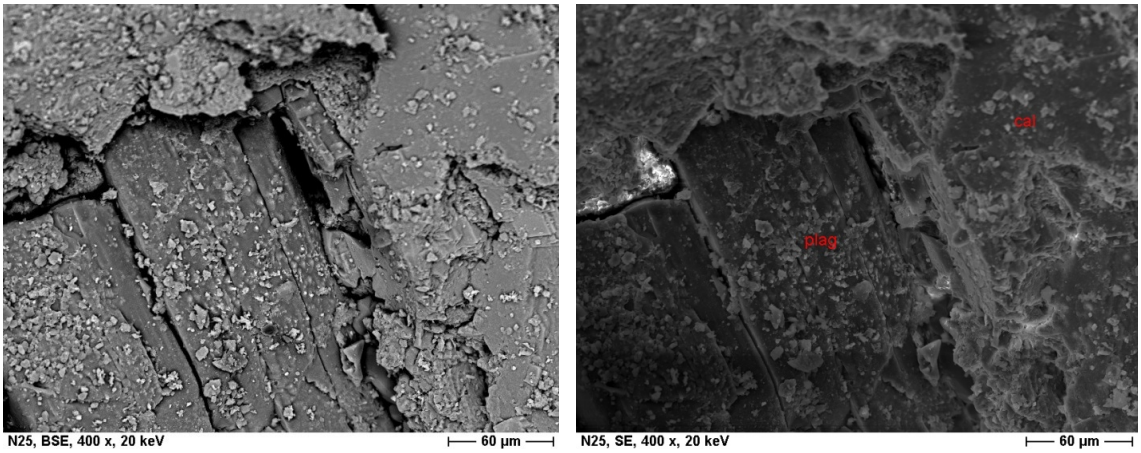

Before reaction with $scCO_2$ surfaces of quartz and plagioclase are typically coated in fine-grained clay minerals presumably smectite that were identified during spectral imaging and XRD analysis. Observing changes in clay minerals on surfaces are important because mobilised clay minerals can potentially block pore throats which reduce porosity and reduce storage potential of host rock. Evenly distributed calcite cements typically exhibit a smooth

surface morphology, consistent with observations made by Marbler *et al.* (2013) of calcareous sandstones prior to reaction with $scCO_2$.

After reaction with $scCO_2$

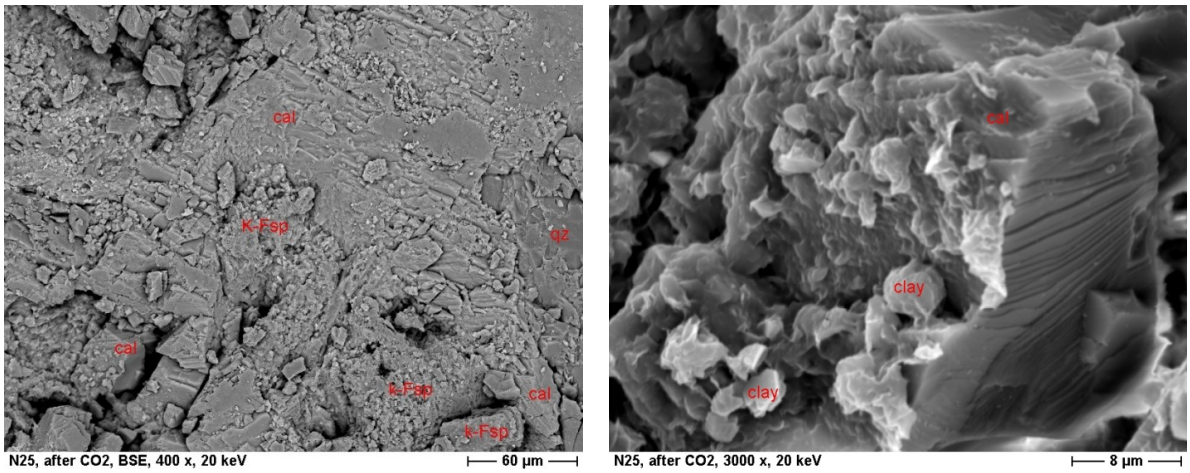

After reaction with $scCO_2$ calcite surfaces are typically rough, exposing cleavage planes due to differential dissolution. The pitted rough calcite mineral grain surfaces exhibit exposed cleavage planes and slightly pitted surfaces. The surfaces of minerals previously coated in fine clays have since mobilised.

Appendix F

Detailed borehole log of NZA with XRF, XRD and spectral imaging results